

Automated Laser Cavity Mirror Alignment & Beam Profiler Modulation System



Senior Design II

Group 10 Members and Majors

Bryce Moon	Electrical Engineering
Anthony DeSantis	Computer Engineering
Nicholas Pinkham	Photonic Sciences and Engineering
William Bowman	Photonic Sciences and Engineering

Table of Contents	
Project Narrative	1
Project Motivation	1
Project Goals.....	1
Project Objectives.....	3
Project Function.....	5
Project Constraints	5
Design Constraints.....	5
Time Constraints.....	6
Financial Constraints	6
Testing Constraints	6
Safety Constraints.....	7
Visual Constraints.....	7
Locationality Constraint	7
Project Standards.....	8
Initial Project Milestones	9
Requirements Specifications	11
Existing Optical Technologies.....	12
Cavity Adjustment Technologies:	12
Automatic cavity tuning for extended cavity diode laser by F. Allard et al.	12
Automatic laser-to-optical-fiber coupling system based on monitoring of Raman scattering signal by Kyoung Duck-Park et al.	13
A simple method for automatic cavity alignment of a solid-state laser ^{106]} by L. Dong et al.	13
Project Comparison with Existing Technology	14
Power Meters	14
Beam Profilers	15
Technology Investigations.....	17
Computer Engineering Technology Investigation.....	17
Supervised Learning Background	17
Supervised Learning Possible Application	17
Unsupervised Learning Background.....	19
Unsupervised Learning Possible Application	19
Reinforcement Learning Background	19
Reinforcement Learning Possible Application:	20

Threshold Search Solution	21
Electrical/Mechanical Components Investigation	23
Electrical Motors	23
Gears.....	29
Metal Gears vs 3D-Printed Gears.....	30
Power Supply/DC-DC Converter.....	31
Optical Engineering Technology Investigation	32
Split Design	32
Reflection/Transmission (R/T) Ratio.....	33
Polarizing and Non-polarizing	33
Narrow wavelength bandwidth or broadband	34
Power Meter	35
Sensors	35
Attenuating Element.....	39
Focusing element(s)	40
Mode Quality Measurements.....	41
Beam Width:	41
Beam Divergence:	44
Beam Waist:	45
Rayleigh Length:	46
Confocal Beam Parameter:.....	47
Beam Quality:	47
Astigmatism:	49
Laser Profile Asymmetry	49
Laser Beam Profiler Investigation	50
Camera-Based Beam Profilers:	50
Scanning-Aperture Profilers:.....	53
CMOS, CCD, Knife-Edge, and Slit Profiler Specification Tabulation.....	56
Design Considerations	57
Total System Integration Design	57
Archipelago Configuration.....	57
Bulk Package Configuration	57
Configuration Decision	58
Power Meter Design	58

Attenuation	58
Photodiode Modes of Operation	60
Noise Equivalent Power, Signal-to-Noise Ratio, and Responsivity	60
Linear Region of Photodiode	63
Power Meter Circuitry	63
Optical Layout Design	69
Product Investigation.....	72
Beam Splitter	73
Neutral Density Filter	73
Profiler Camera.....	74
Microcontroller/Computer.....	75
Servo Motors	76
Power Supply.....	77
Outlet Supply.....	78
Battery Supply.....	78
Selected Product Deep Dive	78
Raspberry Pi HQ Camera	79
Guaranteed Temperature Allowances	79
Spectral Characteristics	80
Pixel Array Size	81
Raspberry Pi 4GB.....	83
Raspberry Pi Pico	84
FEETECH FT90R	84
Vendor Discussion.....	85
Optical Components	85
Raspberry Pi Hardware.....	86
Layouts and Printed Circuit Board (PCB).....	86
Raspberry Pi Computer	86
Testing.....	88
Considerations	89
Component Tests:.....	89
Note: When Using Hantek 2D72 3-in-1.....	89
Passive Components:.....	89
Operational Amplifier:	90

Analog-to-Digital Converter:	90
Beam Profiling Camera:.....	90
Photodiode:.....	91
ND Filters:.....	91
Lenses:.....	91
Beam Splitter:.....	92
System Tests:	92
Power Meter Accuracy Test:	92
Phototransistor Power Meter Demonstration:	93
SBD and Motor Quality Test:	95
Software Test:	95
Fiber Optic Proof of Concept Test:	95
Basic Mode Analysis Test:.....	97
Advanced Mode Analysis Test:	97
Beam Profiler Measurement Test:.....	97
Final Test:.....	97
Project Budgeting and Finance.....	101
Electrical Components:.....	102
Mechanical Components:	102
Optical Components:	102
Power Meter	102
Beam Profiler	103
Miscellaneous Optical	103
Combined Optical	104
Combined Component Cost.....	105
House of Quality Trade-off Table	106
Hardware Block Diagram	107
Optical Subsystems Diagram	108
Software Block Diagram	109
Software Design.....	110
Combined Beam-Profiler/Power Meter Graphical User Interface (GUI):	110
Unprocessed Camera Feed:	111
Color Coded Camera Feed:	111
Live Parameters:.....	112

Desired Parameters:.....	112
Function Tab:	113
Software Logic	114
Beam Profiler:	114
Reinforcement Learning Program Design.....	117
Training Program Functions	117
Training Program Function Descriptions	118
Alignment Program Functions.....	119
Alignment Program Function Descriptions	119
Conclusion	121
Bibliography	122
Computing:	122
Electrical and Mechanical:	122
Optical:	123

Project Narrative

Project Motivation

The motivation for this project is derived from the time and effort it can take to achieve a lasing condition with an open-cavity laser. Above the lasing threshold condition, a laser's output is dominated by stimulated emission as opposed to spontaneous emission, the spectral linewidth drastically decreases, and the slope of the relationship between input power and output power is orders of magnitude greater than in the non-lasing condition. In general, a laser that is lasing produces much greater power than one that is not lasing. An important element in achieving the lasing condition is properly adjusting the output couplers (mirrors) which are located on either end of the cavity. Making these adjustments by hand can often be tedious and frustrating, as the process consists essentially of changing the pitch and angle of the mirrors by twisting knobs on the mirror mounts. As the mirrors are adjusted to their optimal placement, the power generated within the laser cavity will increase, thus indicating if the adjustments are decreasing cavity losses and helping the system reach the lasing condition. The scale of these adjustments becomes exceptionally minute as the lasing condition is approached, and one small mistake can cause major setbacks in progress. We seek to automate this process, removing the need to manually adjust the lasing system and ameliorating any related stress.

Furthermore, our system also performs a qualitative analysis on the laser beam. This is necessary for the second stage of what the system accomplishes. Once the laser has been brought to the lasing condition, the system will seek to maximize output power and mode quality via the power meter and qualitative beam analysis. Through this beam analysis process, elements of the beam, such as intensity distribution, transverse lasing mode, and mode quality are observed and communicated to the user. These factors are all important when deciding what beams to use for differing applications and determining whether or not the beam displays any negative characteristics like astigmatism, jitter, etc.

The issue of manually adjusting an optical system is something that we have frequently encountered, personally by working in the lab and through the complaints of other students and even professors. Thus, we believe that this aspect of the project could reach a niche but certainly existing market, mainly focused in the academic community, for both research, development and teaching applications. The beam profiler broadens the potential market for our system to industry use, while still holding relevance to the aforementioned academic fields. This is especially applicable in the manufacturing of closed cavity lasers, in which both couplers are hard fastened to the cavity. These lasers must be verified to have the highest output power and mode quality possible before permanently aligning the couplers. Automating this alignment process would significantly reduce the potential for human error.

Project Goals

As mentioned above, the overall goal of this project is to automate the process of adjusting an open-cavity laser's output couplers to achieve lasing conditions and maximum power/mode quality. We hope to accomplish this by creating a system that can attach to the mirror mounts that control a laser's output couplers and alter the couplers pitch and tilt until lasing occurs after which maximum conditions are sought. This alteration is done by physically turning the knobs that control the different dimensional parameters. These physical adjustments are predicated off of a feedback-loop between whatever mechanism rotates the knobs—whether that be a gear system, rotating grips, rack and pinion, etc.—and a power meter. These two elements are in constant communication, and each respective reading of the power meter influences the movement of the adjusters.

This information exchange eventually optimizes the coupler dimensions to the point where lasing and subsequent maximum conditions occur. These adjustments affect what the beam profiler observes, but once the system reaches lasing and stabilizes, the profiler can accurately describe the beam's characteristics. We have outlined the primary goals of this project below:

- Construct an optimal power meter for the feedback-loop
- Create a beam profiler that can accurately describe certain elements of the beam
- Encode software into the profiler and power meter that can enable the feedback loop
- Develop a mechanism that can control the knobs connected to the output couplers

- Have the entire system attach to an open-cavity laser and achieve the lasing condition

In addition, we have theorized a set of more advanced goals that, while feasible, were outside of the realistic scope of our two-semester project limitation. However, if the project moves along faster than anticipated, they could be pursued. They are outlined here:

- Fabricate the power meter so it can automatically adjust for different wavelengths
- Extend the basic concept of the feedback loop (both power optimization and profiling) to apply to optical fiber alignment
- Further the scope for beam modulation through the profiler

Lastly, we have come up with some stretch goals potentially beyond our abilities and resources, but which nevertheless are novel extensions of the main principles present in our system. If any of our group members desired to develop the system further, whether that be for entrepreneurial gain or scholastic achievement, these could serve as high level additions to the project. They are as follows:

- Program a computer/ mobile application that can both display all the relevant system information and intake user commands
- Allow the z dimension (parallel to the cavity) to be another axis for adjustment, thus permitting the altering longitudinal modes of the beam in the profiler software
- Enable system operation with high powered pulsed lasers
- Optimize the packaging and design of the system to be mass produced

Project Objectives

This section is dedicated to outlining the major, overarching objectives of the project, while also listing the individual goals that need to be achieved to ensure that each objective is met.

Designing the Optical Power Meter

- Choose the best photodiode for this application
- Select a simple, cost-effective schematic for the meter
- Determine the best vendors to purchase components from, considering: cost, delivery time, reliability, and customer service
- Solder all elements together
- Test meter side by side with a factory-made meter to ensure accuracy
- Design the beam profiler
- Decide on what imaging method to use
 - Perform cost-benefit analysis
 - Purchase imaging system
- Determine what beam characteristics we wish to display and calculate
 - Develop software that can perform calculations for relevant data

Ensuring beam reaches both Profiler and Power Meter

- Determine how to split the beam and in what orientation and split ratio
- Determine correct number of lenses, spacing of lenses, diameters of lenses, and powers of lenses.

Designing the User Interface

- Decide between using a computer program with a GUI or a standalone display with internal processors and input buttons

Integrated GUI

- Determine what operating system is used

- Code the program
 - Successfully implement chosen algorithms
 - Ensure workability with both power meter and beam profiler
- Create a computer application user interface that can output numeric characters to display system information, i.e., wavelength, instantaneous power, and length of time elapsed for the current adjustment cycle
 - Fig. 48 shows where the display would communicate within the context of the system.
 - Consider whether or not the display needs to be able to output information in differing languages. If so, we would of needed to determine which languages and how they will be implemented.
- Integrate a physical emergency shut-off somewhere in the system, perhaps connected to the power supply

Standalone User Interface

- Attach digital input buttons that allow a user to input wavelength and adjust desired output power, or select an automatic maximum power setting
 - Fig. 47 displays the relationships between the correlations on other system parameters for changes in wavelength range.
 - Determine whether the display should feature a full numeric keypad, just up and down buttons to control parameter input, or be completely configured via a peripheral computer keyboard to change parameters within the application itself.
- Have a physical switch on the system that is directly connected to the power supply. Besides acting as the on/off button for the system, the switch will also serve as an emergency shut-off
- Develop a display capable of communicating all relevant information to the user
 - Decide whether this can be monochromatic or needs color imaging
 -

Choose Algorithm with which the computer will Function

- Design feedback-loop
 - Ensure initial loop set will operate based off power meter information and will achieve lasing

- Secondary loop set takes data from profiler and adjusts based on user input (if possible)
- If user inputs are unobtainable, return coupler to its position at the end of the first loop
- Store the adjustor location for when the system reaches lasing

Determine what Single Board Computer (SBC) will Control the Cavity Adjusters and Decode Power Readings

- Compare prices and functionality of different options
- Purchase and integrate into system

Choose the Mechanism with which the Adjustment Arms will Function

- Ensure that the mechanism has a relatively low level of friction, as vibrations could potentially misalign optical elements of the lasing system
- Determine whether we need to create custom elements to replace the rotation knobs on the standard laser output couplers, or design grips to hold and control the factory knobs
- Determine the torque needed in order to adjust the knobs
- Determine the ratio of gears needed so the motors can adjust the knobs of the mirror with ease and accuracy

Project Function

The main apparatus functions as a feedback loop, wherein the SBC decodes readings from the power meter and adjusts the couplers based on said readings. As the adjusters alter the physical parameters of the laser cavity, the power in the cavity changes and is detected by the power meter. The system keeps adjusting the couplers in a one dimensional “sweep” until a defined power maximum is located. The system then repeats the sweep in an orthogonal dimension, replicating the process described above. The system alternates between dimensions of adjustment until the maximum power can no longer be increased, this is considered the true maximum, or optimal, power.

Project Constraints

Design Constraints

A potential design constraint could come from the possibility that ambient light could oversaturate or skew the power sensor data. This could significantly alter the power readings and impact the proposed feedback loop, causing the couplers to misadjust. The sensor may need to compensate for this background light, while ensuring accurate readings from the laser. A potential solution to this constraint could be to have the system conduct a test of background irradiance before it begins measuring the laser power, then factoring this into the adjustment algorithm. In addition, we must be conscious of the level of

vibration the adjustor motors produce, as minute fluctuations in the physical parameters of a laser cavity can have an extreme effect on output power and lasing.

Time Constraints

For the project, our team was using the lasers located in the CREOL building. As a result, availability to those lasers was restricted based on the time that is permitted to our team by the faculty. There is also a clear time limit for completion of the project, as defined by the semester in which we were enrolled in Senior Design I & II. The rough schedule for the remainder of the SD semesters is laid out in Tables 1 and 2.

Financial Constraints

The project is not sponsored by the university or any company as a result, all costs are paid for by the members of the team. Therefore, we wish to keep the cost of the project as low as possible, our specification for this seen in Table 3. This has led to several critical decisions for the project with the most apparent constraint for the project being that the quality of laser we are building the device for are too expensive for our budget. As a result, all testing was be limited to the lasers located on campus in CREOL.

The second financing constraint is that Power Meters (costing anywhere from a couple hundred to thousands of dollars) are quite expensive. To solve this issue our group built and designed our own device to measure the intensity of light. This problem is mirrored with the beam profiler, whose cost can easily surpass ten thousand dollars. As such, we designed and built our own version as well. Although we are confident in the quality of both of these devices, our relative lack of funding certainly limited the quality of the individual elements we purchased for use in these devices. This then had a carry-on effect in the overall devices, potentially decreasing accuracy, working ranges, and degrees of precision. There were also financial considerations in the mechanical and electrical elements of the system. We were limited to purchasing sub-optimal motors, circuitry, etc. due to a financial focus on the optical elements of the system. (Tables 34-40)

Testing Constraints

Testing of the project is limited, as purchasing a laser is entirely unrealistic for our group. We were limited to using lasers at CREOL, which meant we were only be able to use the laser at certain times of the day, and only in the CREOL building. For testing, we used a Helium Neon Laser lent to us by Dr. LiKamWa. This laser model was located in the CREOL Senior Design lab, but only during certain weeks when it is available for us. Another constraint on the project was that each group member is a college senior, and had conflicting school and work schedules with each other, so meeting online, much less in person, was be difficult.

Safety Constraints

Open laser cavities have the potential to be rather dangerous, with some models even having exposed high voltage electrodes. This could constrain our ability not only to test on an open cavity laser model, but also to demo the project prototypes and even showcase it in the final showcase. As with any laser, being that they are by definition highly focused sources of light, there are concerns with the laser light damaging the eyes. We were aware of any potential dangers and took precautions to protect ourselves, such as wearing laser safety eye wear and reviewing laser safety training.

Visual Constraints

While function comes before appearance for the project there is still a constraint the design must adhere to. For the project, the user interface must be simple and understandable so that any users outside the project group are able to use the device with little help/advice from the group. Ideally, operation would not be contingent on understanding English, as valuable information could be conveyed numerically (current power, time, etc.) or audio visually (power failures, resets).

Locationality Constraint

Like any optical system, the environment for our project must be very controlled. Slight physical perturbations can skew the alignment of the system so drastically as completely misalign the laser, removing it from the lasing state. Due to this, the system was restricted to use on an optical breadboard or optical table for testing and demoing.

Furthermore, whenever sensitive electronics are integrated into a system, exposure to extreme temperatures can permanently damage their functionality. While temperatures in this damaging range would likely never be present when testing the system, it is not unfeasible that the system could be stored in a location reaching severe temperatures. For example, the system could easily reach temperatures exceeding 120 degrees Fahrenheit if stored in the trunk of an unshaded car on a hot day. Our group was cognizant of this when selecting components and storing the system.

Project Standards

- Power meter calibration standard
 - ISO/IEC 17025:2017 calibration laboratory standard
- ANSI standards on laser safety (eye safety)
- [Z136.1](#), American National Standard for Safe Use of Lasers
- [Z136.4](#), American National Standard Recommended Practice for Laser Safety Measurements for Hazard Evaluation
- [Z136.8](#), American National Standard for Safe Use of Lasers in Research, Development, or Testing
- NEMA standards for electric motors
- OSHA standards for laboratory safety and testing (electrical equipment, physical hazards)
- [1910.132\(a\) Application](#). Protective equipment, including personal protective equipment for eyes, face, head, and extremities, protective clothing, respiratory devices, and protective shields and barriers, shall be provided, used, and maintained in a sanitary and reliable condition wherever it is necessary by reason of hazards of processes or environment, chemical hazards, radiological hazards, or mechanical irritants encountered in a manner capable of causing injury or impairment in the function of any part of the body through absorption, inhalation or physical contact.
- [29 CFR 1910.303\(g\)\(2\)\(i\)](#) The provision in question, 29 CFR 1910.303(g)(2)(i), generally requires "live parts of electric equipment operating at 50 volts or more" to be "guarded against accidental contact by use of approved cabinets or other forms of approved enclosures" or by other specified means. The guarding requirement does not distinguish between AC and DC voltages. Therefore, the requirement applies to live parts operating at 50 volts or more AC *or* DC

Initial Project Milestones

Number	Task	Start	End	Status	Actionee
Senior Design I					
1	Divide and Conquer 1.0	9/6/21	9/17/21	Complete	Group
2	Technology Investigation for PCB	9/17/21	11/19/21	Complete	Bryce and AJ
	Shopping for different PCB printing options will have to be researched and compared.				
3	Technology Investigation for Open Cavity Lasers and Light Sensors	9/17/21	11/19/21	Complete	Nick and Matt
	Will have to perform research looking at what the tolerances are for the lasing conditions for different kinds of open cavity lasers, specifically as far as mirror offset is concerned.				
4	Finalize Optical Design Goals	9/17/21	11/1/21	Completed	Nick and Matt
	We must speak with Dr. Kar to finalize the scope of the optical design. This might end up altering the scope of the project in general, either by adding more features to the system or slightly altering the goals of the project.				
5	Design PCB	9/17/21	3/28/22	Complete	Bryce and AJ
6	Divide and Conquer 2.0	9/25/21	10/1/21	Complete	Group
7	60 Page Draft	9/27/21	11/5/21	Complete	Group

8	100 Page Draft	11/8/21	11/19/21	Complete	Group
9	CREOL Optical Subset Demo	10/30/21	11/30/21	Complete	Nick and Matt
	Construct a power meter, perform the Accuracy Test to demo function				
10	Final SD1 Document	11/22/21	12/7/21	Complete	Group

Table 1: Senior Design I initial project milestones and objectives

Senior Design II					
10	Implement encoding and decoding components	1/10/22	2/30/22	Complete	Bryce
11	Order and build parts based on PCB	1/10/22	3/30/22	Complete	Bryce and AJ
	Connect proper peripherals to the PCB(s) and verify that all connections within the PCB are valid and functioning properly.				
12	Order parts and construct beam profiler	12/10/21	1/30/22	Complete	Nick and Matt
13	Finish Prototype	2/30/22	4/10/22	Complete	Group
	Connect all hardware together corresponding to the predesigned schematic and verify that all parts speak to each other properly.				
14	Test and Revise	3/30/22	4/30/22	Complete	Group
	Conduct the final test, taking note of where potential pitfalls in the prototype are, and subsequently reconciling the pitfalls.				
15	Finalize SD2 draft	4/10/22	4/17/22	Complete	Group
16	Finalize SD2 Document	4/17/22	4/25/22	Complete	Group

Table 2: Senior Design II initial project milestones and objectives

Requirements Specifications

Spatial Degrees of Freedom	3
Time to Lase	< 5 minutes
Minimum Achievable Output Power	75% of max theoretical power
Workable Laser Wavelength Range	400nm - 700nm
Workable Laser Output Power Range	1nW - 10W
Maximum Laser Beam Half-Angle Divergence	17.5mrad
Workable Laser Beam Diameter	1mm - 10mm
Maximum Workable Laser Beam Divergence	17.5mrad
Data Refresh Rate	60 Hz
Setup Time	< 1 minute
Weight limits	< 6.0 kg
Dimensions	Whole System Storable in a Cubic Foot
Power Consumption	< 20 W

Cost	< \$1000
------	----------

Table 3: Requirement's specifications

Existing Optical Technologies

Although our project goal of delivering a system capable of automatically aligning the cavity mirrors of a laser, optimizing power and modulating the beams profile is certainly novel, it is not the first technology of its kind to exist. In this section we have examined and discussed published research papers which propose similar systems, before rationalizing the uniqueness of our own. In addition, we have provided a tabulation of information regarding existing optical power meters and beam profilers. Through these, we hope to set benchmarks for our own design, and have readily available comparisons for pricing and functionality.

Cavity Adjustment Technologies:

Automatic cavity tuning for extended cavity diode laser by F. Allard et al.

This automated system locks an extended cavity diode laser onto an 852nm cesium line, based off new intracavity etalon architecture. Acousto-optic modulators finely tune the laser frequency and power, while servo motors adjust the cavity dimensions (shown in fig. 1). After the desired parameters are discovered, the system locks the motors in order to support the given frequency. The system also includes a periodic check that confirms the validity of the servo loop, relocking the cavity if necessary.

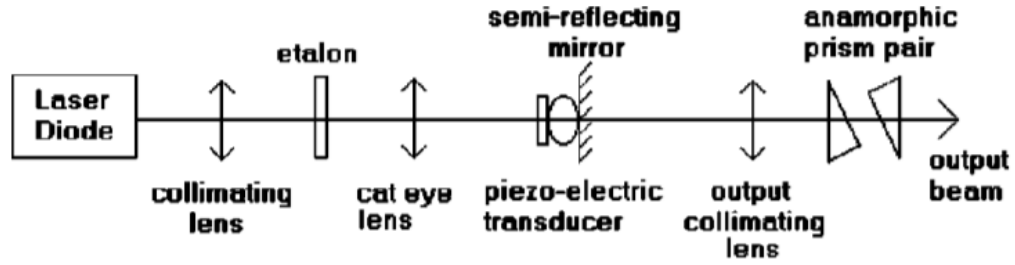


Figure 1: Optical schematic of F. Allard et al.'s open laser cavity

Automatic laser-to-optical-fiber coupling system based on monitoring of Raman scattering signal by Kyoung Duck-Park et al.

Rather than optimizing a lasers output, this system optimizes the coupling between a laser and an optical fiber. It accomplishes this by measuring Raman scattering in both the fiber core and cladding. The scattering is ideally symmetrical around the core, the system can then use this knowledge with the measured data to perfectly align the fiber core centroid with the lasers focal point. Aligning these two should yield the optimal coupling of the laser and fiber. Using precise measurements and motors, the system can adjust the fiber placement rapidly and with extreme accuracy, achieving optimal coupling within a few seconds.

A simple method for automatic cavity alignment of a solid-state laser by L. Dong et al.

Designed to correct intra-cavity misalignment, this system can adjust either input or output couplers in order to maximize the lasers power, even with the misalignment. This is accomplished by first determining the location of the beam spot on the rear mirror, and then replacing either coupler with a tip-tilt mirror, which then automatically can compensate for the misalignment, as seen in Fig. 2. Besides this coupler replacement, the system does not require any external alignment beams or cavity modifications.

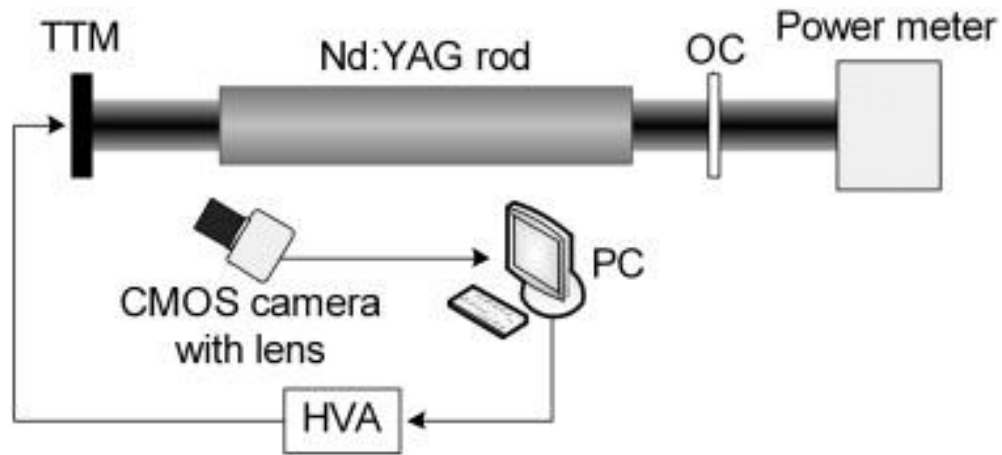


Figure 2: Diagram of L. Dong et al.'s setup

Project Comparison with Existing Technology

The most salient difference between our project and the ones presented above is the applicability of our design. The papers by Duck-Park and Allard are both on the automatic optimization of specific laser systems, while only the Allard paper is written on optimization of a cavity (Duck-Park's work is on optimization of laser-fiber coupling). While the Dong paper can technically be used on any laser, it is more so based off correcting a misaligned cavity by replacing faulty elements, rather than optimizing the output of a valid cavity. In comparison to the first two papers presented above, our project is unique in its broad application to potentially hundreds of different laser systems. We also strive to create our system with significantly less financial outlay than any of the projects above as they all employed exorbitantly priced technical equipment. While this may lead to their projects optimizing the given systems faster, we believe that the relatively low price and broad application of our project makes it a valid and unique contribution to this technological field of automatic laser optimization.

Power Meters

Product	Wavelength Range (nm)	Power Range	Maximum Active Diameter	Price (\$)
Coherent OP-2 VIS Semiconductor Power Sensor	400-1100	10nW-30mW	7.9mm	700.00
Edmund Optics Deluxe Power Meter	210-1080	<11mW	38.1mm	815.00
MKS Ophir PD300 (Fig. 3)	350-1000	500pW - 300mW	10mm	789.00
Swana Pocket Laser Power Meter	400-1100	40uW-40mW	13mm	273.00

Table 4: Laser Power Meter Existing Technologies



Figure 3: Image of MKS Ophir PD300

Beam Profilers

Product	Wavelength Range (nm)	Saturation Threshold	Active Area Size (mm)	Price (\$)
---------	-----------------------	----------------------	-----------------------	------------

Newport LBP2-HR-IR3 Beam Profiler	1440 -1605	50W/cm ²	7.1 x 5.3	6,886.00
Coherent LaserCam HR II - 1/2" USB Camera System	400 - 1100	70W/cm ²	5.9 x 4.8	3,995.00
Edmund Optics Beam Profiler	350 - 1150	10W/cm ²	11.3 x 6.0	2,895.00
MKS Ophir L11059 Beam Profiling Camera	190 - 1100	16W/cm ²	35 x 24	Not Specified

Table 5: Laser Beam Profile Existing Technologies



Figure 4: Image of Coherent LaserCam HR II - 1/2" USB Camera

When comparing the specifications of our beam profiler with the above options, there are a few major contrasts. Most obvious is the massive price difference; we anticipate constructing our profiler for under 400 dollars, less than a sixth of the cost of the cheapest Edmund profiler. However, this relative cost increase with the above profilers does lend itself to some significant performance enhancements. Three out of the four selected profilers feature working wavelength ranges larger than our specified range, with two having both lower working minimum and maximum wavelengths. One profiler quality that varies significantly between all the different models is the imaging area size, as the MKS

Ophir and Coherent LaserCam system (shown in Fig. 4) differ in imaging area by over 800 squared millimeters. While our design specification of a 10-millimeter resolvable spot size maximum would imply that our profiler sensor should have dimensions of at least 10 by 10 millimeters, there are some techniques we can employ to meet this criterion with a smaller sensor. Preliminary research into profiler cameras show most options feature active areas with dimensions similar to the Newport profiler. Unlike all the above profilers, our groups design has a variable saturation threshold predicated on the value of a neutral density filter placed in front of the sensor. Although our designed beam profiler may feature a smaller working wavelength range, it makes up for this deficiency with its low cost, functionally variable saturation threshold, and acceptable active area size.

Technology Investigations

Computer Engineering Technology Investigation

The goal this project is aiming to achieve is, to me, most obviously solved by using machine learning. There are four main types of machine learning: supervised learning, unsupervised learning, semi-supervised learning, and reinforcement learning.

Supervised Learning Background

In supervised learning a model is provided training data to learn from. This data consists of features and labeled target data. The features and labels are then fed into an algorithm to train the model. Through the training process the relationship between the features and labels are determined by the model. Once the model is trained it can take unlabeled features and use the relationships it learned during training to predict the label of the new unlabeled features.

The models created by supervised learning algorithms can be expressed as mathematical functions and fall into one of two categories as seen in figure 1. The first category is regression. The goal of regression is to predict a continuous value based on the features provided. The second category is classification. Classification is used to predict a discrete value for each input.

Supervised Learning Possible Application

In order to use any supervised learning algorithm, we would need to have a set of labeled training data. There are two parts which make up this data, the features, and the target.

- The orientation of the screws which control the mirror's tilt.
- The rotation of the mirror.
The orientation of the screws could be measured in a few different ways.
- The degrees that the screw has been rotated from some predetermined point, for example being completely screwed in.
- The distance from the mirror to the back plate where the screw sits.

The rotation of the mirror could be measured as degrees from perpendicular to the laser with perfectly perpendicular being zero, any angle clockwise being positive, and any angle counterclockwise being negative.

The target value can also be represented in a few different ways.

- It can be represented categorically as either lasing or not lasing. For data collection this would be the simplest approach since we wouldn't need precise measurements from the optical power meter because the contrast of lasing vs not lasing is extremely evident.

- The other option for the target value would be to record the actual value from the optical power meter as opposed to just whether it is lasing or not lasing. The main problem with this approach would be if the optical power meter is not able to precisely determine the value of the laser when it is not lasing.

Both representations of this problem have advantages and disadvantages.

Categorical target advantages:

- Using a categorical target value will be much easier for data collection. Because there are only two categories for the laser, lasing or not lasing, it will be easier to collect a large number of data points for each category.
- Using a categorical target data collection could technically be done without even needing the optical power meter since you can see when the laser begins lasing.

Categorical target disadvantages:

- If we use a categorical target we would have needed some sort of secondary method in order to implement optimization of the power output of the laser.

Continuous target advantages:

- Using a continuous target would make it easier to optimize the output of the laser. Even once the laser begins lasing we should be able to tell when the power is increased further toward the maximum by using the actual value from the optical power meter as opposed to just whether or not lasing is occurring.

Continuous target disadvantages:

- The optical power meter will need to be very precise in order to detect small changes before the laser begins lasing.

Supervised learning models for classification:

- Logistic regression

- K-nearest neighbors
- Naive bayes

Supervised learning models for regression:

- Linear regression
- Lasso regression
- Random forest regression

Unsupervised Learning Background

Unsupervised learning models are used to find patterns in data, and then group data points based on similarity in the patterns it finds. As a result of this pattern recognition approach unsupervised learning can really only be used for classification, not regression. Unlike supervised learning, unsupervised learning uses unlabeled data to train a model. This makes unsupervised learning most useful for problems where it is difficult or impossible for a human to create and assign categories for the data points.

Unsupervised Learning Possible Application

Because of unsupervised learning's main appeal as a tool for pattern detection of unlabeled data points I don't think there is any way to apply this form of machine learning to our problem. No matter which route we decide to go for data collection, either reading the exact value from the optical power meter or just whether or not the laser is lasing, there was always a label associated with the data collected. And while we could technically omit the label I don't see any reason to do that. The option that reads the exact value from the power meter could never work as a problem for unsupervised learning because unsupervised learning can only be used for classification, not regression. And even when our problem is viewed from the perspective of a classification problem I still don't think it would work very well as an unsupervised learning problem. Unsupervised learning works best when there are no obvious categories that humans could apply to the data, but with our data it could be easily observed what state the laser was in.

Reinforcement Learning Background

Reinforcement learning is best applied to problems that focus around behavior and decision making within a specific environment. Reinforcement learning is very different from both supervised learning and unsupervised learning. While the previous two types of machine learning require a large amount of training data to create their models, reinforcement learning does not. In reinforcement learning the algorithm, called the agent, uses information obtained from the environment. The environment includes any component that is interfacing with the agent. The agent interacts with the environment by reading the state of the environment, and performing actions on the environment. The

information received by the agent from the environment is known as the reward. The reward is a measure of how successful the agent's actions are.

The feedback loop of reinforcement learning shown in Figure 5 is as follows:

1. The agent reads the state of the environment.
2. The agent decides what action to perform and performs said action.
3. The environment gives the agent a reward based on that action.
4. The agent stores information about what state and action lead to that reward.

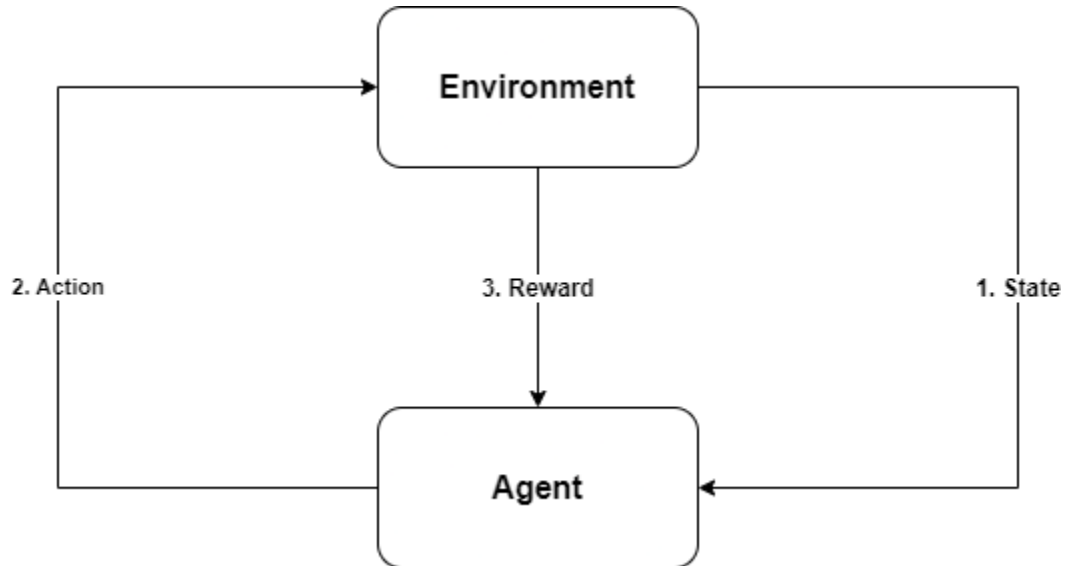


Figure 5: Reinforcement learning diagram

Reinforcement Learning Possible Application:

In order to apply reinforcement learning to our problem, we need to identify what aspects of our problem correspond to components of the general reinforcement model shown in Figure 6.

In our case the environment would include:

- Optical power meter
- Electrical motors

The agent would be whichever algorithm we decide to go with (just to name a few):

- Q-Learning
- Temporal Difference
- Evolving Neural Networks

The actions that can be performed are:

- Rotate the top screw clockwise
- Rotate the top screw counterclockwise

- Rotate the bottom screw clockwise
- Rotate the bottom screw counterclockwise
- Scan the mirror back and forth

The state would just be the current orientation of the screws and mirror.

Initial Reward Concepts:

- The agent has a set amount of time to interact with the environment and tries to attain the highest possible output from the optical power meter.
- The agent has a goal power that it needs to reach, and the faster it reaches that goal power the higher reward it receives.

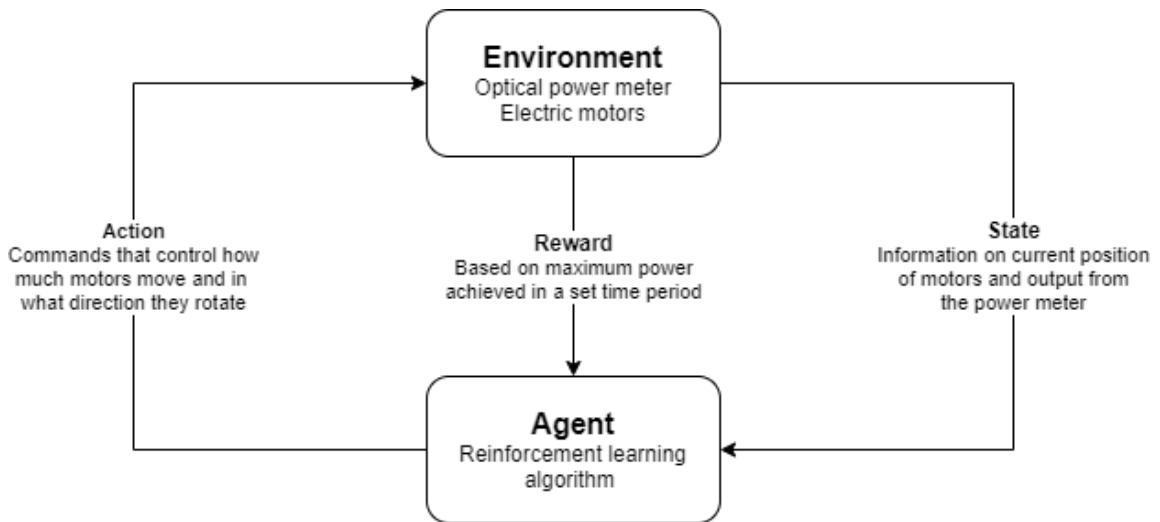


Figure 6: Reinforcement learning diagram

Threshold Search Solution

Our original plan to achieve alignment of the laser was to utilize a Q-Learning based reinforcement learning algorithm to both align the laser and reach maximum power. This initial approach had a few shortcomings which we hadn't foreseen in our initial planning stages. Any differences in the set-up of the physical components of the system would result in any data from previous alignments being useless. As a result, we adapted our approach to utilize a threshold search algorithm. The threshold search algorithm works by scanning vertically with the mirror while sweeping back and forth horizontally until a flash of lasing is detected on the power meter. Once the vertical orientation is located the system begins adjusting the mirror horizontally in small increments until a large jump in intensity is detected by the power meter. This approach proved very effective in aligning the laser as the range of positions that allowed for alignment were large in comparison to the movements we were able to make using the continuous motors. Our approach for finding the max power of the laser was to first run the alignment algorithm for initial lasing.

From that point we would scan vertically until the laser went from lasing to not lasing and find the point which resulted in the highest power. We would then return to that orientation and then scan horizontally once again looking for the max power until the laser reached the boarder of the lasing threshold and returning once again to the max power orientation. This approach did result in finding a higher power than the initial alignment, but since the continuous motors moved at different speeds when moving forward and backward it was inconsistent when trying to return to the exact location of max power.

Algorithm	Pros	Cons
Logistic regression	Easy to implement, no assumptions about distributions, very fast algorithm	Constructs linear boundaries, assumes linearity between dependent and independent variables
K-nearest neighbors	Easy to implement, no training step, can be used for classification and regression	Slow algorithm, sensitive to outliers, bad for imbalanced data
Naive bayes	Resilient to noise, doesn't over fit, works well on large data sets	Can have large bias, can't be used for regression

Linear regression	Easy to implement, best algorithm for linear relationships	Always assumes linear relationship, very sensitive to outliers
Lasso regression	Can select features, avoids over fitting	The selected features are biased
Random forest regression	Automatically handles missing values, only uses 2/3 of data allowing for testing to be done on remaining 1/3	Can be difficult to interpret what the model is doing, has problems with over fitting
Q-Learning	Doesn't need input data, low variance	Biased, struggles with too many actions
Temporal Difference	Doesn't need input data, faster than q learning	May converge to the wrong solution
Evolving Neural Networks	Doesn't need input data, resilient to ruts	Slow to train, very complex

Table 6: Pros and cons of different machine learning algorithms

Electrical/Mechanical Components Investigation

This section will go over the individual components that are to be used in the device covering the electrical motors, motor drivers, gears, power supply, and dc converters. The topics will include the purpose of each component, the costs and benefits of choosing one option over the alternative and what factors played an important role in the decision process.

Electrical Motors

Motor Function

For the project there will be 3 degrees of freedom that will require three individual motors. Two of the motors will be dedicated to adjusting the knobs that control the angle

of the mirror. The stand that holds the mirror being adjusted for this project adjusts so that neither knob on the stand rotates the mirror on the x or y axis but rather the top-right knob causes the mirror to angle up or to the right when tightened while the bottom-left knob controls the change of angle of the mirror to the left or down when tightened. The final motor will be responsible for the rotation of the stand holding mirror on the horizontal axis. This is depicted in Fig. 7. As such for the document the motor controlling the horizontal rotation of the mirror's stand will be designated as the horizontal motor, the motor that controls the top-right knob's rotation will be designated as the right knob motor, and the motor responsible for the rotation of the bottom-left knob will be designated as the left knob motor.

At the start of the calibration to find the lasing state, it is planned to have the knobs initially be at the tightest state then loosen the knobs as time goes on. The sequence of movement for the project is to first have the horizontal motor rotate in a small arc so that at some point in the rotation the stand is perpendicular to the light being emitted. If the power meter returns no value, the next stage in the sequence is to have the right knob motor or left knob motor to loosen their knob in order to adjust the mirror. The horizontal motor will then rotate in the opposite direction, so the stand is once again perpendicular to the light source to check the angle of the mirror. The process is repeated till the correct angle of the mirror is found and the lasing state occurs. At this point the horizontal motor will maintain the angle of the stand while the right knob motor and left knob motor make small increments of change in the angle of the mirror till the max lasing state is found.

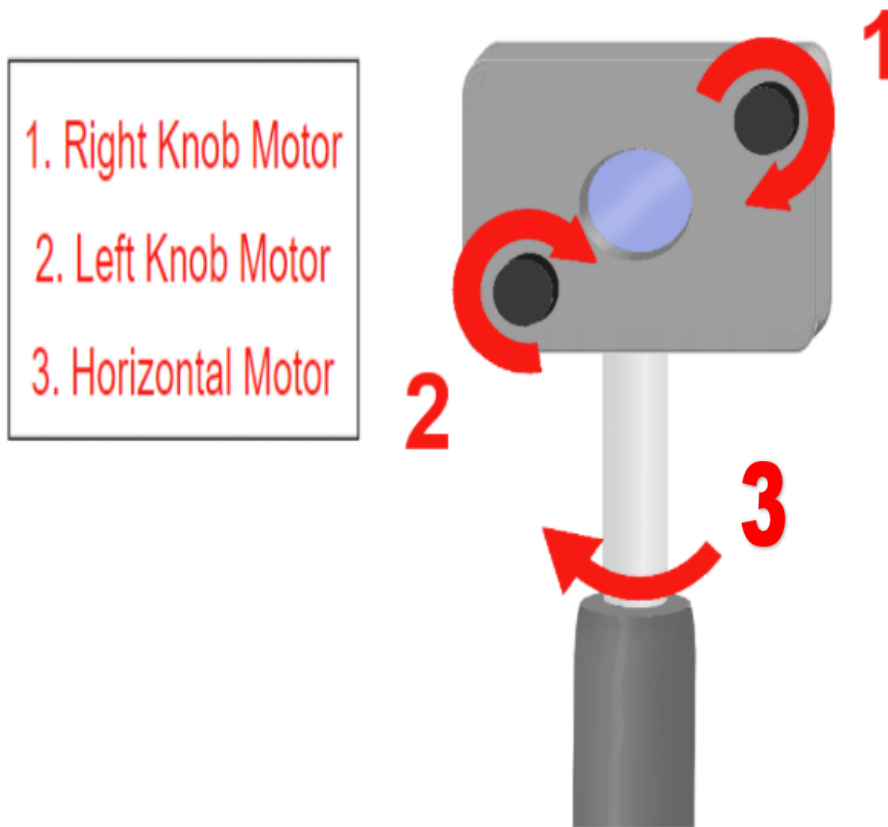


Figure 7: Diagram of mirror mount knob turning

Motor Goals

Horizontal Motor

- Be able to provide enough torque to rotate ~3lbs of equipment with the assistance of gears (small to large ratio)
- Be able to make small and precise movements with the assistance of gears
- Have the motor turn the stand in less than a 30 degree arc from being perpendicular from the laser
- Be able to have some input that allows the computer to know what angle the motor has turned to.

Right/Left Knob Motors

- Be lightweight and small enough to be mounted on the stand and rotated by the horizontal motor
- Provide enough torque to rotate the knobs
- Be able to make small and precise movements with the assistance of gears (small:large ratio)
- Have inputs that allow the microcontroller determine the speed and direction of the controller

Motor Types

DC Standard Electric Motor

This is the simplest of the three listed motors. This motor works by having a rotor with an electric current between two magnets that make the rotor rotate. Brushes connect the rotor to the power source while rotating and are used so that the current continuously flips so that the magnetic poles of the rotor will flip as well making the rotor rotate. These motors will have only two inputs that use the magnitude and sign of the voltage to determine the speed and directions of the motor. Of the three motor types, standard DC motors have great rpm's while offering decent torque at low speeds additionally DC motors are off the cheapest in terms of cost to performance. However, of the three types, the standard DC electric motor is the least capable of making small precise movements. Without any outside sensors to measure its rotation, there is no way for the microcontroller to know the number of rotations or the angle of the electric motor. Lastly, the DC motor cannot perform correctly being connected directly to the microcontroller, instead the motor must be connected to a motor driver to work. A standard L298N motor driver can support up to two DC motors.

Stepper Electric Motor

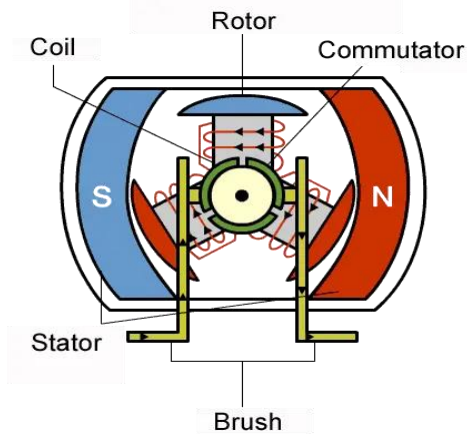


Figure 8: DC Motor Interior Diagram

A stepper motor (shown in Fig. 9) can be seen as the most complex of the three motors requiring four input wires in order to operate and unlike the standard DC motor, has the ability to keep track of how far the motor has turned without the motor having to give feedback. This is down through the fact that the motor will turn at small increments with varying angles such as 1.8 degrees on demand. How this is done is by having one gear acting as the rotor inside a stator that will have varying amounts of wired coils having gear teeth on top facing the rotor. The coils are then turned on and off by the four wires in a synchronous pattern so that the teeth on the rotor will be attracted to and turn to the next teeth on the coil. This process requires no brushes in order for the rotor to rotate. Stepper motors offer the best torque for the rated voltage generally being more efficient electric motor drivers. The main use of stepper motors is for machines that need to make controlled and precise movements that can be tracked. However, there are several disadvantages with the first being that stepper motors struggle to have high rpms compared to the other types of motors, additionally like the DC motor, the stepper motor will require a L298N motor driver dedicated to one stepper motor before being connected to a microcontroller.

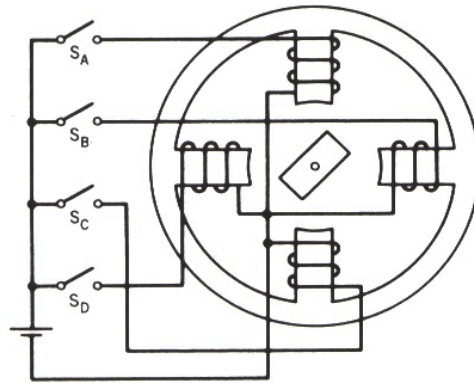


Figure 9: Step Motor Wire Diagram

Servo Motor

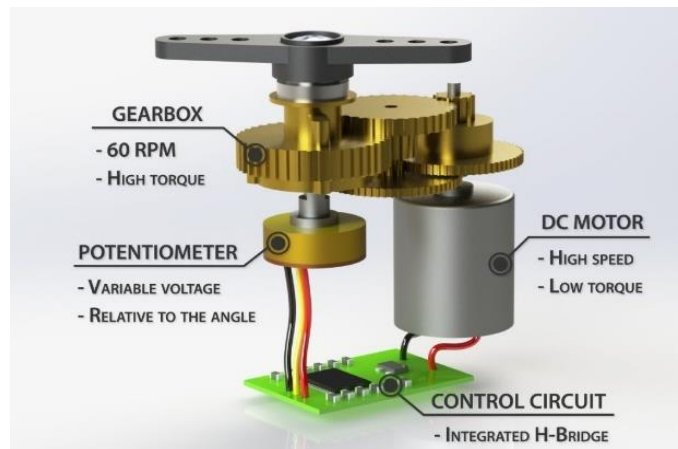


Figure 10: Servo Motor Interior Diagram

A servo motor (shown in Fig. 10) is, in essence, a DC motor that usually offers high speeds and low torque. Moreover, servo motors come with some additions: A gearbox which increases torque, a potentiometer that helps determine the angle of the shaft, and the control circuit that helps determine the motor's direction of rotation. The overall quality of the gearbox can vary from cheap plastic to metal depending on the price, desired weight, and the torque that is expected for the motor to provide. Compared to a standard DC motor, a servo motor will have a greater displacement volume due to the added parts and will also need another wire, bringing the total wire count to three wires. Of the three wires two of the wires are used for the power supply and the third being used as the input for the motor. As a result, unlike the DC motor and the stepper motor, a servo motor will not need a motor driver before being connected to the microcontroller. Servo motors can be divided into two subcategories, positional rotation servos and continuous rotation servos. Each has unique traits, which are outlined below.

Positional Rotation Servo

This type of servo motor is used for when the motor needs to turn to a specific position. In order for the motor to know at what angle the shaft needs to be turned, the wire that is used as an input will send a signal to the motor where the length of a single pulse will determine the angle the shaft will be facing. Unlike any of the other motors a positional rotation servo is only capable of turning between the angles of 0 degrees to 180 degrees.

Continuous Rotation Servo

This type of servo acts very similar to a standard DC motor with a motor driver in which both the direction and the rpm of the motor can be controlled by the microcontroller. This is done by the single input wire connected to the motor in which when the signal is being sent, however instead of making the motor turn to the angle, where the motor reads 0 degrees the motor rotates counterclockwise at full speed while when the motor reads 180 degrees the motor will rotate clockwise at full speed. In the middle where the motor would read 90 degrees the motor instead stops.

Motor Driver

For the standard 5V DC electric motor there are two wires used to power the motor, for stepper motors there are four wires. In order for the microcontroller to be able to control the motor and for the motor to get the correct voltage to power it a motor driver is needed. The most common type of motor driver for use by a microcontroller is the L298N and L293D IC motor driver. The L298N is its own PCB board that is connected through jumper wires while the L293D IC is more akin to an IC chip that can be incorporated into a PCB with the microcontroller. For both motor drivers there are 4 outputs that can connect to either two standard DC electric motors or one stepper motor. Additionally, there are eight separate inputs, four inputs are designated as IN1, IN2, IN3 and IN4. The inputs are connected to the microcontroller to allow the microcontroller to control the direction of the motor. Two inputs called ENA and ENB, these inputs are connected to the microcontroller to control the speed of the motors. Lastly there are the VCC1 and VCC2 inputs, these are

connected to the power supply that will power the motors. While motor drivers are a necessity if our group wants to include a regular electric motor or a step motor, motor drivers still have the downside of needing 4 wires connected to the microcontroller to work properly. This will put a major constraint on our usage of the microcontroller pins with the number of pins needed to control the motors ranging from six pins to a much larger twelve pins. For every pin that is allocated to the motors is on less pin that can be used for the other components such as the light diode or the user input buttons.

Gears

For this project, the range of angles for lasing can be incredibly small requiring the motors to make very small increments of movement, however the quality and strength of the motors may hinder them from making the needed precision and accuracy to make correct movements at such a low rpm. Additionally, for the stand in particular, the increased torque required to rotate the stand will have an overall decrease in the performance of the electric motor for this project. To mitigate this problem the use of gears will be used to increase the torque and precision of the electric motors. This is done through a low:high gear ratio as seen in figure 6, by having a low:high gear ratio the torque of the gear not attached to the motor will increase, while also lowering the amount of movement caused by the motor. Other uses for the gears include help keeping the horizontal angle once it is set and will be placed over the knobs to allow the motors to turn them. The focus for the gears assigned to the right and left knob motors is to maximize the accuracy and precision of the movements. For the gears involved with the horizontal, not only is accuracy and precision key but also torque as compared to the knobs the horizontal needs a greater rotational force to turn about 3 lbs. while keeping accuracy. Calculations for finding the torque and output speed will be found using the equations:

$$\textit{Wheel Torque} = \textit{Motor Torque} \times \frac{\textit{Output Size}}{\textit{Input Size}}$$

$$\textit{Output Speed} = \textit{Input Speed} \times \frac{\textit{Input Size}}{\textit{Output Size}}$$

Metal Gears vs 3D-Printed Gears

There are two types of gears that can be chosen for use in this project. 3D printed gears are gears made by uploading a schematic to a 3D printer, which then ‘prints’ the gear using a plastic polyester. Metal gears are already fabricated in industrial settings and can be found at stores or online and can be made with a variety of different metals.

3D printed gears	
Pros	<p>Customization</p> <ul style="list-style-type: none"> • Able to make custom gears with unique dimensions to allow the gears to meet specific sizes and functions <p>Modifiability</p> <ul style="list-style-type: none"> • Plastic filament is easy to drill/shave into for modification, this is useful for allowing gears to fit onto the motors and nuts to hold in place. <p>Accessibility</p> <ul style="list-style-type: none"> • 3D printers are available on UCF campuses allowing us to print a specific gear that is needed instead of having to buy the gear at a store or online and wait for shipping
Cons	<p>Durability</p> <ul style="list-style-type: none"> • Plastic gears are weaker than the metal counter parts, as a result in order for the gear to maintain structural integrity, it will need to be thicker and wider in cases where more torque is involved

Metal Gears	
Pros	<p>Durability</p> <ul style="list-style-type: none"> • Metal gears are much stronger than 3D printed gears, as a result the probability of the gears breaking and needing to be replaced are much lower compared to 3D printed parts. <p>No work needed to model</p> <ul style="list-style-type: none"> • Metal gears are premade and do not need any effort of the buyer in the process of being manufactured.
Cons	<p>Modifiability</p> <ul style="list-style-type: none"> • Metal compared to plastic filament is much more difficult to drill into and modify, requiring more specialized tools that can drill through metal. • Tools that may be needed to modify gears are expensive for the budget of this project, making us reliant on the tools offered on UCF campuses. <p>Availability</p> <ul style="list-style-type: none"> • Since our group are not the ones producing the gears, we are reliant on if the desired model with the correct size and teeth count is available

Table 7: 3D-Printed and Metal Gears comparison

Power Supply/DC-DC Converter

For this project, the microcontroller/computer that will be used is the Raspberry Pi computer, all available models are powered through a usb-c port with the desired input voltage of 5 Volts and 3 Amps of current. Every model of Raspberry Pi 3 and Raspberry Pi 4 offer a minimum of 40 pins with 2 pins able to supply a voltage of 5 Volts and 2 other pins able to supply a voltage of 3.3 volts. Two motors that are acting as the left knob motor and right knob motor are expected to operate at 5 Volts making it possible for them to be connected to Raspberry Pi as a power supply, however it is strongly recommended to supply the motors with a separate source of power. Additionally, the horizontal motor is expected to be around 8-12 volts and will require a separate connection to a DC voltage converter. There are currently two different sources of electricity that can be used to supply the project with power, these sources are the use of a battery or the use of an outlet. Both sources will come with their own unique advantages and disadvantages which are outlined below:

Wall Plug Outlet	
Pros	<p>Constant/steady supply of power</p> <ul style="list-style-type: none"> ● Since the project is connected to the buildings electrical system, there is there more of a guarantee that the components of the project, specifically the motors will have a similar performance every time the device is calibrating excluding factors such as wear and tear Raspberry Pi compatible ● If the USB-C cable that powers the computer is connected to a wall charger that supports 5 Volts and 3 Amps, the outlets will work without needing a DC converter.
Cons	<p>Location Limitations</p> <ul style="list-style-type: none"> ● Using an outlet will require the project to be in proximity of an outlet or will need to use a long extension cord. ● Problem is partially negated by the fact that the laser will require an outlet guaranteeing that one will always be nearby ● Will require at least two sources of power ● Based on research of existing products, if a USB-C charger is used as the outlet source, another power supply will be required as all rated wall chargers are single ports, and the raspberry pi computer will require a cable dedicated to only it.

Figure 8: Outlet comparison

Battery Power	
Pros	<p data-bbox="662 285 773 315">Mobility</p> <ul data-bbox="615 321 1398 529" style="list-style-type: none"> <li data-bbox="615 321 1398 422">● Does not require an outside source of power, allowing the user to adjust the location of the device without much issue. <li data-bbox="615 428 873 457">● Surge Protection <li data-bbox="615 464 1370 529">● Users will not have to worry of power surges that could potentially damage the circuit.
Cons	<p data-bbox="662 541 935 571">Varying Performance</p> <ul data-bbox="615 577 1390 716" style="list-style-type: none"> <li data-bbox="615 577 1390 716">● Since the power is battery supplied as time goes on the performance of the device will gradually decrease until it stops working unless the batteries are periodically recharged/replaced <p data-bbox="662 722 737 751">Space</p> <ul data-bbox="615 758 1409 1010" style="list-style-type: none"> <li data-bbox="615 758 1409 1010">● Batteries if built into the device will take up plenty of space. For this project the power source will need to supply the microcontroller, the lcd display, three electric motors, a light sensor, a camera, etc. As a result the battery will need to be relatively large compared to standard AA batteries in order for the voltage to stay consistent while it is functioning

Table 9: Battery comparison

Optical Engineering Technology Investigation

The optical design portion of this project can be thought of as comprising of two major subsystems: the optical power meter and the beam profiler. We have the option to design the optical portion via two methodologies. Either the two subsystems are separated, with one being oriented along the optical axis and another perpendicular to the optical axis, or both subsystems are in line with the optical axis.

Split Design

In this design case, the laser beam would first pass through a beam splitter with the normal vector of the splitting interface oriented 45° with respect to the optical axis. This would cause a certain percentage of the power of the beam to be deflected in a direction perpendicular to the optical axis with the remaining percentage continuing parallel with the optical axis.

A major benefit of this split design would be superior spatial maneuverability it provides. Because the two subsystems would entirely spatially separate on orthogonal axes, there would be little to no chance of interference between the two. However, the lower power transmitted into each axis from the splitter could prove troublesome within the

systems. For the power meter, this would obviously impact the reading that the meter generates, as less light is incident on the photodiode. However, this could be accounted for by multiplying the meter reading by the reciprocal of whatever ratio of beam power is sent to its axis. This would act as a computational buffer, compensating for the lost power. Either way, the main purpose of the power meter is to monitor relative power for input into the feedback loop. Ultimately, it would only matter that the meter reads a consistent fraction of the power and not necessarily the full beam power.

In reference to the beam profiler, insufficient light could restrict the accuracy or function of the subsystem. The pixel sensors within the profiler are likely less sensitive than the photodiode, and thus would be more prone to fail in registering low levels of incident light. If there is no information captured by the pixels, then none of the relevant computations done by the profiler could be completed. This issue wouldn't have an easy fix and could only be rectified by increasing the power contained within the profiler's optical axis.

As mentioned above, in the split design choice, a beam splitter would be necessary in order to send the beam down two paths. There are different parameters and configurations that one must consider when choosing a beam splitter.

Reflection/Transmission (R/T) Ratio

In most situations, the amount of light that is transmitted through the beam splitter and how much is reflected is equal, e.g., the incident beam power is split in half. However, in some cases, this is not desirable. It is then when one would wish to alter the R/T ratio. The R/T ratio determines how much light is transmitted through the splitter and how much is reflected. In our case, we decided on a 50/50 R/T ratio.

Polarizing and Non-polarizing

Polarizing beam splitters will separate the S-polarized and P-polarized light, causing one to be completely transmitted and the other to be completely reflected. Non-polarizing beam splitters, on the other hand, will maintain polarization when splitting the beam and will transmit/reflect both polarizations approximately equally. The transmission of non-polarizing beamsplitters is not necessarily exactly equal, as some deviations could occur, as seen for example in Fig. 11. The polarization of the incident beam is of no concern to us, and thus we can work with a non-polarizing splitter.

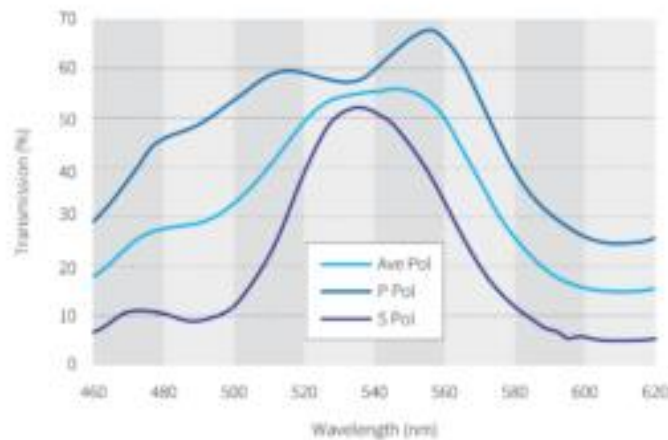


Figure 11: Graph depicting the wavelength dependence for a non-polarizing beam splitter

Narrow wavelength bandwidth or broadband

Clearly, we would desire a beam splitter that is broadband enough to fully capture the visible spectrum that we are interested in, 400nm-700nm. It is perfectly acceptable if the beam splitter's working spectrum goes beyond this range as extraneous wavelengths would not cause problems.

Plate beam splitters

- Plate beam splitters are lighter and smaller than cube beam splitters. This will be a factor to consider when trying to stay within our requirements specifications for weight and size.
- Plates are typically less expensive than cube splitters.
- The optical path lengths of the transmitted and reflected beams are not equal, but this is of no concern as a phase shift between the beam going to the power meter and to the mode profiler would not cause any problems.
- The transmitted beam of the plate splitter will experience a lateral displacement, which can be easily calculated and accounted for
- The angle of incidence of a plate splitter is typically 45° . This can cause extra alignment time when setting up optics from scratch, however the splitter would be permanently fixated within a housing in the system and thus this would not be a concern.

Cube beam splitters

- The angle of incidence is 0° .
- No beam displacement
- No optical path length difference
- More expensive
- Heavier

Order of Operation

The user will start with a laser cavity and detached output coupler that are not producing laser light. It will be necessary that the laser light, once produced, is captured by the power meter.

One option is to stick the power meter right after the output coupler, making them practically touching. This makes it so there is a higher chance the laser flash will be captured. However, this also increases the chance of things getting in the way of the mirror adjustment arms.

Power Meter

The laser power meter will be required to take in incident laser light and provide information on the optical power of said light. There are several ways to design a laser power meter with potential for the inclusion of different types of components. Below is discussed several mandatory components and some that would be necessary in conjunction with other components if chosen.

Sensors

[Photodiode sensors](#) generate a current proportional to the optical power incident on the face of the sensor. A photodiode sensor's power performance range is characterized by a noise floor, linear region, non-linear region, and saturation level. The semiconductor material in which the diode is made of will alter the characteristic power range. These sensors are also wavelength dependent, with different material compositions leading to differing wavelength ranges. The most common denominations of photoconductor sensor types are discussed below.

Germanium photodiodes have a spectral response within the infrared, typically around 900nm-1600nm, shown for example in fig. 12. This range misses our desired range of wavelengths as laid out in the requirement's specifications. These photodiodes saturate at a relatively high power, which would be desirable for the higher power ranges of laser light. However, these diodes exhibit a nonlinear behavior for lower powers, thus requiring the use of some sort of amplifier to access these powers.

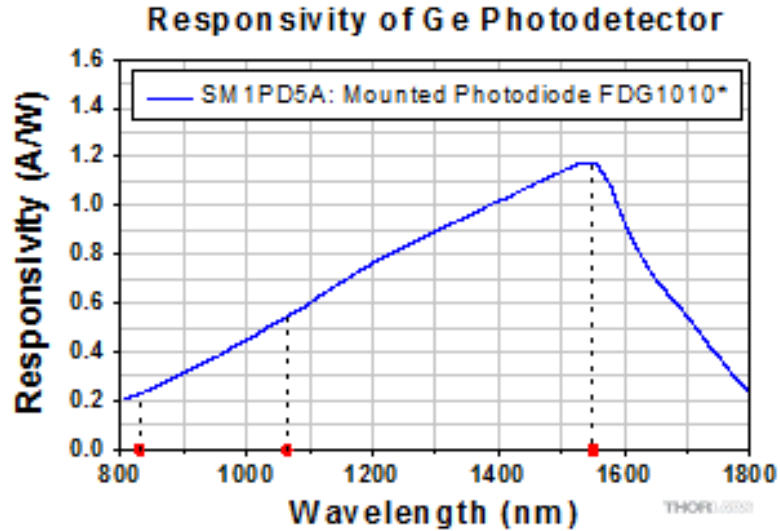


Figure 12: Example responsivity curve for a germanium photodiode

Indium gallium arsenide photodiodes are rather similar in their wavelength and power range performance, the former of which is displayed in fig. 13. However, indium gallium arsenide diodes do saturate at a relatively intermediate power level compared to germanium. This cuts off more of the upper regions of optical power. It should also be noted that these types of sensors are rather expensive, which is certainly not a desired trait.

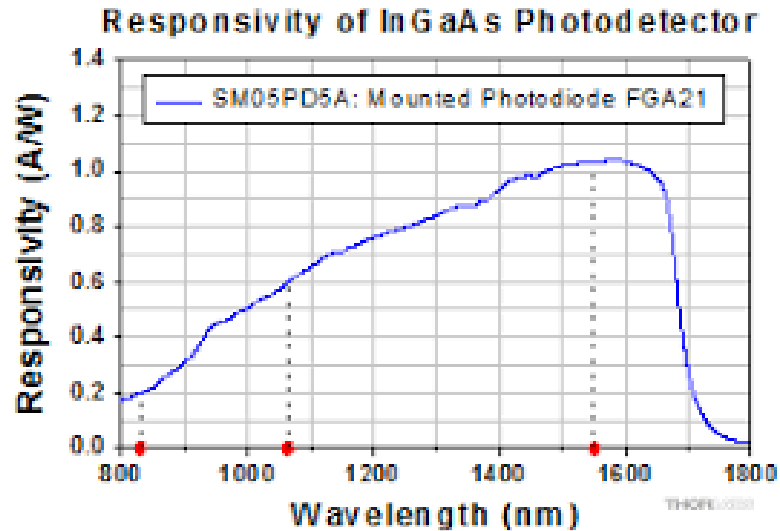


Figure 13: Example responsivity curve for an indium gallium arsenide photodiode

Silicon photodiodes are strongest in their detection capabilities in the visible to the beginnings of the infrared spectrums. In some cases, silicon diodes can even extend into the ultraviolet range. These are very attractive qualities for the wavelength response as this would help to ensure that even the lowest wavelengths of our desired range will be captured with a sufficient responsivity. Silicon photodiodes saturate at relatively low power,

typically on the order of 1mW. The noise floor for these diodes is also relatively low. It is also the case that these photodiodes are very linear within the region between the noise floor and saturation level, as shown for example in fig. 14. These power qualities would allow us to reach into the lower optical power ranges but leave us wanting in the upper levels. Additional elements such as an attenuator would need to be considered in this case.

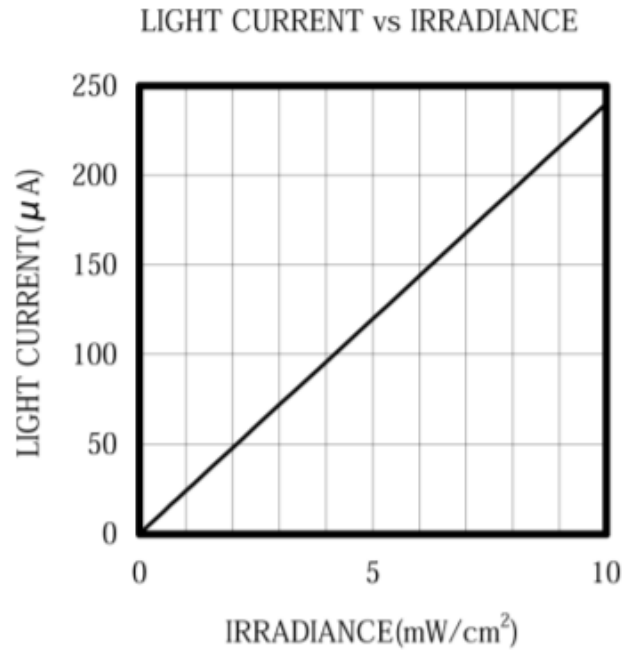


Figure 14: Example plot displaying the linearity of a Si photodiode

[Thermophile laser sensor](#) create a voltage from an incident laser power source heating the sensor. These sensors are characterized by a higher power performance when compared to photodiode sensors. There are two types of thermopile laser sensor types: volume and surface sensors.

Volume sensors are relatively thick and large, which allows for a high power to be detected without damaging the sensor. The size of these however contribute to a decrease in the response time. A characteristic plot showing the slow rise times of two types of thermopiles is displayed in fig. 15. These sensors are most applicable to short pulses of laser light. Therefore, while they may not be the best choice for the main goals of our project, they could potentially be leveraged for use in the stretch goals of high powered pulsed laser qualification.

Surface sensors are thin and small compared to volume sensors. This naturally means that the power range is lessened to lower powers so as to keep the sensor from being damaged. The smaller size however increases the response time. These sensors are useful for long pulse and continuous wave styles laser operation.

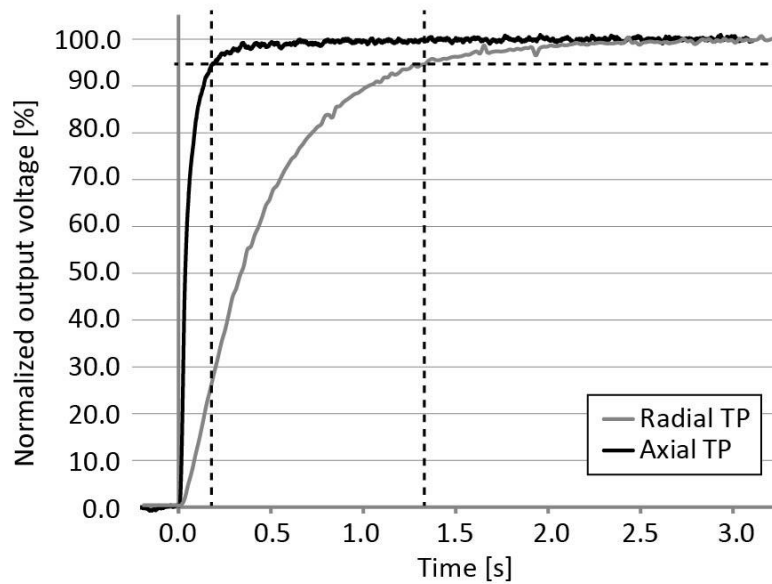


Figure 15: Plot showcasing the very slow response times of radial and axial thermopiles.

Pyroelectric detectors generate a voltage due to a change in thermal energy cause by the optical power incident on the sensor. These sensors are typically operated in the infrared region. They also exhibit a broader spectral response when compared to photodiode sensors. Since pyroelectric detectors work by sensing the *change* in optical power, they are truly only useful for detecting laser pulses. This is very clearly shown in fig. 16, in which the response of the detector rapidly falls in response to a step pulse. This would not work for the main objective of the project but should be considered when thinking of the stretch goal of expanding the systems operation to pulsed lasers.

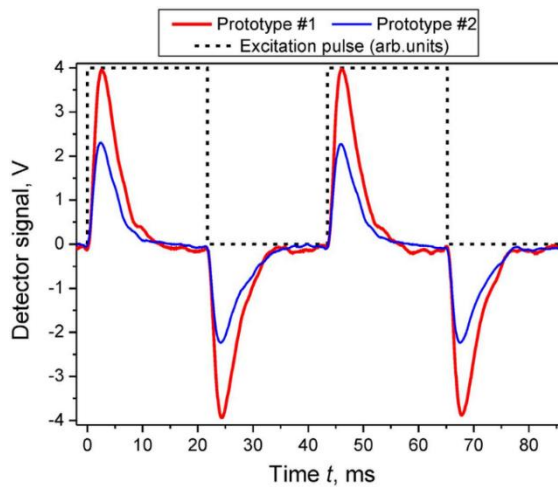


Figure 16: Plot showcasing the rise and subsequent rapid fall time for a pyroelectric sensor.

Attenuating Element

An attenuating element would be mandatory in the case in which we choose a sensor with a low saturation or linearity threshold, such as a photodiode (especially silicon photodiodes). Some potential technologies for such an attenuating element are described below.

Liquid crystal variable attenuators can be controlled electronically to allow for continuous and completely variable attenuation of light, which is an attractive quality. They are inexpensive for compact designs such as those used in fiber optics, but this would require coupling into a fiber which would greatly increase the complexity of our design. They are rather expensive for free space designs (thousands of dollars), thus making them a not viable option for our budget.

[Neutral density filters](#) provide a broad spectrum of attenuation. This being said, they do not necessarily attenuate all wavelengths equally. Attenuation is typically approximately equal for the target visible spectrum of 400nm-700nm, although minor errors are possible at the lower end of the spectrum. It must be noted that plain neutral density filters do not allow for continuous and variable control of attenuation. They allow only for discrete attenuation – either the filter is placed in the path of the beam and is attenuating to whichever amount it is rated for or it is not in the path and is not attenuating. Despite this, it is most likely that our power does not need variable control of attenuation and the relatively low cost of these filters makes them a compelling choice. (It must also be noted that it is possible to create very inexpensive neutral density filters from welder's glass; however, this glass is typically only rated to highly attenuate ultraviolet light, which is not within the range of our requirement's specifications.)

It may become apparent later in the design that it must be necessary to have variable attenuation. In this case, instead of opting for the rather expensive and cumbersome choices outlined at the beginning of this section, we could consider the following choices.

Linear polarizers could potentially be utilized in the same fashion as the filter wheel described above. If two linear polarizers are placed one after the other, then one of them can be turned through 0° - 90° to alter the attenuation of the incident beam. A negative of this choice is that it will be unclear what the polarization of the laser being operated will be. Thus, since linear polarizers are orientation specific, it would be much more complicated to implement these elements.

Neutral density filter wheels are essentially the variable upgrade of the neutral density filter. They consist of two circular filters that instead of having a uniform attenuation across the entire area of the filters, have density gradients that travel circumferentially around the filters. These two filters can then be turned with respect to each other to attain attenuation that varies from 0% to 100% of the max attenuation of both filters. A benefit of this choice is that it ignores polarization and allows the beam to propagate with unchanged polarization. This also implies that orientation of the filter with respect to the polarization of the beam is not important.

Focusing element(s)

It is possible that the sensor choice that most ideally suits our requirements specifications will have too small of a detectable area to meet our workable beam diameter requirement. It is in this case that we must use a focusing element(s) to bring all the laser light upon the active region of the sensor.

The first option is to use a singular focusing lens, such as a biconvex lens. This option is attractive as it uses only one element and would thus reduce cost. However, using only a single lens to bring a beam from diverging to converging is typically undesirable. Tasking a single lens to make this sign change alone would increase the likelihood of aberrations, which could impact the ability of the system to completely feed all the beam light onto the photodiode.

The second option is to use two focusing lenses, such as two plano-convex lenses. While this option would be potentially more expensive as two lenses would need to be purchased, splitting the focusing job across two lenses would be beneficial in reducing aberrations.

Material of the lens is also an important consideration when designing a lens system. The material is what defines the lens' refractive index, which is integral to the overall design to the power and properties of a lens. It is typical when designing complex lens systems that the power of the many lenses in the design are able to differ from each other, sometimes wildly, in order to attain the necessary system optical parameters. However, in our case, there will most likely only be one lens for each path of the optical system, at most two. This means that instead of attempting to optimize the lens design to a rather high degree, we can instead opt for a potentially less optimal but cheaper and easier to obtain material option.

One such material option is an industry standard of lens material, N-BK7. This is one of the most ubiquitous lens materials for its comfortable refractive index of around 1.5, very low chromatic dispersion, consistent transmission (as shown in fig. 17), low cost, and availability.

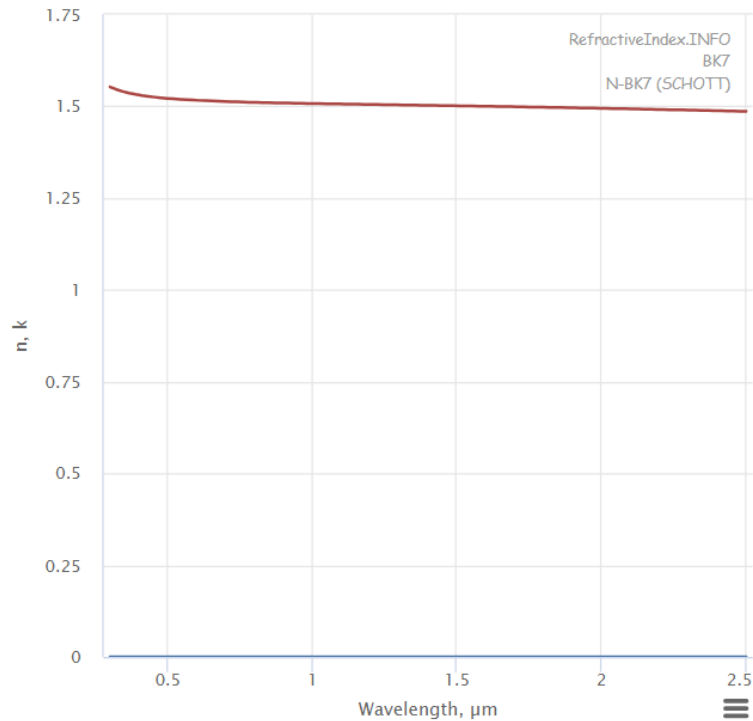


Figure 17: Plot showing the low variability in refractive index for N-BK7 glass

Mode Quality Measurements

This section of the report will investigate different elements of laser beams and determine which the group designed beam profiler will be able to identify and, ideally, adjust in accordance with user inputs.

Beam Width:

Beam width, or diameter, refers to the diameter of the laser intersecting the axis of propagation. As laser beams usually have Gaussian intensities, the edges of the beam are weakly defined. Due to this, there are a variety of different ways to characterize the beam width. The four main methods are briefly touched upon below.

Full Width at Half Maximum (FWHM): The simplest definition of beam width, this measurement is given by the two opposite points on the marginal distribution at which the beam's irradiance is equivalent to half of the maximum irradiance (-3 dB). This metric is also referred to as Half-Power Beam Width (HPBW). FWHM measurements are very common throughout optics and are not only used to define beam widths (shown in Fig. 18).

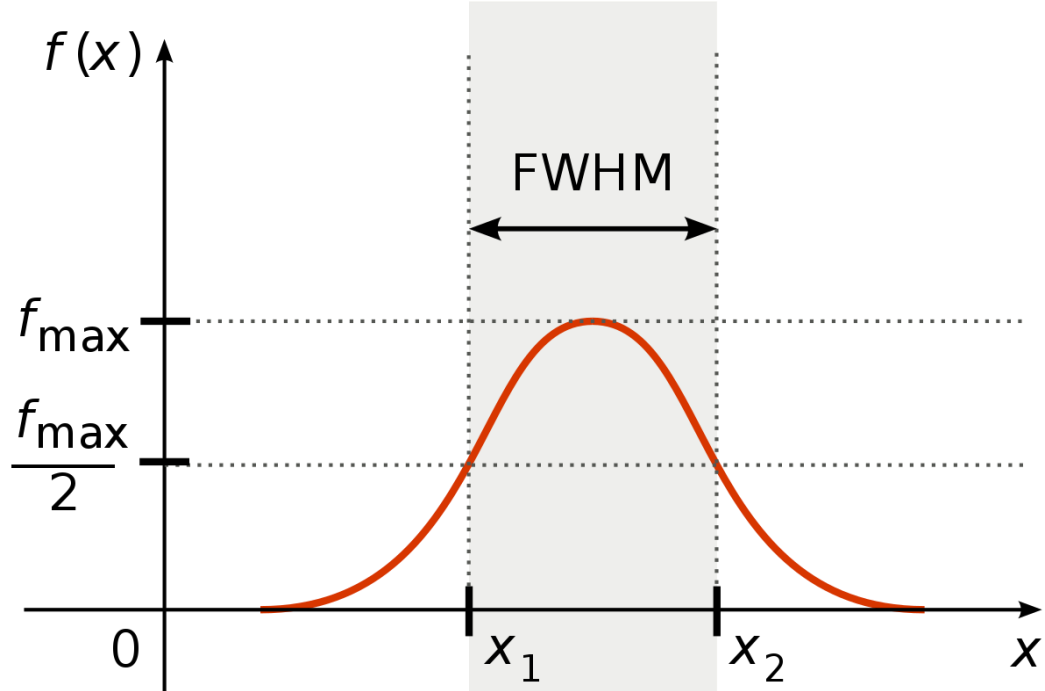


Figure 18: Full-Width Half Max range imposed over a Gaussian Distribution

$1/e^2$ Width: This width measurement is predicated on the distance between two points on the distribution which both have intensities equivalent to 13.5% ($1/e^2 = 0.135$) of the maximum power. It should be noted that The American National Standard Z136.1-2007 for Safe Use of Lasers (p. 6) defines the beam diameter as the distance between two points whose intensities are equivalent to $1/e$ of the maximum power. As both the $1/e^2$ width and the FWHM are based on the distance between points that give a specified ratio of the maximum power, they can be related by the following equation:

$$w_{1/e^2} = \frac{\sqrt{2} \times w_{FWHM}}{\sqrt{\ln(2)}} = 1.699 \times w_{FWHM}$$

Second Moment Width ($D4\sigma$): Significantly more complex than the widths above, the $D4\sigma$ width in a vertical or horizontal direction is four times the standard deviation of the beam in the respective direction. Algebraically, the $D4\sigma$ width in the x direction of an intensity profile $I(x,y)$ can be described below, where \bar{x} is the beam centroid in the x direction.

$$D4\sigma = 4\sigma = 4 \sqrt{\frac{\iint_{-\infty}^{\infty} I(x,y)(x - \bar{x})^2 dx dy}{\iint_{-\infty}^{\infty} I(x,y) dx dy}}$$

$$\bar{x} = \frac{\iint_{-\infty}^{\infty} I(x, y)x \, dx \, dy}{\iint_{-\infty}^{\infty} I(x, y) \, dx \, dy}$$

Unlike the FWHM and $1/e^2$ Width mentioned above, which are predicated off the intensity distribution along one axis, the Second Moment Width considers the overall beam profile. It should be noted that in a perfectly Gaussian beam with no noise in the measurements, the Second Moment Width and $1/e^2$ Width will be identical. If there is a significant presence of noise in the system, then the calculated $D4\sigma$ width will be greater than the real value. For this reason, $D4\sigma$ width should always be taken with background readings in order to subtract them from the data.

D86 Width: Given as the diameter of a circle located at the beam centroid containing 86% of the beam's peak power, the D86 width is not derived from the beam's marginal distribution. This measurement is often used in applications when power density is important. 86 is the chosen percentage as it correlates to a circular Gaussian beam profile integrated down to $1/e^2$ of its peak value.

Beam width is one of the most broadly useful and easily identifiable characteristics of a laser beam, so it is paramount that our profiler can measure it. Due to its ease of calculation, dependency on the intensity distribution, simple relationship to the $1/e^2$ width and wide acceptance in many different laser applications, our beam profiler will express beam diameter in terms of FWHM.

Although the second moment width is also a widely used standard, we did not use it due to its vulnerability to noise. As our system is meant to be applicable to multiple laser cavities and environments, the level of background noise could vary greatly and, in some scenarios, it could be difficult to avoid. In addition, its desired price, size, weight, and set up time are all opposed to the inclusion to many optical baffles, covers, and other instruments meant to reduce background light. With this being said, a toggle could be included in the software to change the beam width characterization method.

Beam Divergence:

While a laser may seem to travel in a perfect line, the rays which it consists of do gradually spread over time. The pattern of this spreading, or divergence, is described separately in two regions at different distances from the laser output. In the closer and shorter distance, known as the near-field, the beam divergence follows a parabolic curve. In the further and infinite range, called the far-field, the beam divergence is essentially linear. If this linearity is traced back to the beam's origin, an angle will be formed with the beam's axis of propagation. This angle is classified as half of the beam divergence. Laser divergence should be symmetric around an axis, so the full angle between the 'top' and 'bottom' of the linear beam in the far-field is the true beam divergence. There are two main methods of measuring the beam divergence. The first is a somewhat brute force method of measurement and involves taking the beam width at two separate points in the far field. The divergence can then be solved trigonometrically as follows, where Θ is the beam divergence angle, l is the distance between the two measurement locations, while D_f and D_i are the beam widths at further and closer distances, respectively.

$$\Theta = 2 \tan^{-1} \left(\frac{D_f - D_i}{2L} \right)$$

Although this method is perfectly valid, the need for two beam width measurements requires movement of the beam profiler. The second method forgoes this displacement, although it does require the addition of an auxiliary optic. If a focusing lens is placed in front of the profiler, the divergence angle can be found only using the focal length of the beam and a sole width measurement (shown in Fig. 19). (f is the focal length of the objective lens and D_m is the width)

$$\Theta = \frac{D_m}{f}$$

It should be noted that for this method, the sensor plane of the profiler (the location at which the beam waist is imaged) needs to be placed at the focal point of the objective lens. This technique operates on the principle that collimated light entering a lens should focus to a point at the lens's focal length; the divergence angle of spreading, non-collimated light can then be extrapolated based on the spot size which the light is focused down to, rather than an ideal point.

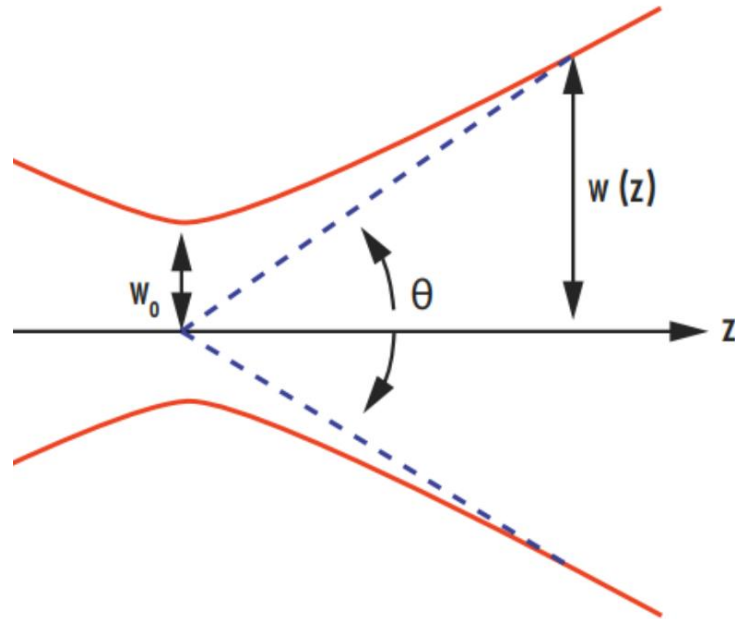


Figure 19: Showcasing the inflection point between near and far-fields with beam divergence. Adapted from [Edmund](#).

Beam Divergence is a very rudimentary element of a laser and is directly involved in the calculation of the overall beam quality. Due to this, it is necessary to include it as a feature of our profiler. Between the two measurement methods presented above, we pursued the latter, as even though the introduction of an objective lens increased the price of the system, the requirement for multiple beam width measurements in the first method introduces significant complexity to the system. This is because the measurement of widths would require either manual movement of the profiler itself, or the creation of a rail system which could laterally displace the profiler in the axis of the beam. In addition, it is very possible that an objective lens could be borrowed or repurposed from a facility in CREOL, removing or at least reducing any additional financial burdens. An objective lens with a small focal length should be used for this application, as we don't want to increase the physical distance within of the system significantly. Doing so could make the system infeasible for usage in smaller spaces, impeding the systems design criteria of being usable in many different beam cavities and lab settings.

Beam Waist:

An extension of beam diameter, beam waist is most readily identified as the beam radius of the laser at its smallest point, i.e., in the lasing cavity. As measuring equipment cannot be placed inside the cavity for this design, an analytical relationship can be defined to determine the waist, which is as follows.

$$\tan(\theta) = \lambda / (\pi \times w_0)$$

Where w_0 is the beam waist and θ is the *divergence half angle*. Rearranging to solve for the waist, we arrive at

$$w_0 = \lambda / [\tan(\theta) \times \pi]$$

Although not evident now, beam waist is a necessary component for determining beam quality (see below). While it is not a highly sought after nor important element of a beam, the fact that we gather all the requisite data to calculate beam waist makes its inclusion in our profiler a formality. It may not warrant immediate display on the system's GUI, but we should include the option to view it somewhere. However, the user could always calculate it themselves based on other elements displayed by the system if we find it difficult to fit all the information on the viewing screen.

Rayleigh Length:

Although far-field and near-field ranges were mentioned above, the designations between the two were not discussed. Enter, Rayleigh length. It is the distance from the laser output at which the near-field ends, and the far-field begins (shown in Fig. 20). As far-field is an imperfect approximation of laser divergence, the Rayleigh length itself is essentially a construct. It is defined as the point where the laser waist expands to a factor of $\sqrt{2}$ (1.414) of its original value. It can be calculated using the formula below:

$$Z_R = (\pi \times w_0^2) / \lambda$$

Similar to the beam waist, the Rayleigh length isn't a particularly significant factor of a beam. It can be important though if a user would like to deploy their beam to operate specifically in the near-field or far-field, so its exclusion would not be trivial. As discussed with the waist, even if we are unable to fit it on the viewing screen with the other beam profile information, it can be easily calculated by the user. As determining the waist was based off another formula, combining the two to solve for the Rayleigh length can be done like so:

$$Z_R = \{ \pi \times [\lambda / (\tan(\theta) \times \pi)^2] \} / \lambda$$

This is further simplified to

$$Z_R = \lambda / [\tan^2(\theta) \times \pi]$$

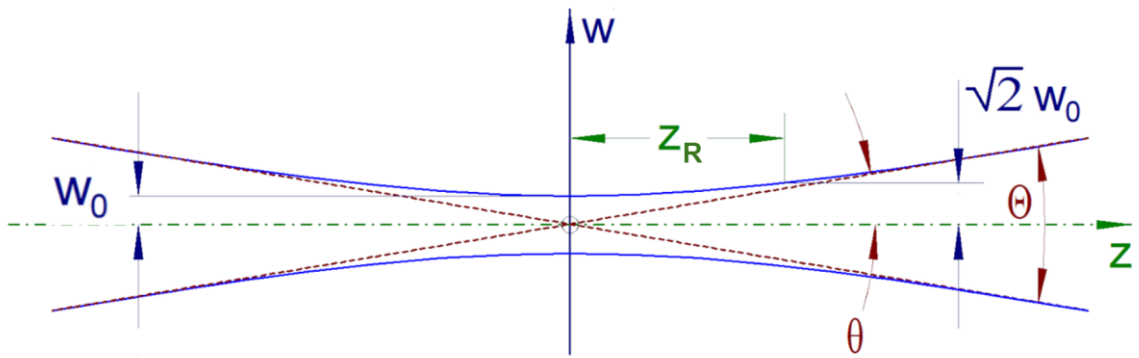


Figure 20: Pictorial representation of the relationships between the half waist (w_0), divergence (Θ), divergence half angle (θ) and rayleigh length (Z_R) . Adapted from [Bautsch](#)

Confocal Beam Parameter:

Fairly abstruse compared to the other metrics in this section, a beams confocal parameter (B) is thought of as a bi-directional range wherein either end of the range contains the points where the beam wavefront curvature is at its greatest. Fortunately, this is also the criterion of the mono-directional Rayleigh Length. Thus, the confocal beam parameter is just the Rayleigh Length in both axial directions from the cavity center, or

$$B = \pm Z_R$$

$$B = 2 \times Z_R$$

Similarly to the Rayleigh Length, the confocal beam parameter is not one of the highlights of our system, as it is a lesser known beam metric without broad recognition. While we may choose to include it somewhere within the system software, it won't be front and center and will likely be accessed through specific user commands.

Beam Quality:

A somewhat broad and abstract quantity related to a laser beam, simply put, Beam Quality is a way to measure how tightly a laser beam can be focused. This can be understood by visualizing the wavefronts of a beam. A laser exhibiting good beam quality will have smooth, uniform wavefronts, while poor quality beams will have scrambled, nonuniform wavefronts, as seen in Fig. 21. The latter example will lead to the beam diffracting more and thus reducing how well it can be focused. Beam quality is usually classified by one of two parameters, Beam Parameter Product and M^2 , which will both be discussed further below.

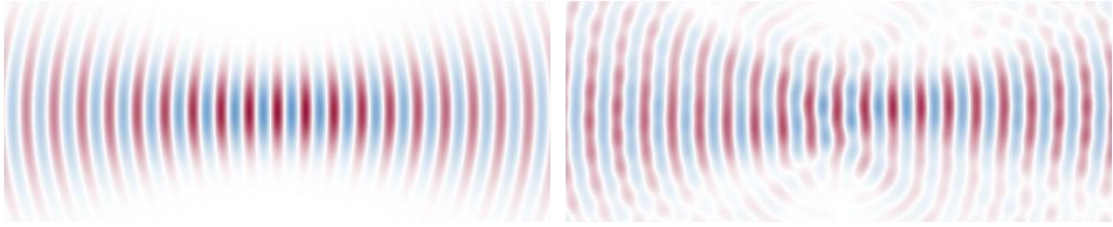


Figure 21: High-quality wavefront (left) and Low-quality wavefront (right)

Beam Parameter Product (BPP): The simplest way to describe beam quality, BPP is defined as the product of the beam divergence half angle and beam waist.

$$BPP = \theta \times w_0$$

As it is such a rudimentary measurement, it has a broad range of applications, and is valid for gaussian and non-gaussian beams. Defining BPP for non-gaussian beams requires employing the second moment methods in measuring waist and divergence to ensure accuracy. In addition, BPP is valid for elliptical beams, exhibiting unique values for the major and minor axes of the beam. Lower numerical values for BPP implies a better beam quality, and the minimum possible BPP exhibited by a perfect gaussian is equal to λ / π .

M Squared (M^2): Directly related to a laser's beam parameter product, the M^2 parameter is the ratio of a laser's BPP to the perfectly gaussian BPP value defined above. Unlike BPP, M^2 is a unitless quantity with a maximum achievable value of 1. M^2 is generally preferred over BPP and is recognized as the [ISO standard](#). Combining the original BPP formula with the perfect gaussian into a ratio, M^2 can be simplified to

$$M^2 = [\lambda / (\pi \times \theta \times w_0)]^{-1}$$

As beam quality is the element of the beam we hope to optimize through our automatic mirror adjusters, we obviously had to display it. While the measurement system for beam quality mentioned above is valid, we came across a significant amount of documentation referencing a different, more complex, but potentially more accurate method for determining beam quality. This method involved taking the $D4\sigma$ width at multiple points along the beam's axis and then reducing the data and deriving M^2 . As this method of calculation relies on a beam waist measurement we weren't on using, we did not use this and focused on the method outlined above, yielding a amplified M^2 parameter.

Astigmatism:

Arising from a variety of reasons, astigmatism refers to when focusing a beam, the vertical and horizontal axes of the beam do not focus on at the same distance. This is frequently due to either a defect in an optical element (lens scratches, glass impurities, etc.) or from an aberration in the imaging system itself. While it would be possible to quantify with our profiler design, it seems that to do so the profiler would have to be physically moved along the beam axis. As mentioned above, we do not plan on doing this, so measuring astigmatism will not be a feature of our system. Also, as it is a quality induced by not the beam itself but rather the optical elements it interacts with, it seems like a superfluous addition to our specific project.

Laser Profile Asymmetry

The least quantifiable measurement of all those listed, laser mode asymmetry refers to the axial beam dissimilarities on either side of the beam's centroid. This can be defined along any central axis of the beam, or through integrating these 2-D slices into a 3-D intensity profile (shown in Fig. 22). Essentially, the beams asymmetry can be considered a measurement of difference between two halves of the intensity profile. Quantifying this value can be challenging and obfuscating, especially when the beam profiler will provide a live image of the beam's spatial characteristics and relative intensity. Due to this visual representation, we have not been displaying a quantification of asymmetry. However, in order to ensure that the computer software can gauge symmetry, we have designed a value we call the Beam Asymmetry Parameter. This values derivation will be touched on further in the document, but is it essentially a construct of the beam profiler sensor array used to gauge the average intensity difference between points equidistant from the beam center, or area of maximum intensity.

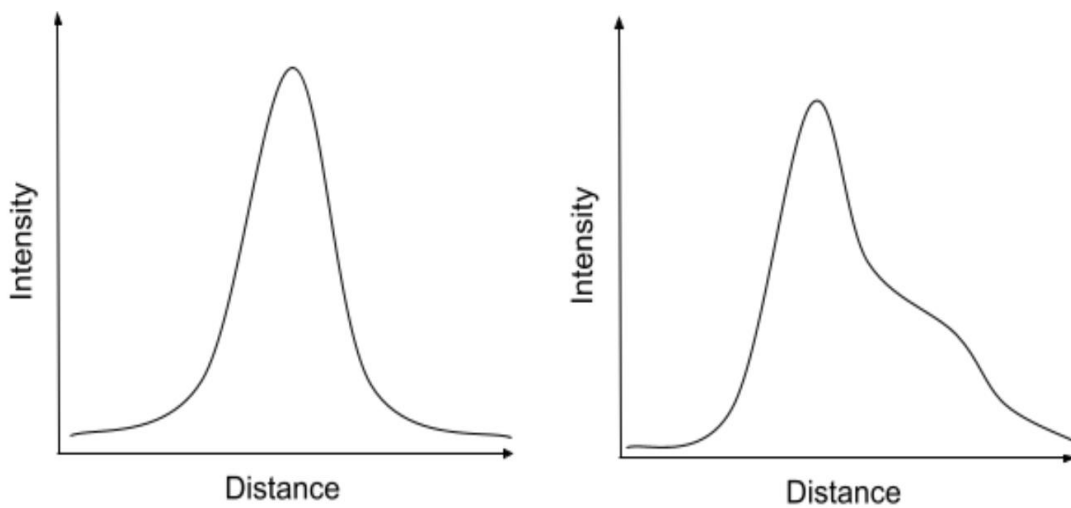


Figure 22: Highly Symmetric (left) and Highly Asymmetric (right) beam profiles

Laser Beam Profiler Investigation

Camera-Based Beam Profilers:

Camera based beam profilers work by shining a laser onto the camera sensor and imaging the beam directly. There are two separate camera systems used for these profilers, the Charge-coupled Device (CCD) and Complementary Metal-Oxide Semiconductor (CMOS) systems. While people tend to think that both systems employ an array of wavelength specific, light sensitive cells called pixels to image, this is usually not true. Rather, cameras tend to employ a patterned filter, known as a Bayer filter (shown in Fig. 23), which arranges a Red-Green-Blue (RGB) array upon light collecting photosensors (sometimes called photosites). For every blue and red pixel, there are two green pixels, as most light contains some element of 'green' wavelengths. Both systems convert the optical signal received into an electrical one which is then processed into image data.

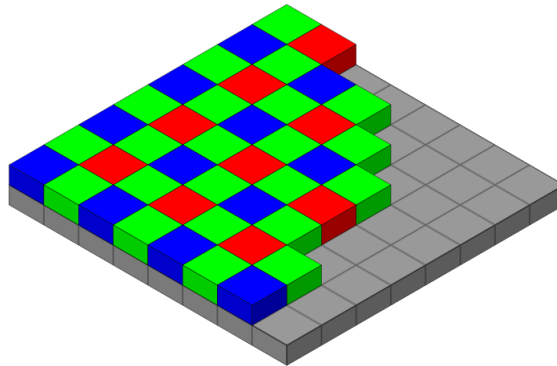


Figure 23: A Bayer filter imposed over photosensors.
Public Domain, courtesy of [C. Burnett](#)

The main distinction between the CMOS and CCD is that CCDs are analog, while CMOSs are digital. Although not immediately present when comparing between the two, this distinction impacts the production and operation of the devices significantly, so the correlated differences are outlined below.

CCD Systems

Seemingly counterintuitive to their superior resolution and higher price, CCD cameras are unique in the sense that their photosites are passive elements. The signal incident on them is immediately transferred, amplified, and then processed, row by row. This high-level processing can lead to great resolution, linearity, and noise reduction, but tends to be power intensive. An unfortunate side effect of the row processing is a CCD-specific effect called blooming, occurring from electron build up in the photosites due to high numbers of incident photons. These excess electrons then leak into adjacent sites and corrupt the image through 'smearing' the area of high intensity.

CMOS Systems

CMOS cameras, in stark contrast to CCDs, perform their light processing individually at each photosite, which contain their own amplifiers. This site-specific processing raises framerate, although it does also increase transfer time. In addition, it can potentially lead to rolling artifacts, which are caused by the camera scene changing faster than the photosites processing speed. Local amplifiers, along with integrating digital-analog converters and timers, help conserve space, and CMOS systems tend to be the smallest around, being able to fit on single chips. Their production can also be done on most standard silicon production lines, reducing cost.

Summary and Comparison for Camera Based Profilers

When analyzing CCDs and CMOS systems for use in our project, it is not as simple as one being cheaper, but inferior, to the other. The unique mechanisms contained within each lead to unique issues for both. Between the two major harmful phenomena that occur for each system, blooming and rolling artifacts, blooming would likely be more detrimental to our system than rollers. This is because blooming would be much more probable to occur in our system and it would also impact system performance more heavily than a rolling artifact. Rollers occur when a scene changes at a speed higher than the camera framerate, and while the laser is almost guaranteed to morph at a rate exceeding the cameras framerate, the change is unlikely to warp the image to a harmful degree. Blooming (see Figure 24), on the other hand, could very easily happen, especially if using a narrow-linewidth laser with a small spot size. The small spot could quickly oversaturate a region of the sensor and would continue to until the incident was reduced or interrupted. While an ND filter could help with controlling this and the mirror adjustors would likely cause the cavity to enter and exit the lasing condition, the effect of a bloom would be incredibly detrimental to the profiler's performance. Any camera-based profiler would measure the beam size based off its intensity profile, which could be axially distorted with bloom.



Figure 24: Telescopic astral photograph exhibiting bloom

In most other aspects, CCD cameras do perform better than CMOS systems. Resolution tends to be higher, and the row processing method can help computationally remove noise. While these would both be beneficial to the profiler, our resolution specification of a 1 mm spot size is achievable for both camera types, and our system is being designed to operate with a reasonable level of noise. Another element of CCDs that is usually beneficial, but is superfluous for our project, is their superior sensitivity. As we would be imaging lasers, it is exceptionally unlikely that a CMOS would lack the sensitivity to image a beam, even after passing through the system's beam splitter. It is more likely that this increased sensitivity would be a drawback, as it could lead to more blooming and potential photosensor array damage.

More relevant to our design specifications are the relative costs and size of each camera system. In both scenarios, CMOS systems are superior. Easy mass production of CMOS cameras reduces their price to a fraction of the harder to manufacture CCDs, while the localization of amplifiers and further chip integration in CMOSs make them smaller as well. As both size and cost are part of our defining features of our system, these are important distinctions.

Overall, both camera systems exhibit the very relevant ability to provide live imaging of the beam, and through this, our system will be rapidly able to update the beams parameters, increasing the frequency of the adjustment loop and reducing down-time. This is incredibly significant, as having our system induce the lasing condition on a given cavity is one of our major design criteria. As these systems both output an image array, processing that information into beam parameters and a beam visualization will be relatively easy.

Although CMOS and CCDs each are relatively limited wavelength ranges-they're usually designed for imaging visible light-the range our group selected for our project, 400-700nm, is well within the operating limits for practically all models of both systems. The increased power sensitivity of cameras is not particularly relevant for similar reasons, as although the power density of the most extreme laser our system is specified to profile (1mm spot size, 10-Watt output power) would be huge and potentially damaging to any sensor, the presence of an ND filter could mitigate this concern. As well as this, the extreme laser parameters described above are almost exclusively found in industrial machining lasers. These lasers are a) closed cavity and b) not used by our target environments of research and teaching labs. Because of this, it is highly unlikely our system would interact with such a laser cavity.

While cameras can certainly be expensive, with some optical grade CCDs running for thousands, if not hundreds of thousands of dollars, there are also very affordable options for both CMOS and CCDs. Camera performance will likely increase with price, but with reference to all of our design considerations, our project truly does not require a particularly advanced camera system. Due to this, price would not be a restrictive factor for using a camera-based profiler.

Scanning-Aperture Profilers:

Unlike camera profilers, scanning-aperture profilers operate by using a power meter and measuring the relative beam intensity as the meter is obstructed to different degrees by an aperture. With enough data of both the measured intensity and the relative level of obstruction, the beam can have its spatial characteristics algorithmically reconstructed. The two most popular forms of aperture profilers are discussed below.

Knife-Edge Technique

Utilizing the knife edge technique requires placing a straight edge in front of a power meter and measuring the transmitted power of the beam as the edge chops it. Then, charting intensity versus the edge position yields a one directional integrated beam intensity profile, as depicted in Fig. 25. After doing this with multiple blade orientations, the full spatial characteristics of the beam can be algorithmically profiled.

Although this method is simple in application and requires rudimentary equipment, it does not provide an exceptionally detailed beam profile, and only captures a composite snapshot of the beam, rather than providing a live feed image.

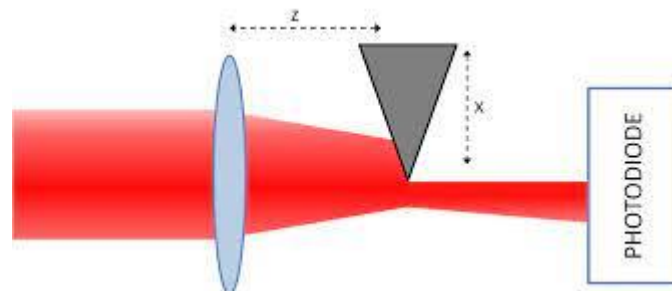


Figure 25: Diagram of Knife-Edge Technique

Scanning-Slit Technique

Similarly, to the knife-edge method, the scanning-technique measures beam power in relation to the location of two orthogonal slits in front of the power meter. As there are two slits rather than just the knife edge, fewer relative orientations of the slit are needed to garner the same amount of information.

With the being said, obtaining the equipment for the scanning-slit technique could prove troublesome. Machining the slits themselves via a 3-D printer could be relatively affordable, but the accuracy of production would be far too low for valid, precise measurements. This is because the slits themselves need to be exceptionally thin, straight, and exactly perpendicular to one another. Laser machining could likely produce the desired results, but our group lacks familiarity with this technique, and it is more expensive. Purchasing the scanning-slit equipment from a vendor would also be costly.

Summary and Comparison for Scanning-Apertures Profilers

Between the two scanning aperture methods outlines above, the knife edge technique can tend to be thought of as the cheaper alternative to a scanning slit method. Knife-edge scanners require more measurements to obtain the same amount of information as a slit scanner, due to the mono-directional edge of the knife in comparison to the two orthogonal slits. Because of this, the time of operation would be likely doubled for a knife-edge system, which is an important design criterion, as our adjustors will need large amounts of input data to properly adjust, and the faster that data is input, the faster the adjustors will alter the cavity. Due to our design specification of reaching lasing in under five minutes, data refresh rate is highly relevant.

Both systems predicate their power sensitivity and wavelength range on their paired power meter, and each will require developing an automation system. The knife-edge technique tends to be performed manually, so a significant amount of development would be required to automate the process. Scanning-slits, however, frequently have some degree of automation through pre-existing profiler software packages bought through a vendor. However, our group plans to create our own software, so while their may be foundational elements to build software upon for the slit method, both techniques will require creation of custom automation software.

There are both a litany of potential benefits and drawbacks for employing scanning-aperture profilers within our project. One major advantage of this profiler type is its viability for all wavelengths of light detectable on a power meter, which tend to have a much larger operational range than cameras. This is because power meters usually extend beyond the visible spectrum, whereas many cameras exclusively image that small wavelength range. However, we specified a relatively small operable wavelength range, so this is fairly insignificant. On a similar note, the allowed power in a scanning-aperture system would likely be higher than that of a camera system, as power meters tend to allow more saturation than camera pixels. This is somewhat irrelevant, as in either scenario of employing a camera or scanning system, we would likely include a neutral density filter in order to ensure system functionality with high powered lasers.

As implied in the above statements, using a scanning-aperture in our profiler would require the use of another power meter, separate from the one our group will design. This would bring to question whether or not we should duplicate our design, our purchase a

factory model. In either scenario, an additional, nontrivial financial outlay would be required.

The need for another power meter is perhaps counterbalanced by the superior resolution of scanning-aperture profilers, which can far exceed that of camera-based systems. Scanning-aperture systems can accurately characterize beam spots as small as a singular micron, far exceeding the resolution offered by camera profilers. Bleeding-edge cameras are just reaching sub-micron sized pixels. Even if our group could afford a system of such clarity, Nyquist sampling theorem dictates that to resolve a spot size of 1 μm , sampling must occur twice within that frame, or rather, that a camera resolving such a small feature must have pixels of size (at most) 0.5 microns. So even the most advanced, expensive camera systems are beaten-in terms of resolution-by scanning apertures. However, our design specifications list the minimum resolvable laser spot size as 1 mm, so the above point is essentially moot when considering the design of our project.

The major drawback with scanning-aperture systems is that they do not provide a live image of the beam. This is very significant to the design of our system, as the parameters of the beam need to be constantly refreshed in order for the feedback-loop to update the mirror adjustors quickly. While our group could potentially optimally automate the scanning process to gather the beam profile information at a high frequency, the process would, realistically, still take seconds per iteration. In comparison to the refresh rates of camera (at least 30 frames per second), the difference is gargantuan.

In addition, we would need to develop our own techniques within our projects software in order to both calculate the beam parameters and display a visualization of the beams spatial profile from the scanning techniques. These would be significantly more involved than the pixel conversions involved with camera systems. While it is unlikely these calculations would push the limits of our computational power, it is still a possible consideration, especially if the system would refresh at high speeds.

Although the high price of scanning-slit apertures was previously mentioned, it would likely still be less expensive than many CCD camera systems. Knife edge scanners would probably be the cheapest option of all, even over inexpensive CMOS cameras. This is because the system needs very few optical elements and can employ regular, everyday utensils, albeit potentially at the detriment of ease and accuracy.

CMOS, CCD, Knife-Edge, and Slit Profiler Specification Tabulation

Profiler Type	Cost	Live Imaging	Wavelength Range	Power Range	Intensity of Computation	Resolvable Spot Size
CMOS	Low	Yes	Visible, NIR	Small	Low	Small
CCD	High	Yes	Visible, NIR	Small	Low	Smaller
Knife Edge	Lowest	No	Limited by Power Meter	Large	High	Small
Slit	High	No	Limited by Power Meter	Large	High	Smallest

Table 10: Profiler Decision Table

For a litany of reasons, our group has decided to move forward with building a beam profiler featuring a camera system. This is due camera-based profilers being easier to integrate within our optical system, as less automation and computational software will need to be developed. More significant than this is their ability to perform live imaging on the beam, which will greatly increase the frequency of the adjustment loop, which will reduce the lasing time. Although cameras have lower resolutions, working wavelength ranges, and power allowances in comparison to scanning profilers, these benefits would all exist outside of our stated design specifications. When choosing between CMOS and CCD systems, we selected CMOS, as much like with scanning profilers, the benefits of a CCD camera would occur mainly beyond the scope of our initial requirements for the system. Furthermore, CMOS cameras are among the cheapest options available on the market, helping us meet our desired price range of under a thousand dollars. However, we still may employ a knife-edge profiling technique in conjunction with our designed power meter as method of confirming the accuracy of our camera-based profiler.

Design Considerations

Total System Integration Design

The entire system will consist of multiple components that must be situated together in order to properly function as a unit. There are several ways in which we could configure all the components of the system.

Archipelago Configuration

In this design choice, the mirror mount adjusters, the power meter, and the beam profiler are all not necessarily physically attached. The adjusters would individually mount to the optical breadboard/table and extend upwards towards the mirror mount, much like manufacturing robot arms. The power meter and beam profiler would be separately mounted on the optical table/breadboard via optical posts.

This system configuration has some significant advantages, mainly the reduced spatial density achieved through the ‘archipelago’ layout of components. The elements of the system would not be tightly packed, and thus there would be more space in between each element. This would be beneficial if some element of the design was done improperly, and additional optics or other equipment were required in between design elements. Moreover, any individual errors or equipment failures unique to a subsystem could easily be isolated and dealt with, rather than having to take apart a bulk-packaged system.

This ease of isolating an individual part is a two-sided coin however, as more loose, disconnected parts require higher levels of organization and tracking. Employing the ‘archipelago’ layout would likely increase the chances of our group misplacing a component, potentially causing significant delays to the system development. As well as this, more loose parts increase the complexity of setting up the system, which in turn increases the time required for system set up. Quick and easy system implementation is a design specification, so we need to be wary of using too many disconnected elements which could make setting up the system laborious or confusing.

Bulk Package Configuration

In this design choice, all components of the system are physically combined into a single module. This would be done by creating a small, dense frame which encompasses all the disparate (non-laser adjusting) elements of the system. This frame would then be placed at a distance from the laser coupler, and light from said coupler would enter the frame before being directed to the relevant subsystems. This frame would likely be either fabricated through a 3-D printer, or manually constructed through an easy to work with material, such as wood.

Unlike the ‘archipelago’ configuration, this system layout would essentially reduce the non-adjustment elements to a singular unit. While this would decrease the likelihood of losing small parts and the like, it could be very troublesome if the entire frame was misplaced, or an individual part was damaged. We would then have to deconstruct the frame, removing the misfiring part before fixing it and rebuilding the frame. This issue could be accounted for by designing the frame to allow for easy removal of system parts, through perhaps latches, clamps, or screws. Beyond this, a bulk package would vastly reduce set up time, a clear benefit to the system as described by the set up time design specification.

As shown by the above section, many of the benefits of one system layout mirror the negative elements of the other. This is further demonstrated by the increased spatial density of the bulk configuration. The overall package could become fairly large, cumbersome, and heavy, especially if using a wooden frame. As our requirements table states, we need the system to weigh under 6 kilograms, so we need to be aware of this potential limitation of the bulk layout. In addition to increasing weight, designing a frame would expend resources, both financial and time related. Even if using cheap materials, there would be a significant amount of effort expended in the design and creation of the frame, effort that could perhaps better be placed elsewhere. The frame would also limit the inclusion of additional elements. While careful design and consideration would ideally make it so that no other elements would be needed beyond what are outlined in this paper, it is always a possibility that unforeseen circumstances would require us to include an additional optic or other piece of equipment. Beyond this, as our system is designed primarily for teaching or research environments, it is logical that users would seek to customize it to some degree. The bulk package would obviously limit their ability to do so.

Configuration Decision

While the bulk-package system configuration certainly has benefits, our group is currently planning on using the ‘archipelago’ layout. We made this decision based off the decreased cost and weight of the ‘archipelago’ layout. Beyond this, the increased time requirement for designing and fabricating the frame for the bulk package was taken into account. With ideal funding amounts and no time requirements, the bulk package may be a better option, but under current circumstances the ‘archipelago’ layout seems the superior option. Choosing this no means rules out the possibility of later designing a frame to hold system elements together, though, as we may determine it is a net positive to connect specific elements (such as the beam profiler sensor array and objective lens) with a framework.

Power Meter Design

Attenuation

Choosing a photodiode with linearity between 1nW - 1mW. This means nonlinear response would occur above powers of 1mW, which is undesirable. Attenuation must be

used to bring higher powers into the linear region of the diode. This can be done with an ND filter or combination of ND filters. The attenuating strength of ND filters is described by the following equation,

$$\frac{I}{I_0} = 10^{-d}$$

where I is the output optical intensity, I₀ is the input optical intensity, and d is the neutral density factor. To bring the maximum power of the requirements specifications into the linear region of the diode, it must be attenuated to the maximum power a photodiode can read and remain within a linear response. This would mean bringing an optical power of 10W down to 1mW, or a decrease in optical power of around 4 decades. Thus, the corresponding neutral density factor of the ND filter (or combination of ND filters) would be 4.0. The following are potential components that would suit this requirement.

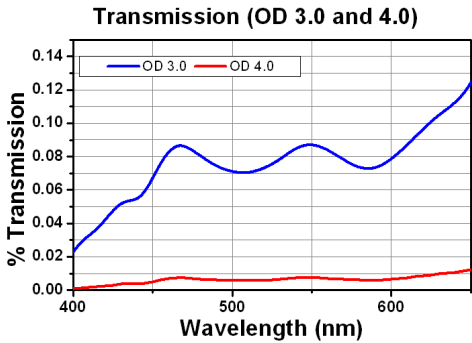
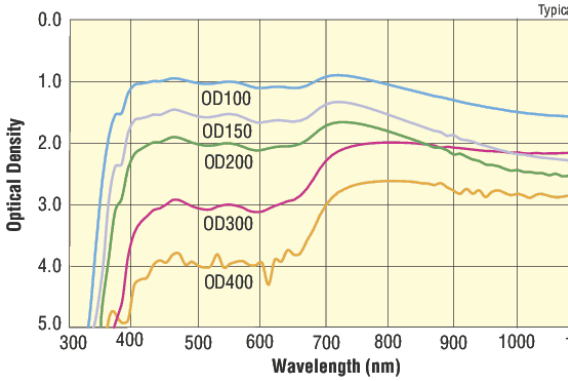
Product Name	Transmission/Optical Density Variation Plot	Cost (\$)
<p>NE540B - Unmounted Ø1/2" Absorptive ND Filter, Optical Density: 4.0</p>	 <p>The plot shows % Transmission on the y-axis (0.00 to 0.14) and Wavelength (nm) on the x-axis (400 to 600). Two curves are shown: OD 3.0 (blue) and OD 4.0 (red). The OD 3.0 curve shows higher transmission, fluctuating between approximately 0.07 and 0.12. The OD 4.0 curve shows very low transmission, near 0.00 across the entire wavelength range.</p>	21.45
<p>Neutral Density Filter, Absorptive, 25.4 mm, 4.0 OD at 546.1 nm</p>	 <p>The plot shows Optical Density on the y-axis (0.0 to 5.0, inverted) and Wavelength (nm) on the x-axis (300 to 1000). Multiple curves represent different OD values: OD100 (light blue), OD150 (medium blue), OD200 (green), OD300 (orange), and OD400 (red). All curves show a sharp increase in OD starting around 350-400 nm, reaching a plateau between 500 nm and 1000 nm. The OD400 curve reaches an optical density of 4.0 at 546.1 nm.</p>	38.00

Table 11: ND filter potential products table

It can be clearly seen that the transmission of the filters is not exactly constant across the spectrum of wavelengths. This variation in transmission will have to be determined as a function of wavelength and taken into consideration when calculating the true power of the laser being measured.

Photodiode Modes of Operation

There are two ways to operate a photodiode: photoconductive mode and photovoltaic mode. In the photoconductive mode, the diode is operated with a reverse bias voltage, which causes a dark current to flow. This makes precision measurement of optical power more complicated and increases noise, making this mode of operation undesirable for our application. In the photovoltaic mode, the diode is operated with a bias voltage of 0V. This naturally eliminates dark current, thus making it an attractive choice due to the decreased noise.

Noise Equivalent Power, Signal-to-Noise Ratio, and Responsivity

Noise equivalent power (NEP) is defined as the power level that is equal to that of the noise of a system. For a photodiode, the NEP is a description of the current that is necessary for the diode to produce in order to overcome its own current noise. The NEP of a photodiode is dominated by a few different types of noise: Johnson (or thermal) noise, shot noise, and flicker noise. Johnson noise, I_j (A), is described as follows:

$$I_j = \sqrt{\frac{4k_B T B}{R_L}}$$

Where k_B (J/K) is Boltzmann's constant, T (K) is temperature of the diode, B (Hz) is the bandwidth of the system and R_L (Ω) is the load resistance. One can see that as temperature of the diode increases, so does the Johnson noise. This is something to consider as the laser could heat the diode up to create non-negligible thermal noise effects.

Shot noise, I_s , is described as follows:

$$I_s = \sqrt{2q(I_{ph} + I_D + I_B)B}$$

Where q (C) is the charge of an electron, I_{ph} (A) is photocurrent, I_D (A) is dark current, I_B (A) is background current, and B (Hz) is again bandwidth of the system. Shot noise is strongly influenced by the dark current that is generated when the diode is being operated with a bias voltage. Since we have been operating our diode in the photovoltaic mode with bias voltage equal to 0V, the dark current term can be ignored. It is also worth noting that the background current in the shot noise expression typically only manifests in high field applications and is thus negligible. Flicker noise only occurs at low frequencies of laser amplitude modulation, which is not how the laser in question will be operated, and thus can be ignored altogether.

We can now consider the noise generated by the photodiode circuit in reference to the signal-to-noise ratio (SNR). The SNR is related to the current noise terms and photocurrent as follows:

$$SNR = \frac{I_{ph}^2}{I_s^2 + I_j^2}$$

Requirement's specifications state that the SNR of the power meter must be at least 30dB. The SNR in decibels is related to the SNR in terms of a ratio as follows:

$$SNR = 10 \log \left(\frac{I_{ph}}{I_{noise}} \right)$$

This results in a SNR current ratio of 1000. Rearranging the equations for Johnson noise, shot noise, and SNR to solve for the photocurrent, we arrive at the following expression:

$$I_{ph} = qB \frac{S}{N} \pm \sqrt{qB \frac{S}{N} + 4 \left(\frac{k_B T B}{R_L} \right)}$$

Bandwidth of the system is given by

$$B = \frac{1}{\tau} = \frac{1}{R_L C}$$

where C (F) is capacitance. Assuming a load resistance of $R_L = 10G\Omega$, capacitance of $C = 0.1\mu F$, and diode temperature of $T = 293K$, we arrive at the photocurrent that is necessary to attain the required SNR, $I_{ph} = 50.494pA$.

Responsivity of a photodiode is a characteristic that determines how much photocurrent will be produced given a certain impinging optical power. Responsivity, \mathcal{R} (A/W), is given by the following expression:

$$\mathcal{R} = \frac{I_{ph}}{P_{opt}}$$

Where P_{opt} (W) is the optical power incident upon the photodiode. Plugging in the previously acquired minimum photocurrent and using the minimum laser power that the system should be able to detect, we arrive at the minimum required responsivity of the photodiode, $\mathcal{R} = 0.0505A/W$. Now that we have a number for the important metric that is responsivity, we can tabulate and compare various choices for photodiodes from the market. (see tables 12 and 13)

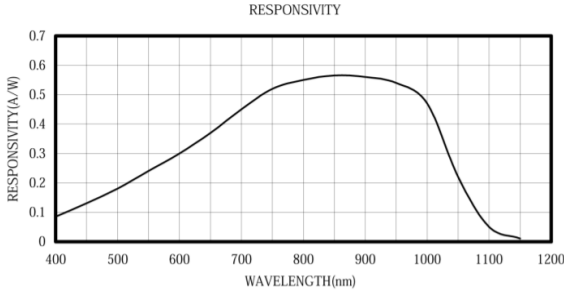
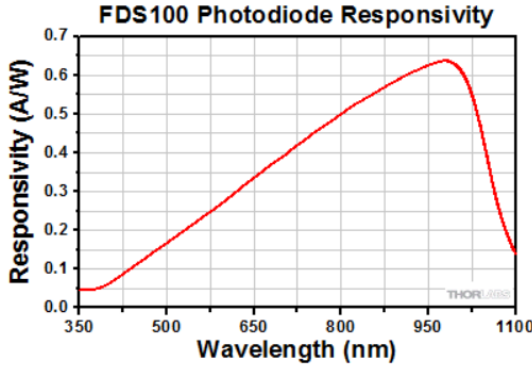
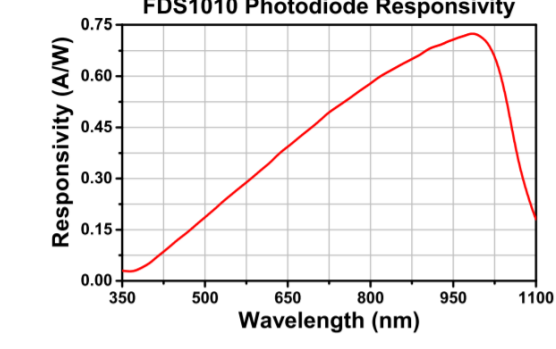
Product Name	Responsivity Plot	Cost (\$)
Marktech MTD5010N	 <p>The plot shows the responsivity of the Marktech MTD5010N photodiode. The x-axis is labeled 'WAVELENGTH(nm)' and ranges from 400 to 1200. The y-axis is labeled 'RESPONSIVITY(A/W)' and ranges from 0 to 0.7. The curve starts at approximately 0.1 A/W at 400 nm, rises to a peak of about 0.55 A/W between 800 nm and 900 nm, and then falls to near zero by 1100 nm.</p>	5.32
Thorlabs FDS100 - Si Photodiode	 <p>The plot shows the responsivity of the Thorlabs FDS100 photodiode. The x-axis is labeled 'Wavelength (nm)' and ranges from 350 to 1100. The y-axis is labeled 'Responsivity (A/W)' and ranges from 0.0 to 0.7. The curve starts at approximately 0.05 A/W at 350 nm, rises to a peak of about 0.65 A/W at 950 nm, and then drops to about 0.15 A/W at 1100 nm.</p>	14.94
Thorlabs FDS1010 - Si Photodiode	 <p>The plot shows the responsivity of the Thorlabs FDS1010 photodiode. The x-axis is labeled 'Wavelength (nm)' and ranges from 350 to 1100. The y-axis is labeled 'Responsivity (A/W)' and ranges from 0.00 to 0.75. The curve starts at approximately 0.05 A/W at 350 nm, rises to a peak of about 0.7 A/W at 950 nm, and then drops to about 0.2 A/W at 1100 nm.</p>	55.73

Table 12: Photodiode potential products table

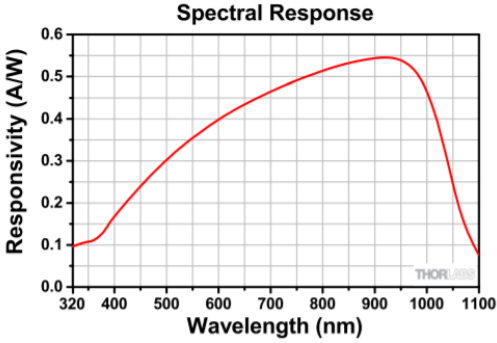
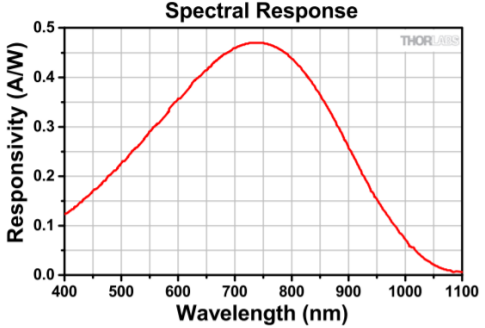
Product Name	Responsivity Plot	Cost (\$)
Thorlabs FD11A - Si Photodiode		14.58
Thorlabs FDS025 - Si Photodiode		34.36

Table 13: Photodiode potential products table continued

Due to the characteristic wavelength/responsivity relationship that typical diodes have, the upper range of our requirement's specifications workable wavelength range will be covered with no problem when considering silicon photodiodes. The lower end of the range is where it will be challenging to find suitable diodes.

[Linear Region of Photodiode](#)

The linear region of a photodiode is dictated by the noise equivalent power and the saturation level.

Power Meter Circuitry

A popular method of configuring a photodiode power meter is by utilizing a transimpedance amplifier to keep the voltage across the PD at a virtual zero volts. This allows one to drastically reduce dark current through the system, thus reducing shot noise and improving detection.

A simulation of a simple transimpedance amplifier, shown below in Fig. 26, was simulated in Multisim Live. A DC current source was used to represent a photodiode.

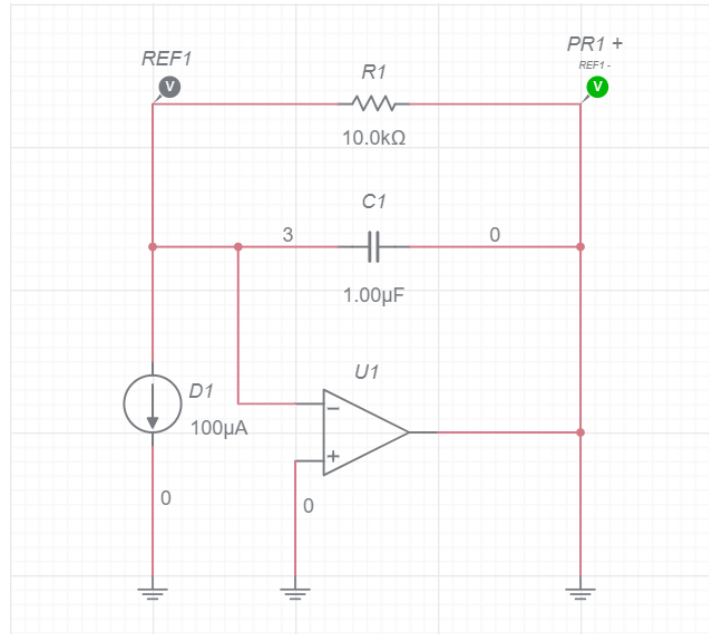


Figure 26: Schematic of an optical power detecting transimpedance amplifier circuit.

This model can be used to see the effects of changing the current produced by the photodiode (D1) and the measurement resistor (R1) on the voltage measurement (PR1). First, let's look at the minimum condition of a photodiode current of 100pA for different cases of the R1 resistance.

R1 Value	PR1 Simulated Value	PR1 Ideal Value	Percent Error (%)
1kΩ	99.997nV	100nV	0.00300
10kΩ	999.67nV	1000nV	0.03300
100kΩ	9.9668µV	10µV	0.33200
1MΩ	96.774µV	100µV	3.22600
10MΩ	749.99µV	1000µV	25.00100
100MΩ	2.3076mV	10mV	76.92400
1GΩ	2.9125mV	100mV	97.08750
10GΩ	2.9909mV	1000mV	99.70091

Table 14: Resistor simulation values

For lower $R1$ values, such as those below $1\text{M}\Omega$, the simulated voltage reading measurement is rather close to the ideal value, with low percentage errors. However, the voltages that these resistance values produce are miniscule due to the combination with the very low picoamp current. This poses a problem as Raspberry PI would struggle to resolve microvolt level voltages.

Thus, we look towards higher voltage readings and consequently higher measurement resistance values. However, as shown in Table 15, the percent error of the voltage readings using resistances higher than $1\text{M}\Omega$ are quite substantial, and in some cases even approaching 100% error. This phenomenon is caused by a current division that occurs due to the relatively low op-amp input resistance compared to the large measurement resistor resistance. The solution for this is to increase the input resistance of the op-amp. One way to do this is to simply add a hefty resistor on the negative terminal of the op-amp, as shown below in Fig. 27.

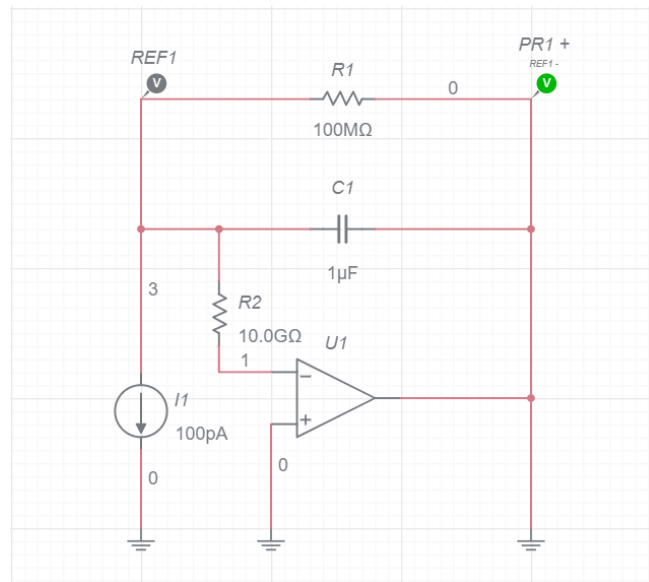


Figure 27: Power Meter Circuit

Now let us look at the effect of the added op-amp input resistor (R2) on PR1 while keeping R1's resistance and I1's current at a constant 100MΩ and 100pA, respectively. The ideal value of the PR1 simulated value for each case is 10mV.

R2 Value	R1 Simulated Value (mV)	Percent Error (%)
1MΩ	2.3663	76.337
10MΩ	2.8570	71.43
100MΩ	5.6518	43.482
1GΩ	9.1142	8.858
10GΩ	9.9003	0.997
100GΩ	9.9890	0.110
1TΩ	9.9980	0.020

Table 15: Table of simulated voltage and R2 values

As expected, the percent error between the simulated PR1 reading and the ideal reading decreases as the input resistor to the op-amp increases in resistance. However, favorable percent errors of less than one percent only begin to occur after R2 has reached tens of GΩ and beyond. It would be excellent to choose a 1TΩ and have low deviation in voltage readings, but cost must be considered at ohmage this high. Below in table 16 we have compiled a table comparing typical prices between high ohmage resistors a few decades of resistance apart.

Resistance (Ω)	Price (\$)
1G	2.00
10G	10.00
100G	40.00
1T	80.00

Table 16: Table compiling typical costs of high ohmage resistors

Now let's take a look at the ranges of optical power for which we must account for. Since our requirement's specifications for measurable laser power span such a wide range, it would be useful to display the spread logarithmically. The following figure, fig. 28, visually displays the ranges.

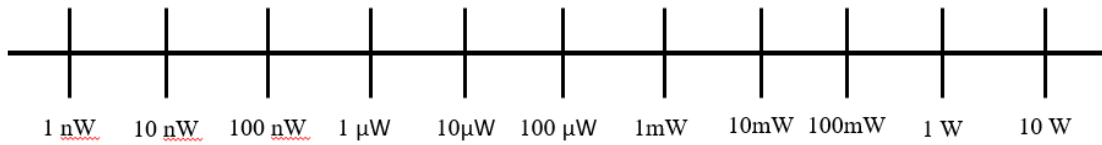


Figure 28: Decade divisions of input power range

It would now be of use to look at the decade divisions for the subsequent current produced by the photodiode. First, we look at the case in which the responsivity is lowest, corresponding to the lowest range of current. This would be a responsivity of 0.1A/W , shown in Fig. 29.

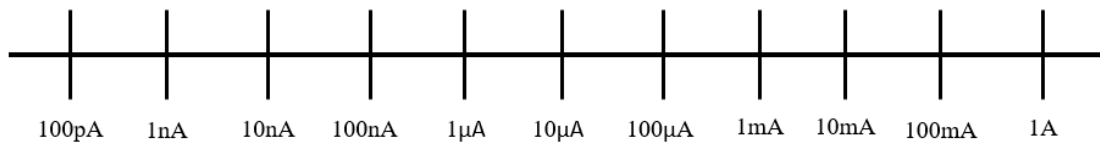


Figure 29: Decade divisions of photocurrent for responsivity of 0.1A/W

The next case would be for the maximum responsivity, or a responsivity of 0.6A/W , shown in Fig. 30.



Figure 30: Decade divisions of photocurrent for responsivity of 0.6A/W

In all cases, it can be seen that our range spans 11 decades. A single load measurement resistor can be used to cover a range of these values, however if one uses a single resistor, one would need to also utilize a voltmeter with a subsequently rather wide range of measurable voltages. Thus, it would be of use to use not one, but multiple load resistors to be able to breach the full breadth of required measurement ranges. The trickiest range would be in the lower regions of the photocurrent, since as the load resistor increases in resistance, the voltage division from the op-amp increases, thus decreasing the accuracy of the measurements.

In a situation in which the number of load resistors that can be used is not restricted, then we would have an ideal case in which resistors could be used to represent each decade of photocurrent, corresponding to a subsequent voltage range of, say, 0.1V to 6V .

However, it must also be considered that each of these voltages created by the load resistors will need to be measured by a voltmeter. The GPIO pins of the Raspberry Pi are able to take inputs in the form of voltage. However, it is of importance to note that these pins only accept digital voltage signals - analog voltage is not acceptable.

Thus, if we wished to use the GPIO pins of the Raspberry Pi to take our voltmeter measurements, it would be necessary to convert the analog signal coming from the photodiode transimpedance amplifier circuit load resistors into digital signals. For this, one could utilize an ADC to convert the analog signal to a digital one that could be read by the GPIO pins.

The two most pertinent characteristics of ADC's are their sampling rate (temporal resolution) and their bit-length (amplitude resolution).

Sampling rate describes the frequency at which samples of the analog waveform are taken for digitization. In most cases, sampling rate is most concerned with when dealing with AC signals in which periodic frequencies will occur. It is possible for the frequency of the analog signal to increase past the maximum obtainable frequency for a given sampling rate, as per the Nyquist sampling theorem.

In our situation, while we are not dealing with periodic signals, we are dealing with potential spikes or impulses in optical power. It is entirely possible that one of these spikes, especially that for when attempting to bring the laser into the lasing condition, could be so brief that they are missed by the sampling of the ADC.

Below is described the Nyquist sampling theorem in equation form.

$$f_N = 2f_{Max}$$

Where f_N is the Nyquist sampling rate and f_{Max} is the maximum frequency of the analog signal being converted. We do not necessarily care for the maximum frequency that we can sample, but rather the minimum duration of signal we can sample. Thus, we instead would wish to describe the Nyquist equation in the following manner.

$$f_N = \frac{2}{T_{Min}}$$

The second important characteristic of an ADC is its bit-length. The bit-length of an ADC determines the resolution with which it can distinguish different values of analog input. The greater the bit-length of the ADC, the greater the resolution of the amplitude sampling. In essence, we wish to have as high of a bit-length as possible, so as to maximize the level of scrutiny we can hold over the voltmeter of the power meter.

Bit-length	Levels	Step Size (For 5V)
6	64	78.13mV
8	256	19.53mV
10	1024	4.88mV
12	4096	1.22mV
16	65536	76.3 μ V
18	262144	1.91 μ V
20	1048576	4.77 μ V

Table 17: Levels and step sizes for varying bit-lengths

Since the minimum of our measurable voltage range is 0.1mV, then technically any of the bit-lengths shown in table 17 would suffice. As mentioned prior, the higher the bit-length, the better our resolution. However, as bit-length increases, so does the price of the ADC as well. Below is compiled a table of typical prices of ADC for each bit-length.

Optical Layout Design

The laser beam in question will have to propagate from the output coupler, into the aperture of the device, and then be split and travel to the power meter and profiler camera. When approximating the beam divergence, one assumes that the location of the beam waist is where the divergence begins from the optical axis. The beam waist of a laser can lie at any point within the cavity of the beam and its location is determined by the curvatures of the two couplers. There are two boundary cases that we must consider when performing the design calculations. The first case is when the back coupler is flat, thus making the beam waist be located at the back coupler and subsequently farthest away from our system. The second case is when the output coupler is flat, thus making the beam waist be located at the output coupler and subsequently closest to our system.

Some distances along the optical path are defined below:

d_{1max} = maximum distance from beam waist to device aperture = 600mm

d_{1min} = maximum distance from beam waist to device aperture = 0mm

d_2 = distance from device aperture to beam splitter = 60mm

d_3 = distance from beam splitter to focusing lens = 40mm

d_4 = distance from focusing lens to photodiode = 40mm

It would be desirable for the imaging lens to the mode profiler to have as small of a power as possible, which would require the distance separating them to be as large as possible. The distance of the imaging lens to the mode profiler must fit within the size of the entire device as laid out in the requirement's specifications.

d_5 = distance from beam splitter to objective lens = 10mm
 d_6 = distance from beam splitter to mode profiler = 190mm

Let's begin by considering the beam path to the power meter. This would consist of distances $d_{1(max/min)}$, d_2 , d_3 , and d_4 . Assuming a maximum case scenario in which the beam waist is 700mm from the collimating lens and maximum half-angle beam divergence is 17.5mrad, we can calculate the approximated diameter of the beam incident, D_c (mm), on the focusing lens by the following equation:

$$D_c = 2(d_{1max} + d_2 + d_3)\tan(\theta)$$

Where θ (rads) is the half-angle divergence. Calculating using the aforementioned values, we arrive at a beam diameter on the collimating lens of 24.503mm.

Since we have two boundary cases in which the divergence is either at full divergence or the beam is actually collimated, we must consider the fact that the spot size of the beam will be different on the face of the photodiode within the range of divergences. Let us consider the scenario in which the photodiode is placed at the focal length of the focusing lens. In this instance, when the beam is collimated, the beam will focus directly onto the photodiode. This is illustrated in fig. 31. As divergence increases from here, so too does the distance at which the beam focuses on to the optical axis. This corresponds to a broadening of the beam spot size at the face of the photodiode, as seen in Fig. 32. The power and distance of the lens must be chosen so that the beam spot still fits on the face of the photodiode in either case.

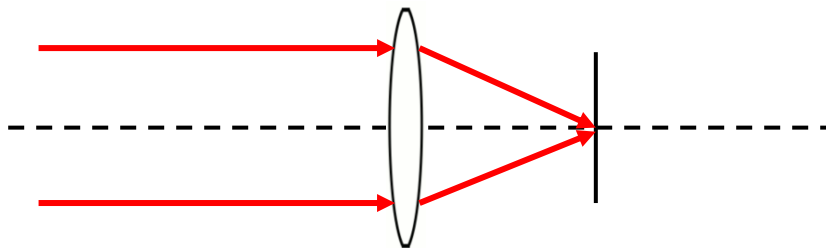


Figure 31: Diagram showing how light with zero divergence would be focused

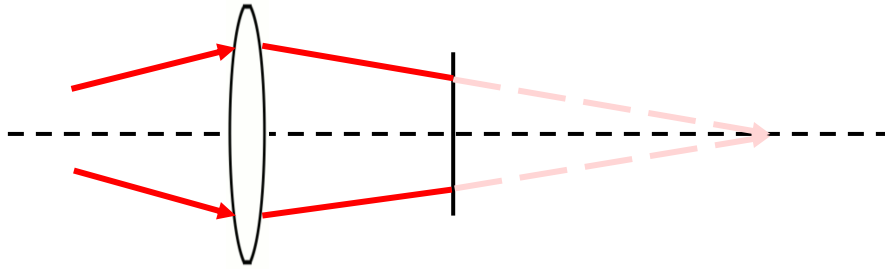


Figure 32: Diagram showing how light with non-zero divergence would be focused relative to the focal point of the lens.

Let us begin by utilizing the thin lens approximation imaging equation, shown below, to determine the focal length of the focusing lens.

$$\frac{1}{d_o} + \frac{1}{d_i} = \frac{1}{f}$$

Where d_o (mm) is the object distance, d_i (mm) is the image distance and f (mm) is the focal length of the lens. Looking at the simplest case, where the beam is collimated, we say that the object distance is at infinity, which consequently makes the image distance equal to the focal distance. Since the image distance in this case is equivalent to the spacing between the focusing lens and photodetector, the focal length, f , is therefore equal to d_i , 40mm.

Next, let's examine the case in which the input beam is not collimated, but is in fact diverging. This would cause the beam not to focus on the focal point of the lens after passing through it, but instead be focused some distance after the focal point. We can find that for the maximum case in which the beam is diverging at 17.5mrad and strikes the lens at 12.25 mm on the lens from the optical axis, the object distance can be calculated by the following equation:

$$\tan(\theta) = \frac{D_c}{2d_o}$$

We then find that the object distance, d_o is equal to 700mm. By applying the same imaging equation used further above, we can find that the image location, i.e. the location at which the beam will be focused is 42.424 mm from the lens. We can then use the geometry of similar triangles to find the height of the diffuse image that would be created at the focal point of the lens. The equation describing this relationship is outlined below.

$$\frac{D_p}{D_c} = \frac{d_i - f}{d_i}$$

Where D_p is the minimum required diameter of the photodiode active region. Solving for D_p , we find the minimum diameter of the photodiode to be 0.00233mm, or 2.3321 μ m.

Since we know the focal length of our lens, we also know the power as they are inverses of each other. This makes the total power of our lens 0.025mm⁻¹.

We have performed these design calculations for the thin lens approximation. It would not be of importance to perform some thick lens analysis and design in order to ensure that these calculations would translate to the real world. Below in table 18 is outlined the prescription for the paraxial approximation we have performed above.

	Object	S1	S2	Image
Radius (mm ⁻¹)	Infinite	0.01	0.01	Infinite
Thickness (mm)	Infinite	5	40	0
Material (mm)	Air	N-BK7	Air	Air
Diameter (mm)	24.5	24.5	24.5	

Table 18: Paraxial approximation Zemax prescription of power meter path

Product Investigation

For this section we investigated and compared the options available for each component of the project. Aspects that we have considered when deciding on a product will include, the price, vendor, time to ship the product, quality of the product, performance of the product for the job, and the specifications (weight, dimensions, etc.). However, for the tables comparing the products, not all the mentioned categories will be included due to being less important than the listed categories or not having enough relevance in the decision of the product. After each table will be a paragraph or more explaining why one product was chosen over the options, this section of the product investigation may include some of the mentioned categories that weren't listed.

Beam Splitter

Product Name	Type	Wavelength Range (nm)	R/T Ratio	Price (\$)
EO 12 x 19mm, 10R/90T, Plate Beamsplitter	Plate	400-700	10/90	29.00
EBS1 - Economy 50:50 Beamsplitter, Ø1", AOI: 45°	Plate	450-650	50/50	34.91
Newport 05FC16PB.3 Polarizing Cube Beam Splitter	Cube	~632	99/90	269

Table 19: Product comparisons of beam splitters

From the beam splitters provided above in table 19, our group will likely employ the Edmund Optics 10R/90T splitter. Its working wavelength range matches our requirements specifications and the price point is very reasonable. The difference between cube and plate splitters has little effect on the system performance, so it being a plate splitter is of no concern. Ideally, we would like a splitter with a RT ratio closer to 50/50 to ensure that enough light reaches both the profiler and power meter, but the 10/90 ratio should be acceptable, as the 10% of the minimum specified power (1 mw) is 0.1 mW, high enough to register on the profilers pixel array and the power meters photodiode. However, we should perhaps look for a model with a more equal RT ratio.

Neutral Density Filter

Product Name	Optical Density Range	Size (mm)	Variability	Price (\$)
Polar Pro VND, Peter McKinnon Edition II	0.6-1.5, 1.8-2.7	67, 77, 82 Diameter	Polarizing Rotational	250
Continuously Variable ND Filter, Edmund	0.4-1	76x24	Continuous Linear	89
K&F Concept 40.5mm Variable Neutral Density Filter Pack	0.3-2.5	40.5 Diameter	Polarizing Rotational	25

Table 20: Product Comparison of Neutral Density Filters

With respect to our design considerations and the specifications in table 20, the K&F Filter pack seems like the best choice for implementation into our system design. It meets our needs for attenuation, as it is capable of lowering the optical power density of the most extreme beam (high power, low size) to a level which wont damage the optical elements in either the power meter or beam profiler. The diameter is significantly larger than the maximum beam diameter specified, which will only make aligning the filter into the system easier, with more room for error. A polarizing rotational filter does have the possibility of interacting with a beams polarization state in an obfuscating manner, but polarization is not an element of our system so this concern is irrelevant. Besides all of these points, the K&F filter pack is also the cheapest of the bunch, and will help us meet our goal of low system costs.

Profiler Camera

Name	Price (\$)	Resolution (MP)	Pixels	Pixel Size (µm)	Sensor Area (mm)	FPS
Basler-Ace acA1300 GigE	875	1.3	1280x1024	5.3x5.3	6.78x5.43	60
MU1000B	330	10	3584x2746	1.67x1.67	6.44x4.62	35
Raspberry Pi HQ 12	50	12.3	4056x3040	1.55x1.55	6.28x4.71	30
Arducam 5	15	5	2592x1994	1.4x1.4	3.62x2.79	30

Table 21: Profiler CMOS Camera

At this point in time, it seems likely that our group will employ the Raspberry Pi HQ 12 camera system. As a RP product, it should be extremely accessible and easy to integrate into our system. At an attractive price point many times lower than cameras from optics-specific companies (see table 21), it still meets our resolution criteria. The sensor size is acceptable, and while the frames per second lags behind some other options, 30 fps should be more than enough. In addition, I have found outside examples of this camera successfully being integrated into optical systems, thus I am confident in its selection. Although the camera itself is \$50, we would have needed to buy a raspberry pi module to accompany it. This module should not exceed \$100, however, so it's still a cost-effective option.

Microcontroller/Computer

Name	Price (\$)	RAM (GB)	GPU Speed (MHz)	CPU Speed (GHz)	Operating Current (A)	USB Port Count
Raspberry Pi 4 M-B, 4GB	64	4 SD	500	1.5	3	4 Total 2 USB-2 2 USB-S
Raspberry Pi 4 M-B, 8GB	85	8 SD	500	1.5	3	4 Total 2 USB-2 2 USB-S
Raspberry Pi 3 MB	35	1	250-400	1.4	2.5	4 USB-2
Raspberry Pi 3 MB+	40	1 SD	250-400	1.4	2.5	4 USB-2

Table 22: RP Model Tabulation

*It should be noted that although the prices above are consistent across multiple vendors, issues in chip production have severely impacted backstock for practically all RP models. As such, many vendors are out entirely out of stock. Due to this, we may be forced to pay a gouged rate, or buy a RP package bundled with other items.

After careful considerations, our group is leaning towards purchasing the Raspberry Pi 4, 4GB. Processing power is superior in every category when comparing the 3rd generation to the 4th generation. While the 3rd gen models likely will perform adequately, the increased speed the newer models offer will be greatly beneficial to system operation. As processing speed increases, so too does computational speed, which would raise the frequency of the adjustor-profiler-power feedback loop, ultimately lowering the time it takes for our system to induce lasing within a cavity. 4GB of on-chip solid-state memory should be more than enough for the system, so purchasing the 8GB option would be an unnecessary financial outlay in a project were cost are both a limiting factor and a design specification. (See table 22)

Name	Price (\$)	RAM (KB)	CPU (MHz)	Operating Voltage (V)
Raspberry Pi Pico	4	264	133	1.8-5.5
Arduino Nano RP 2040	25	264	133	3.3
Msp430 FR6989IPZR	6	128		1.8-3.6

Table 23: Microcontroller Tabulation

After some thought, our group has found the Raspberry Pi Pico as the best option for our microcontroller. Ultimately, the Raspberry Pi Pico was chosen over the other microcontrollers due to it offering decent RAM and a USB-C port for a price much lower than the closest performance wise microcontroller had to offer. Additionally, being made by Raspberry Pi, the form of coding language will be the same as the Raspberry Pi 4 making integration between the two devices easier while saving our group time from having to learn the parameters of a different microcontroller.

Servo Motors

For this project it has been decided that all three motors will be servos with two of the three motors being a lower torque, rotational servo acting as the left/right knob motors and the third motor being a higher torque positional motor. Based on the information listed in table 24 it has been chosen that the left and right knob motors will be the FEETECH FT90R. This is due to the fact that the FT90R motor is best suited for our desired specifications for the motor being relatively light weight while also providing enough torque to turn the knob at a reasonable rpm. As for the horizontal motor, it has been decided that the best option will be WEISE DS3218, this is because the motor has more than adequate torque at the specified voltage of 6V. Furthermore, for cost per performance, the WEISE DS3218 was the best by a large margin. Weight and rpm are not a deciding factor for choosing the horizontal motor.

Name	Type	Price (\$)	RPM (max)	Torque (max) (Oz-in)	Voltage Range (V)
HS-5645MG	Positional	~46	55.55	168	4.8-6
FEETECH FT90R	Continuous	~8	135	21	4.8-6
FEETECH FS5106R	Continuous	~24	95	83	4.8-6
WEISE DS3218	Positional	~15	71.4	298	5-6.8
FEETECH FS5115M-FB	Positional	~22	62.5	215	4.8-6
Pololu 1248	Continuous	~13	71.4	66.7	4.8-6

Table 24: Servo Motor Tabulation

Power Supply

For this project we decided to use the MPD BH4DL as our battery supply and the 4 Slot D Cell Battery Holder as our second option in case the battery holder from digikey is out of stock or having issues being shipped. Overall, we chose the D battery pack due to the battery being able to deliver 6 volts of electricity over a longer period compared to the smaller batteries. While the MPD BH4DL is the best option so far, the battery holder may be replaced for a larger battery in the future that is able to supply at least 6V. This conclusion was reached after comparing tables 25 and 26.

Outlet Supply

Name	Price (\$)	Voltage Rating (V)	On/Off Switch
Raspberry Pi 15 Watt USB-C	8.48	5.1	None
5 Volt, 3 Amp USB-C Power Supply Adapter with Switch	6.99	5	Included

Table 25: Outlet Supply Tabulation

Battery Supply

Name	Price (\$)	Voltage (V)	Battery Type	Battery Count	Vendor
4 Slot D Cell Battery Holder	2 for 8.49	6	D	4	Amazon
Keystone electronics 2478 Holders	1.89	6	AA	4	Digikey
MPD BH4CL	3.89	6	C	4	Digikey
MPD BH4DW	4.60	6	D	4	Digikey

Table 26: Battery Tabulation

Selected Product Deep Dive

As the Product Investigation sought to determine which products we have employed within our system through brief comparisons between options, this section will act as a much more in-depth examination of our chosen products. We have outlined any potential concerns with them, and further discuss their characteristics and idiosyncrasies. As not all system elements are created with equal importance or complexity, we restricted our analysis to a select few products.

Raspberry Pi HQ Camera

Although naming conventions would imply otherwise the RP camera we have chosen for our system does not feature a custom in-house sensor array, instead opting for a Sony IMX477 CMOS sensor. With reference to the Sony provided data sheets, this subsection will be dedicated to discussing sensor elements which are relevant to our projects design specifications.

Guaranteed Temperature Allowances

Temperature Classification	Range in Celsius	Range in Fahrenheit
Operating	-20 to 75	-4 to 167
Storage	-30 to 80	-22 to 176
Performance	-20 to 60	-4 to 140

Table 27: Guaranteed temperature ranges for Sony IMX477 sensor

Through observing the above parameters in table 27, we can clearly see the RP camera will not realistically limit our systems testing environment or storage environment. As our team is located in Florida, the coldest allowable temperatures are far beyond what we could reasonably expect anywhere in the state. The guaranteed performance temperature maximums for operation and performance are both irrelevant, as testing will be in the temperature controlled CREOL building on UCFs campus. The safe storage temperature maximum of 176 degrees Fahrenheit certainly gives our group a lot of leeway, but we should still be careful to store the camera in cool, shaded locations. A good idea would be to never leave the camera in a car, storage unit, or outside.

Spectral Characteristics

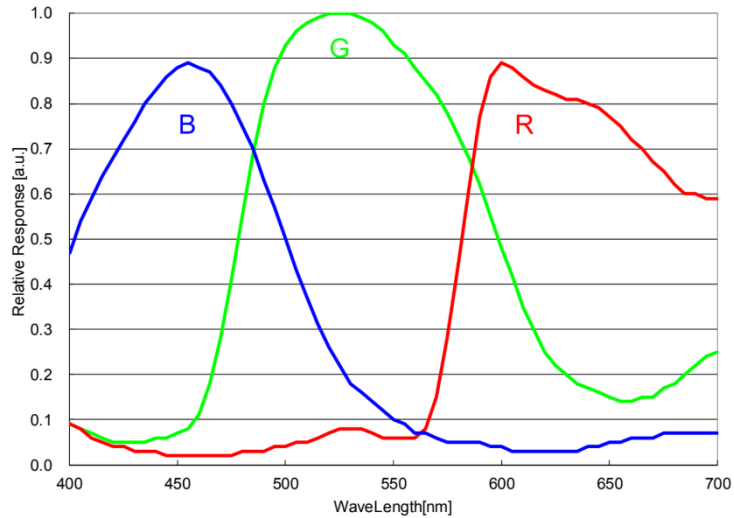


Figure 33: Spectral Response of Sony IMX477 Sensor, courtesy of Sony

As seen above in Fig. 33, the camera exhibits a relatively high and steady spectral response along our designated operable wavelength (400-700 nm). While the response does drop to around 50% near either ends of the wavelength range, this would only prove troublesome when imaging the lowest power lasers specified for use within our system (1 mW). Even in this situation, the ND filter can be adjusted or removed from the beam path, eliminating potential attenuation and maximizing incident light on the sensor array.

The differing spectral responses between the RGB cells on the sensor array are not problematic in our systems design, as the narrow emissions from lasers are not complex enough to induce a response error. Beyond this, the software logic of the beam profiler is based solely off the spatial intensity profile of the beam. A beams spectrum does not change significantly across its spatial profile, so potential intensity mismeasurements due to the sensor's response are unrealistic for lasers. A polychromatic laser could theoretically induce such errors, but as their polychromism is a function of gratings which interact with the beam post-output, there is no reason such a laser would need to exhibit its polychromism when used within our system.

Pixel Array Size

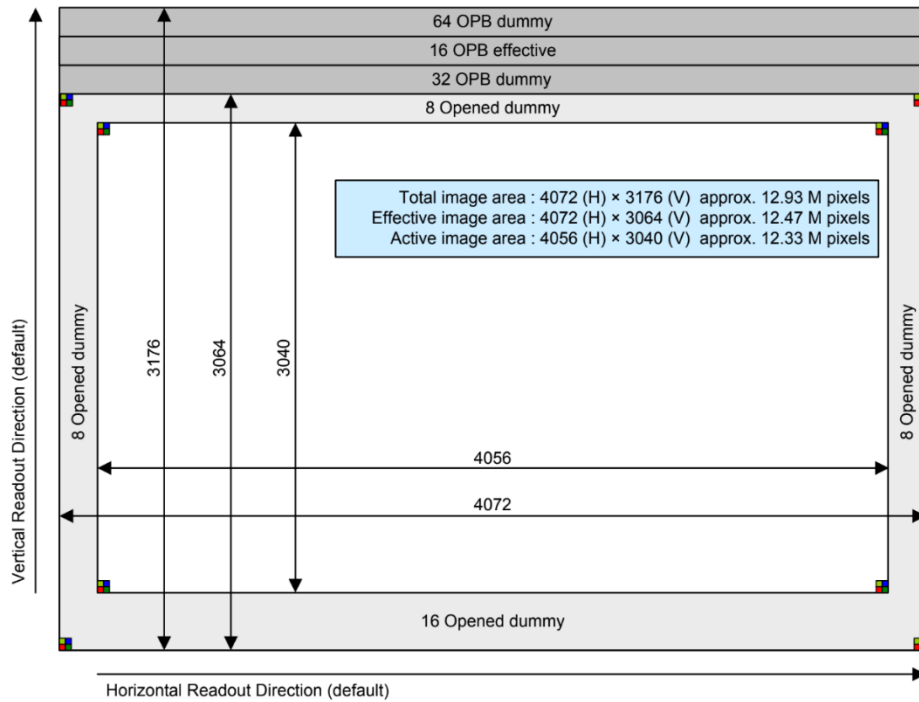


Figure 34: Sony IMX477 Sensor Dimensions, courtesy of Sony

When referencing our design specifications that state a maximum laser spot size of 10 millimeters, we seemingly are at odds with the given sensor dimensions given above in Fig. 34. The pixel size itself is symmetric, 1.55 microns in either dimension, so the vertical array size of 3040 pixels is the limiting feature of the array. Simple computation of the pixel size and the pixel count reveals the vertical dimensions of the array to be 4.7 millimeters, less than half than of the specified size! However, for multiple reasons which will be discussed further, this seeming contradiction should not actually limit our system in analyzing beam spots of 10 millimeters.

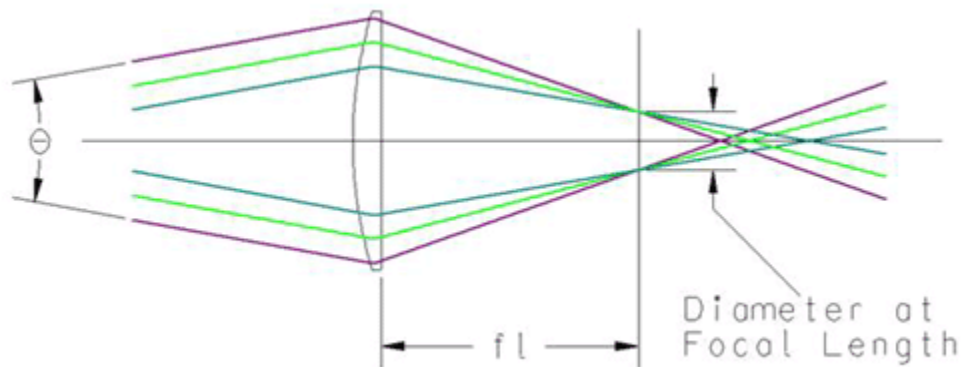


Figure 35: Focusing a divergent beam via an objective lens

The first, and most significant reason as to why the pixel array dimensions won't limit out system is that the objective lens will significantly reduce the size of a beam spot incident on the profiler. As seen in figure 35, the lens will eventually force the beam to focus, but as the beam enters the lens un-collimated, this focused point will occur beyond the beams given focal length. The spot size reduction at the focal length is predicated on the beam's divergence angle; wider divergences will cause the beam to focus 'slower' (at a distance further beyond the lens's focus) and thus increase the spot size at the focal plane. This focal plane is where the profiler will be placed in the system. While it is possible for a beam to have a strong enough divergence to where it would still exceed the size of the sensor array at the lens's focal plane, there are a few techniques that can be employed to ensure the system can still accurately characterize the beam.

The simplest of these techniques involves just centering the beam upon the profiler. Even if the entirety of the beams spatial intensity profile isn't captured by the profilers imaging sensor, as long as the 50% maximum intensity pixels are captured by the sensor, the profiler will be able to perform all of its requisite calculations in order to arrive at the simplified M^2 value. Although live imaging of the beam would fail in capturing the entirety of the beam's spatial characteristics, it is a sacrifice necessary to meet our design requirements. Even with this imaging limitation, most of the interesting beam features would be within the FWHM range so not too much information would truly be lost. If the above method fails in successfully characterizing large beam spots, there is one last technique we can employ to ensure operation. If the center of the beam (i.e. the maximum intensity pixel) is placed in a corner of the sensor array, with its vertical and horizontal axes aligned roughly along the edges of the sensor, so that the camera essentially cuts into a quarter of the beam spot, the profiler should be able to extract the required parameters (shown in Fig. 36). This is because the profiler only needs the location of the maximum intensity pixel (which doesn't need to be centered) and its relative distances in the vertical and horizontal directions to its 50% intensity counterpart in order to perform its calculations. Much like the aforementioned technique, not even the full spatial characteristics of the beams quarter-slice are needed, only the maximum and 50% maximum pixels.

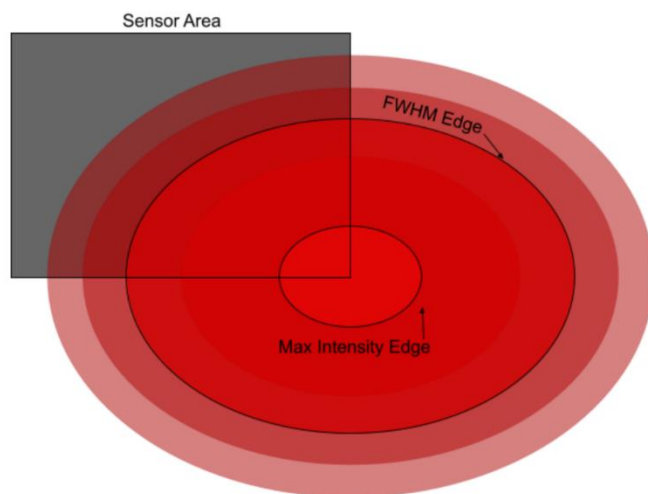


Figure 36: Visualization of Quarter-Slice technique for profiling large beam spots

This method does certainly come with some drawbacks, however. First and foremost, if the beam had any obvious asymmetries, profiling just one quarter of the spot could yield misleading data. This could be ameliorated by visually checking the beam for any clear asymmetries before profiling, or by profiling each quarter-slice of the beam and averaging the results. Obviously, the whole beam won't be incident on the camera and thus won't be fully visualized in the profiler software. Even with these limitations, the quarter slice method will still be useful in profiling larger beam spots, enabling our group to meet the preset design requirements of 10 millimeters. Usage of this technique essentially quadruples the maximum spot size that our system can profile and will likely allow us to analyze beams significantly larger than the 10-millimeter maximum specified.

Raspberry Pi 4GB

The Raspberry PI 4 will be the main component to run all the codes that will interpret the values from the power meter and camera then send signals telling the motors and lcd display what to do. The Raspberry Pi computer is produced by the Raspberry Pi Foundation, a UK based Charity Group. The specific model Raspberry Pi 4GB, is very similar to the other Raspberry Pi 4 models with the main difference being the 4 GB of ram available. Besides the ram all Raspberry pi 4 models share the following specifications in table 28:

Voltage/Current Rating:	5.1V/ 3A	Number of pins:	40
Processor:	Quad core Cortex 64 Bit SOC 1.5GHz	Power Source:	5v UCB-C, 5V GPIO Header
Temperature Range(C°):	0 -50	USB Ports:	2 USB 2.0 ports 2 USB 3.0 ports
RAM:	4GB LPDDR4-3200	HDMI ports:	2 micro-HDMI with 4k 60 fps
Camera Port:	2-lane MIPI CSI	Display Port:	2-lane MIPI DSI
Video Port:	4-pole stereo audio and composite video	Connectivity:	5.0 Bluetooth, BLE Gigabit Ethernet
GPIO pin header ratings:	3.3V, 5 V	Operation temperature (Celsius):	0-50
Vendor:	The Pi Hut	Price (\$):	85

Table 28: Raspberry Pi 4 4GB specification

Raspberry Pi Pico

The Raspberry Pi Pico will be the microcontroller implemented into the pcb design that will communicate with the computer and send commands to the motors. Raspberry Pi is produced by the company Raspberry PI foundation, a UK based charity organization. This model was introduced to the market in January 2021 and will continue to receive support till 2028. The raspberry pi uses the RP2040 microcontroller chip designed by Raspberry Pi and was designed for PCB use. The Raspberry Pi Pico has the following specifications below in table 29.

Voltage/Current Rating:	1.8-5.5 V/3A	Number of GPIO pins:	26
Microcontroller Chip:	RP2040	Ports:	1 USB-c
Ram (KB):	264	CPU (MHz):	133
Memory:	2Mb onboard QSPI Flash	Timer:	Accurate on-chip clock
Dimensions	51mm x 21mm	Channels:	2×SPI, 2×I2C, 2×UART, 3×12-bit ADC, 16×controllable PWM channels
Vendor	The Pi Hut	Price (\$):	4

Table 29: Raspberry Pi Pico specifications

FEETECH FT90R

The FEETECH FT90R is a continuous servo motor that will act as the two left/right knob motors for the project. The FEETECH FT90R is a very common servo motor and can be found at many vendors such as Amazon and Digikey. Of all the motors it was the cheapest at \$7.99 at most vendors. While it is believed to be able to deliver enough torque to turn a knob, test will be done to determine its performance. Additional information regarding the performance of the servo motor is as follows in table 30:

Voltage Range	4.8V-6V	Weight(grams)	9
Max RPM	135	Min RPM	108
Max Torque(oz-in)	21	Minimum Torque(oz-in)	18

Table 30: FEETECH FT90R specifications

WEISE DS3218

The WEISE DS3218 is a high torque positional servo motor. Of all the options the WEISE DS3218 offered the best performance in torque for the price. The WEISE DS3218 like many of the positional servo motors listed are originally design for remote control vehicular use. When searching for the specifications of the motor, there was no data on the accuracy of the motor to turn to a specific angle, as a result, tests will need to be done to determine the quality of the more. Other specification of the WEISE DS3218 are listed below in table 31:

Voltage Range	5V-6.8V	Weight(grams)	99.8
Max RPM	71.4	Min RPM	62.5
Max Torque(oz-in)	298	Minimum Torque(oz-in)	263.86

Table 31: WEISE DS3218 Specifications

Vendor Discussion

While obviously not as important as the parts themselves, the decision of what vendors to use when ordering said parts nevertheless is an element of project development which warrants consideration. In this section, we discussed the vendors (see tabl 32) we expect to use for various elements of our system, both in broad generalizations (Optical Components, Electrical Components, etc.) and in more detailed case-by-case examples (Camera, Photodiode, etc.)

Vendor Options:

Vendor	Country of manufacturing
OSH Park	United States
Sunstone Circuits	United States
Advanced Circuits	United States
PCBWay	China

Table 32: vendor comparisons

Optical Components

Our group is anticipating that many optical elements can be borrowed through various entities within CREOL. Currently, we are being lent an open cavity laser and its couplers via Dr. LiKamWa's research group. Many components needed to integrate

elements with an optical breadboard, such as posts, mounts, and holders, are available through either the senior design or teaching labs at CREOL, as well as the optical breadboard itself. For parts we would have to purchase, there are a variety of vendors we could use. Integral components, which need to be free of aberrations and defects, optic-specific manufacturers, such as Edmund or Newport, should be used to guarantee quality. Both of these companies have excellent support centers as well, so any issues we have with products purchased from them should be relatively easy to solve. For less important components, we could likely purchase them from Amazon or another mass retailer, where bulk purchases are significantly cheaper than from optic-specific brands. Although optics purchased from a mass distributor would likely be of lower quality, we would restrict these purchases to elements we expected to break and replace, or where the optical integrity of the elements is not of particular importance.

Raspberry Pi Hardware

Surprisingly, Raspberry Pi does not sell any hardware directly from its website. A product page on the RP domain will send you to a list of RP approved reseller if one attempts to purchase a product. There are a number of companies listed, including Adafruit, Digi-Key, Newark, and Cana Kit. Our group should try to limit purchases of RP equipment to these retailers. However, we have found that many products are currently out of stock. Because of this, we would have likely have to use third party retailers like Amazon to purchase these components. This is unfortunate, as these retailers rarely have good customer support centers or any guarantee on product authenticity. To avoid this, our group may decide to purchase a Raspberry Pi bundle, which contains the RP 4B model, power source, and various other components at a reduced cost compared to buying the elements ala carte. While we would likely end up with superfluous components, many of these bundles are still in stock at reputable resellers. In addition, the cost of the bundles does not significantly exceed the combined costs of the necessary Pi elements.

Layouts and Printed Circuit Board (PCB)

This section is dedicated to the discussion of layout/schematics of the components for the project specifically the PCB. There are three main segments that make up this project, these segments will include the Raspberry Pi computer, PCB board and user display. Important details that will be included in the discussion will be how each segment will be connected to each other, a brief overview of the layout of the segments, and for the PCB, a more detailed schematic based on the Autodesk Eagle program will be provided.

Raspberry Pi Computer

The raspberry pi computer (shown in Fig. 37) will be the centerpiece of the design being responsible for processing the values from the sensors and determining what the motors will do in response. Both the laser sensor and the motors are part of the PCB being directly connected to the microcontroller as a result, the computer cannot send commands directly to the components. To send and receive signals to the PCB, the Raspberry Pi

computer will be connected via a USB-C cable and will send instructions through Uart messaging. The components of the project that involve the user interface will be connected directly to the Raspberry Pi computer with three input buttons being connected to pins , and. The led display showing the modes and results of the coding will being connected to one of the two html ports included in the computer. The last component being connected to the computer will be the Raspberry Pi HQ computer which will be connected through one of the USB ports.

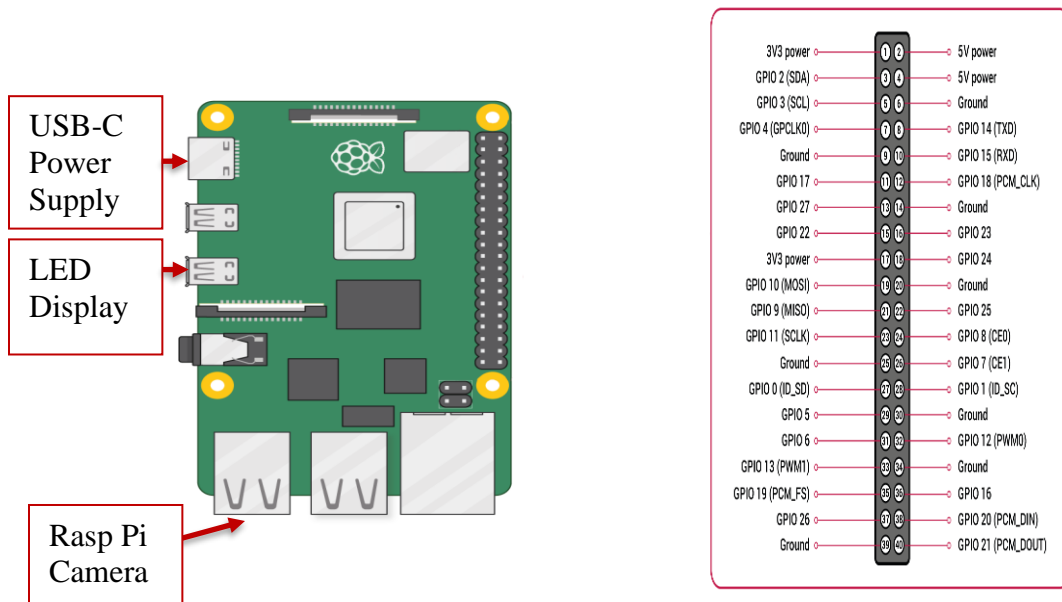


Figure 37: Connections to Raspberry Pi

PCB Power Meter Design

For Senior design 1 the original plan for the PCB was to have a 6v 4xD battery holder, a light diode with resistor and capacitors, and the Raspberry Pi Pico (shown in Fig. 38). While the Raspberry Pi computer will be where the main code will be held the Raspberry Pi Pico will be responsible for sending instructions to the computers and receiving the values from the light diode. The Raspberry Pi Pico will communicate to the computer using a USB-c cable which will send Uart instructions. Initially it was planned to power the microcontroller through the battery with a voltage converter, however with the USB-c connection the system will receive power from the computer instead.

However, for the final PCB design there were several alterations that occurred due to several reasons including component supply, change of goal priorities from SD1 to SD2 and time constraints. For this project, designing of the PCB board was done on Autodesk Eagle software. As seen in figure 38, the power meter and the mirror mount motors were relocated to each side of the Raspberry Pi Pico with the mirror mount motors dealing with pins 1-20 while the power meter is connected to various pins between pins 23-38. Though

the PCB contains the power meter and the motor system, initially the plan for the PCB was to include much more such as the power supply and multiple voltage converters. However, over the course of the project the PCB design drop the mentioned components for several reasons. For the voltage converter the main reason as to why it was dropped was due to supply shortages. When designing the voltage converter, the website Webench was used, but for each design the same issue occurred where key components were out of stock, eventually making a DC converter unfeasible with the projects time restraints. As a result of this, a prebuilt DC converter was bought instead. For the voltage supply, a BHDL4xD battery pack was used, however, having a whole area on the PCB for the battery pack proved unnecessary. Its spot aboard the PCB was replaced with pin holes connected to the ground and voltage inputs of all the major components. As a result of the constant changes, additional pin holes were placed in the PCB board, mainly for ground voltage inputs and voltage outputs. These acted as redundancies in the PCB design, in case of any more problems arising while developing the project

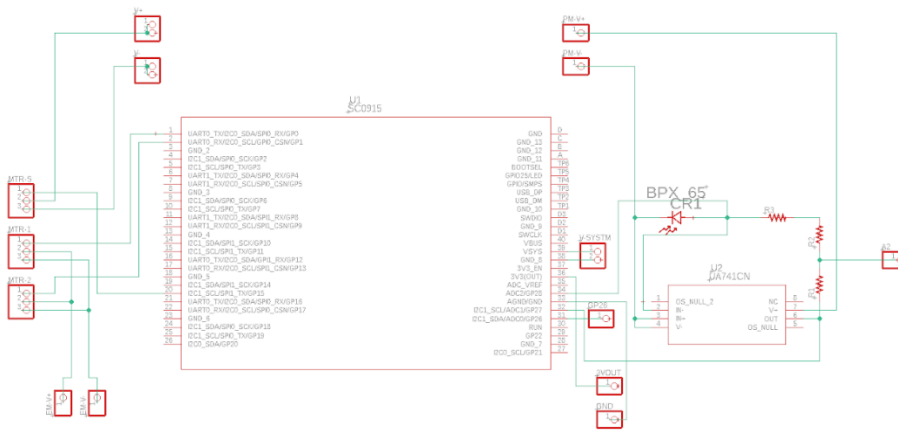


Figure 38: Schematic design for the power meter

User Interface

Originally the plan for the layout of components involving the user interface was to be three to four touch push buttons and the Raspberry Pi LCD display. The display will be connected to the computer through one of the micro-HDMI ports while the buttons will be connected to GPIO pins 17, 27, and 22. However at the end of the project it was decided to have all the user interface be relocated to the PC desktop as the PCB was already going to be connected. All the interaction between the user and the machine was going to be on the code using the micro-python program.

Testing

Included in this section are an outline of a number of tests we expect to perform over our project's development, as well as a brief summary of some considerations we should consider for conducting said tests.

Considerations

Testing will be restricted to labs within CREOL, either in the undergraduate laboratory or the Senior Design laboratory. This is because laser systems require high levels environmental stability, which can be ensured with the usage of the optical breadboards found in CREOL. As we would be performing our tests in CREOL, members of the group are subject to the rules and regulations of the facility. Any violations of these rules and regulations can lead to disciplinary action including-but not limited to-losing permission to access campus labs.

Component Tests:

Note: When Using Hantek 2D72 3-in-1

The Hantek 2D72 3-in-1 has function generator capabilities that allow one to produce a range of different AC profiles with varying frequency, voltage amplitude, DC offset, and duty cycle. However, there is no option for DC supply. In many cases throughout testing, it is of importance to utilize a DC supply for constant voltage. In order to accomplish this, one can rectify the AC signal of the function generator into a DC signal by means of a Wheatstone bridge, as depicted in fig. 39.

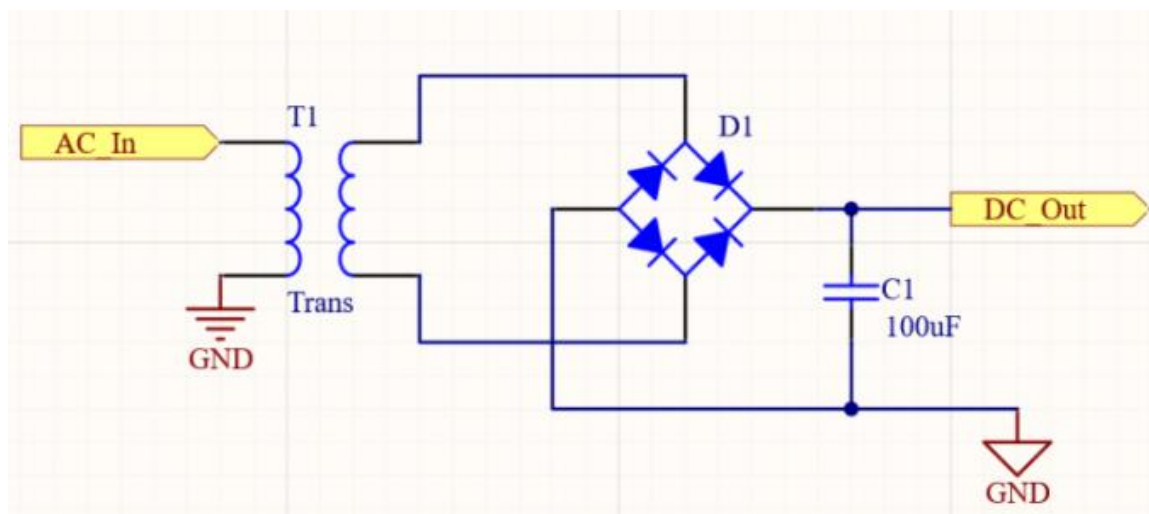


Figure 39: AC to DC converting circuit for Hantek voltage supply

Passive Components:

Simple tests of the passive components being used in the project can be conducted with a multimeter to determine their deviations from their expected values and whether any components are faulty. This would include performing resistance measurements across resistors to determine their true resistance, capacitance measurements across capacitors to determine their true capacitance and diode measurements across diodes to determine their true diode capabilities. An example of how values can deviate is given in Fig. 40.

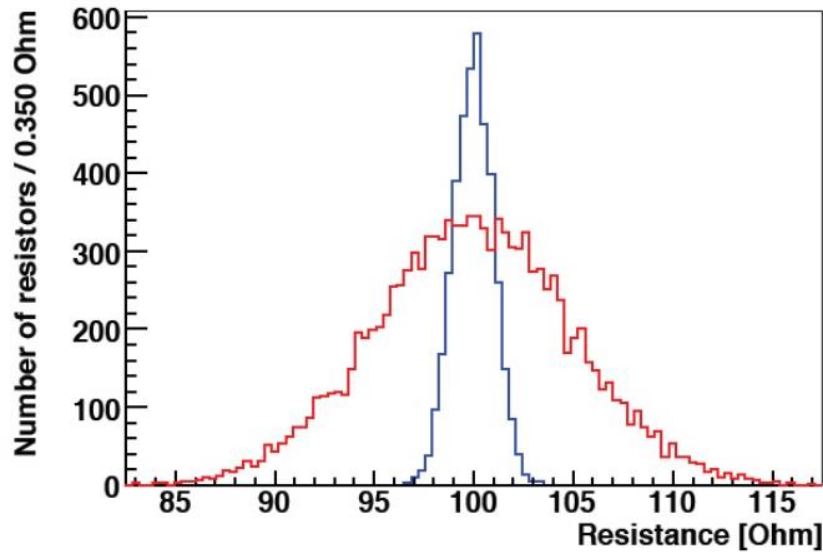


Figure 40: Graph depicting variance of true resistance values

Operational Amplifier:

The operational amplifier for the optical power meter holds the task of maintaining the voltage across the photodiode at a virtual zero volts. This can be tested for by supplying a current source through where the photodiode would be placed within the transimpedance amplifier configuration and measuring the voltage at the positive node of the current source.

Analog-to-Digital Converter:

The ADC for the optical power meter holds the task of converting the analog voltage of the load resistor within the transimpedance amplifier setup into a digital voltage to then be read by the Raspberry Pi GPIO pins. It is of importance that the ADC returns the correct digital signal for a given input analog signal. In order to test this, we take a variable DC power supply that can output and sustain a constant voltage of our choosing. This the voltage would then be fed to the analog input of the ADC. The subsequent digital signal of the ADC would be read using an oscilloscope and compared against what the expected digital value should be. This would be repeated for every pair of input pins and output pins for the given ADC.

Beam Profiling Camera:

Testing the camera is simple and consists of ensuring that a live feed of the image sensor can be obtained and quantized on the connected RP computer. This image should be visually inspected for color accuracy, dimensions, and other obvious errors.

Photodiode:

The first test of the chosen photodiode will be that of a simple photovoltaic mode configuration, consisting of the photodiode and a load resistor in series. A voltmeter will be attached in parallel to the load resistor and an ammeter will be attached in series between the photodiode and load resistor, as depicted in Fig. 41. Since the photodiode will be operated in the photovoltaic mode, no external bias voltage will be required. A range of laser light powers of known power and wavelength will be measured by a Newport optical power meter. These ranges of incident light powers will then be shone on the photodiode. Measurements of the produced photocurrent and subsequent voltage will be taken to determine performance of the diode.

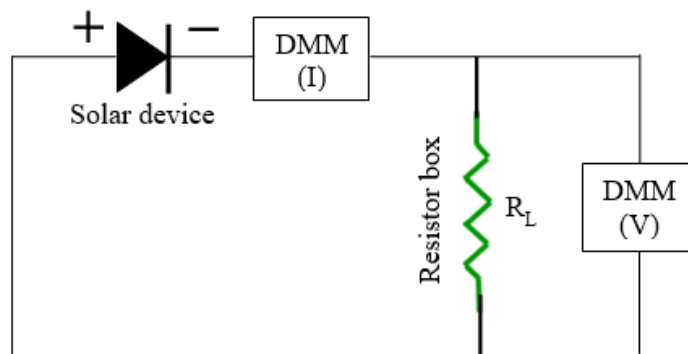


Figure 41: Simple testing configuration for photodiode

The second test for the photodiode would be that of an actual transimpedance amplifier configuration, so as to determine the photodiode's performance in such a situation.

ND Filters:

A range of known laser light powers will be shone through the filters and measured by a Newport optical power meter on the other side to determine the attenuation capabilities of the filters. It would also be of importance to perform this test for various transverse locations across the ND filters, to ensure that the power attenuation is constant across the surfaces of the filters.

Lenses:

Light of various distances from the lens and divergences will be shone through the lens, while measuring the location and subsequent spot size of the focal point. The determining of the spot size can be done using a variety of methods such as the knife-edge method or simply imaging the spot onto a camera. If we utilized the CCD camera found in the CREOL undergraduate lab, we would be able to image the focal point of the lens onto the camera and use the accompanying software to determine the diameter of the spot size in terms of pixels of the camera. Knowing the sizes of the pixels of the camera, we would then be able to calculate the true diameter of the spot. In order to measure the location of the focused spot, we would utilize an optical rail with ruled markings to measure the distances between components setup on the rail itself such as the light source, lens, and camera.

Beam Splitter:

There are two major elements to consider when testing the beam splitter. First, that the split beam exits the element at the expected normal orientation, and second, that the reflected and transmitted beam powers match the expected ratio. Testing both of these elements can be done simultaneously with a single set up, as depicted in Fig. 42. Using an optical breadboard is necessary, but that can be done in CREOL. First, we should align the beam splitter along optical breadboard bores, confirming that the actual output orientations match the expected and that beam leaves normal to the splitter faces. If optical power meters are placed along each beam path, the R/T ratio can also be checked. The beams output power should be noted as well, to see how much power is absorbed via the beam splitter.

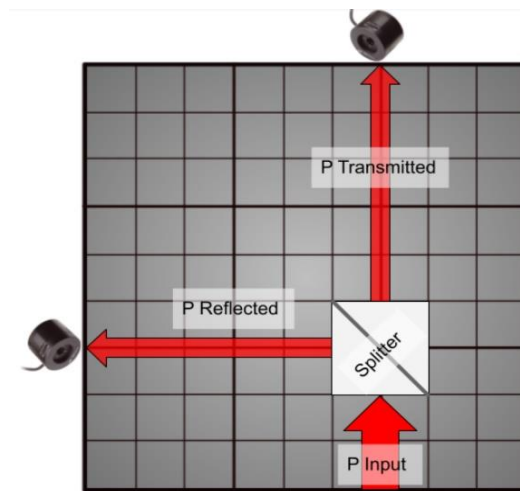


Figure 42: Beam splitter testing configuration

System Tests:

Power Meter Accuracy Test:

As the power meter is a central tenant to the operation of the system as a whole, it is of utmost importance to test its accuracy in measuring power. This could be done by using a source with a known power output. However, testing via this method could be susceptible to defects in the source and the presence of ambient light sources in the test setting. These could both alter the power incident on the meter, leading to a power reading that differs from the stated output power of the source and leading to the meter to be deemed falsely inaccurate. Another drawback of this testing method is that many different sources with defined power outputs would be needed to check the accuracy of the meter at different wavelengths. A superior method of testing would be to alternate testing a source with the group made power meter and one or more factory-made meters. Comparison between our own meter and the factory meters would then confirm or refute our devices accuracy. This method is less susceptible to inaccuracies, as the testing setting would be nearly identical for all the meters, reducing the potential for any inaccuracies due to ambient light. While there is a possibility for a factory-made power meter to incorrectly measure the source—thus skewing the apparent accuracy of the group device—the use of multiple power meters would seemingly eliminate this possibility, as the likelihood of multiple factory meters having identical power misreadings would be exceptionally improbable.

Phototransistor Power Meter Demonstration:

A physical demonstration of a rudimentary optical power meter was constructed as a proof of concept for the project. This demonstration was constructed using the components outlined in table 33.

Electrical Breadboard
Hantek 2D72 3-in-3
HeNe Laser
2kΩ Resistor
10MΩ Resistor
100μF Capacitor
22pF Capacitor
Phototransistor (3DU5C)
Diode
Operational Amplifier (UA741)

Table 33: List of parts for demonstration

Upon attempting to utilize the phototransistor in the photoconductive mode as one would operate a photodiode, i.e. without a bias voltage applied to the circuit, There was no relationship between the measured voltage across the load resistor and the amount of light incident upon the phototransistor. It was thus determined that the phototransistor could not be utilized in the photoconductive mode as a photodiode would be. The transimpedance amplifier circuit as outlined in Fig 43 was used in order to apply a bias voltage to the circuit to gain this light-voltage dependence that we sought.

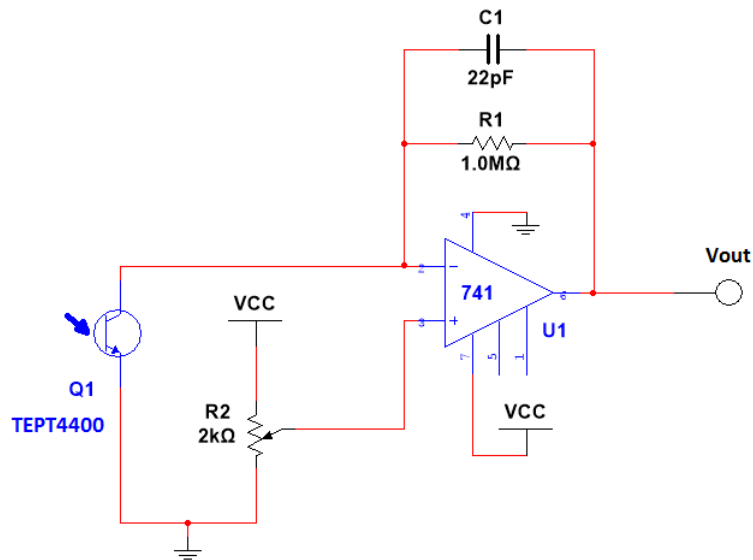


Figure 43: Circuit diagram used for demonstration

Various resistances for the load resistor, R1, were tested to determine which seemed to provide the best response given the circumstances of the testing environment. This demonstration was performed in the undergraduate teaching lab, in which the lights were fully on, creating a rather high ambient light amount.

With this test, the success of the results was not completely ideal, but still promising. When the laser light was not incident upon the phototransistor, the multimeter read a certain voltage that indicated the background (this included the dark current of the transistor and the ambient light of the testing location). Upon bringing more laser light upon the phototransistor, the reading on the multimeter began to increase. This is the exact response we wish to see for the functionality of increasing the output power of the laser.

However, at a certain point of scanning the laser beam across the face of the phototransistor, the voltage being measured across the load resistor capped and did not increase further for greater incident light. This indicates that the phototransistor was saturated before the laser light could reach its maximum incident power.

SBD and Motor Quality Test:

This test will be used in order to understand the qualities of the motors used to adjust the angles of the mirror. Some of these tests will include measuring the rotations per minute of both motors at various rates of power. The goal of these tests is to compare the two motors to find any difference in performance and allow us to determine the gear ratio needed to adjust the knobs of the mirror. The next test of the motors is to see how close the change of angle made by the motor is to the actual change of angle. This is done to measure the accuracy of the motors being used.

Software Test:

Unit tests will be performed throughout the development process to ensure that individual functions are able to produce the expected output given specific inputs. AJ will use a sigmoid function to test and simulate the functionality of aligning the mirrors to increase the output power of the laser. The input of the function will be defined by the degrees of separation between the two mirrors. The output of the function will be the power of the laser in watts. The program will be given a random input angle for both mirrors and will need to find the most efficient way to make them parallel by using the power of the laser to check if it is correct.

Fiber Optic Proof of Concept Test:

After ensuring both the adjuster system and the power meter are working individually, we seeked to test the combined mechanism. This will be done by attempting to optimally couple a fiber to a light source. We deem this a valid proof of concept test because much like the couplers in a laser cavity, a fiber coupling is adjusted by rotating knobs which control minute displacements of the fiber head in three orthogonal dimensions. As the laser cavity couplers are only changeable in two dimensions, this proof-of-concept test will only alter the x and y dimensions of the fiber. Due to the dependence on the three-dimensional adjustment to reach optimal power, before testing we hand-adjusted the fiber to optimal, before randomly displacing it in the x and y dimensions. After this, we connected the adjusters and test if the system can return the fiber to its optimal x-y coordinates.

A schematic of the test is included below in Figure 44, but the basic layout is as follows: First, the fiber will be stripped, cleaned and cleaved on either side, with one end being placed into an adapter feeding directly into our power meter, mitigating almost all background light. The other end will be linked into a coupler, which is then fed through a fiber adjustment mount. It is this adjustment mount that our group's adjusters will connect to and alter. The bare end of the fiber attached to the mount will then be placed closely to a light source.

There are three potential options for the source: an LED, laser diode, or normal laser. An LED would be the simplest and cheapest option, but it's output power would be difficult to gauge due to its large cone of emission. Thus, determine whether the fiber

couples successfully (transmitting approximately 50% of source power) is infeasible. However, as we would first manually couple the fiber to the light before running the test, we could simply observe whether or not the adjusting system returns the output power to the hand-tuned power level. The laser diode is also relatively cheap, and it would have a known output power. LDs emit a somewhat elliptical output, obviously at odds with the cylindrical structure of the fiber. They also feature strong beam divergence, due to the physical parameters of the semiconductor. So to truly couple the fiber and the diode, we would need an intermediary cylindrical lens between the two optics to mitigate the elliptical misalignment and beam divergence.

In addition, retro-reflections from the fiber head onto the diode could damage its internal elements, so the fiber would have to be rotated slightly off axis with the diode. A normal laser would also require a focusing lens to reduce divergence, however, as the beam diverges less the lens would require less power, and likely be cheaper. The potential for retro reflections still exists, and the whole lasing system would certainly be more expensive than a laser diode or an LED, but one could likely be borrowed from CREOL. While every potential light source has a drawback, due to the comparative cost of the LED, and the simplicity of the set up, we conducted the test using an LED, even though we would not be able to validate whether the light is coupled to 50% of the input power.

Ultimately, this test will be considered a success if the automatic adjusters can process readings from the power meter and use them to inform their positioning. This will be demonstrated by the auto adjusters returning the fiber to its optimal placement for maximum output power in the x-y plane.

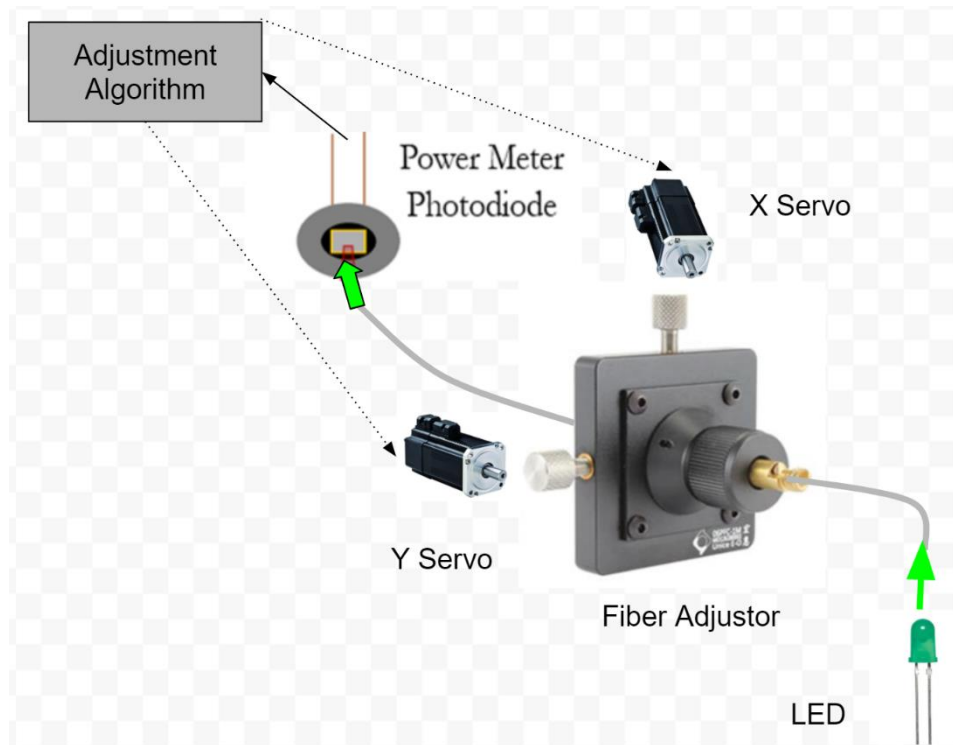


Figure 44: Fiber Optic Coupling Proof of Concept Test

Basic Mode Analysis Test:

The basic mode analysis test would be conducted to determine the effectiveness of the beam mode analyzing portion of the design in determining the quality of a single mode. This test would require the use of a laser whose spatial profile and beam characteristics are predetermined and known to us. An easy option for such a laser would be a (insert part number here) HeNe laser utilized in the CREOL undergraduate teaching lab. This laser produces an output optical power of about 1.5mW and has a well-defined TEM01 spatial mode profile, beam waist, and divergence. The test would consist of verifying these characteristics of the beam with standard manual methods.

Upon verifying the characteristics, the automatic beam profiler would be used in an attempt to attain the same results. The differences in the two sets of data would be compared and adjustments made to reconcile the differences. The manual tests to obtain reference data would be predicated off measuring, by hand, the beam radius at different far-field distances. After this, the data should be combined graphically, and the slope of the line determined. Then, taking the inverse tangent of the slope would yield the divergence half angle. As this method uses more data points than the first method described in Mode Quality Measurements: Beam Divergence, it should yield a more accurate angle. The other values are extrapolated from this divergence, so no further hand measurements are required.

Advanced Mode Analysis Test:

The advanced version of the mode analysis test would look similar in methodology to the basic test. However, in this case a different laser that can produce multiple different modes or several different mode lasers will have to be used. In this test, the methodology of the basic test would be repeated for several different modes.

Beam Profiler Measurement Test:

Before integration into the system, the beam profiler must be shown to accurately obtain its measurements of beam divergence and spot size. Only these two need to be measured, as other measurements are extrapolated from these two. Initially for this test, the profiler will analyze the beam and output its findings. The spot size will then be checked by replacing the profiler with a screen and manually measuring the size of the beam. Divergence will be confirmed by then moving the screen away from its original position and re-measuring the beam spot. After obtaining enough data points, the relative spot sizes can be graphed, and the divergence angle can be garnered from said graph.

Final Test:

The final test will fulfill the project goal of automatically adjusting a laser's output couplers until lasing is achieved. In a similar manner to the Proof-of-Concept Test, the automatic adjusters will be connected to the x and y displacement knobs of both couplers. (See Figure 45) While the PoC test only controlled two knobs on a single adjustment frame,

the Final test will control four knobs total on two separate couplers. One the couplers is fully reflective, while the other only partially so. The laser output emits from the partially reflective coupler; thus the power meter will be aligned directly behind this coupler. It should be noted though that the photodiode in the power meter could potentially become oversaturated if exposed to a laser of high wattage, so we have been cognizant of this and take any further measures to protect the integrity of the photodiode, if needed.

After the power supply to the laser is turned on, the power meter will begin to detect some sub-lasing photon emission from the cavity, and the automatic adjustment process will begin. An adjuster connected to the x or y knobs on either coupler (the order is arbitrary) will begin to alter the knob in an attempt to find a local maximum power. It will do this in a scanning manner by rotating the knob a significant amount, storing where a local power maximum was detected, and reverting its position to that maximum. After this is accomplished by one adjuster, the orthogonal adjuster on the same coupler will perform an identical process to the one described above.

Once both adjusters on a coupler have completed a dimensional alteration cycle, the process will begin again on the other coupler, and so on and so forth. (Figure 4 contains a block diagram of the feedback loop) It is difficult to estimate a realistic number of cycles for the process before the cavity lases, but the goal is to achieve lasing in under five minutes. Even if this condition can't be met, if the cavity can be made to lase at all, the project will be considered a success, as the process's speed could certainly be improved with more expensive motors and optimized software. As mentioned in the PoC test, there must be some precautions taken during this test. A retro reflection off the power meter could reflect back into the lasers optics and severely damage them, so we should displace the meter angularly off axis with the laser cavity. In addition, the photodiode in the meter's operating range should be considered and compared to the laser's output wattage to ensure its integrity.

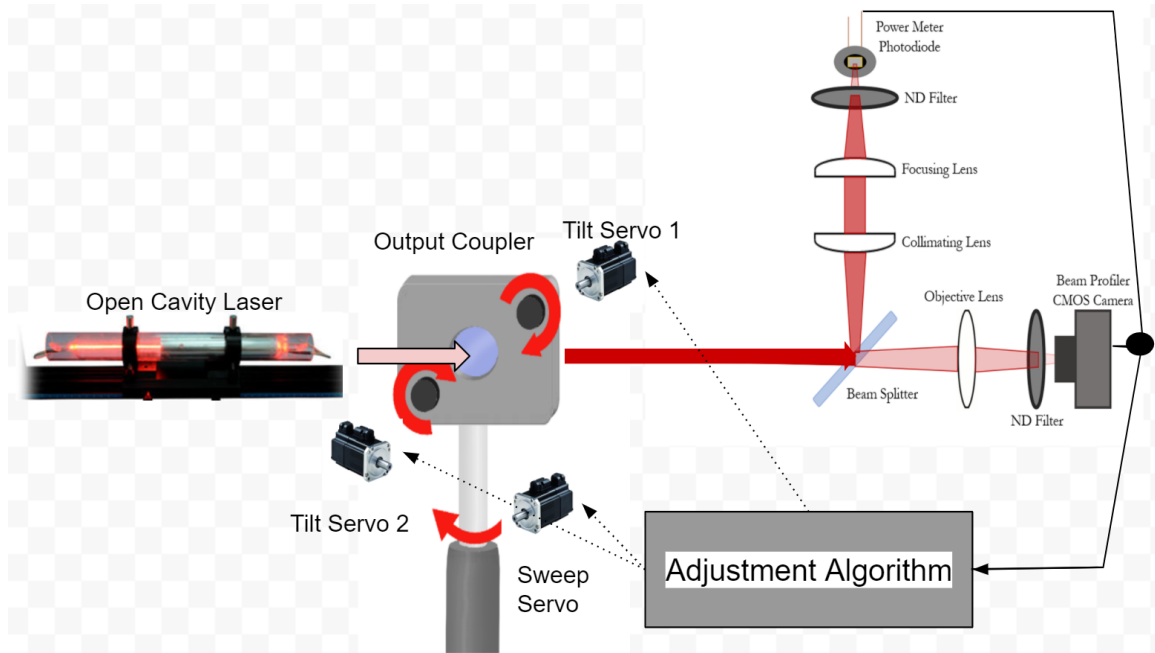


Figure 45: Final test diagram

HOUSINGS

One of the primary design challenges our group faced in developing this project was how to interface between the output coupler adjustment knobs and the motors themselves. While the coupler has only two knobs, one for vertical tilt and one for horizontal, our experience with manually achieving lasing had taught us that one of the best methods involved performing large rotations of the coupler itself, performing a sweep, in essence. To perform this type of sweep, we realized that we would need to be able to rotate the optical post upon which the coupler rests. The knob rotation was decided to be controlled by the continuous motors, while the post rotation would be dictated by the servo motor. For the adjustment knob interface, our group designed a ring-like holder with a notch separating the two ends, allowing the ring to bend and expand in order to fit around knobs of different sizes. A triangular protrusion was then created on the back face of the ring, which we affixed the continuous motors rotating propellor to. This design was then 3-D printed with plastic filament. The plastic offered very low friction with the metal of the adjustment knobs, so to ensure that the two would move in unison, we applied tacky electrical tape to the inside of the ring, greatly increasing friction and allowing the mount knobs to be turned with the rotation of the motors.



Figure 1, Adjustment Knob Mount

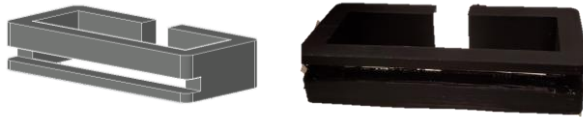


Figure 2, Adjust Motor Housing

Unless the knob motors themselves are anchored in a fashion that restricts their movement, rotation of the motors would simply rotate the motor housings rather than the adjustment knobs. To circumnavigate this issue, a motor casing was designed to house both motors to keep their position static as they applied torque to the adjustment knobs. Other considerations had to be accounted for when designing this casing, as it would need to have a negative space clearing in order to allow the beam of the laser to pass through unobstructed. Furthermore, the wires of the motors had to retain their connection to the adjustment systems PCB, explaining the small slit on one edge of the casing. Also important was the fact that the casing could not be hard fastened to the optic mount itself as the stand motor would rotate and alter the casing's position.

As well as this, a mechanism for rotation of the couplers post had to be designed, since the positional servo motor could not be easily located underneath or above the couplers mount in order to rotate it about the axis of the optical post. The rotation of the positional motor was simply translated linearly to the location of the stand post via two arms and a spacer for the post to allow the stand to be rotated at a distance by the motor. The two elements below with holes on either end are the arms, whereas the piece with the circular ring extrusion wraps around the coupler's optical post. This piece also has a hole bored into its side, to allow for a screw to be threaded through it and ensure maximum friction between the coupler post and the part. On the other side of the arms lies the piece which connects to the servo motor. This connection was created by etching an imprint of the servo motors propellor into the bottom of the piece and recessing it deep enough to allow it to fit snugly over the propellor.

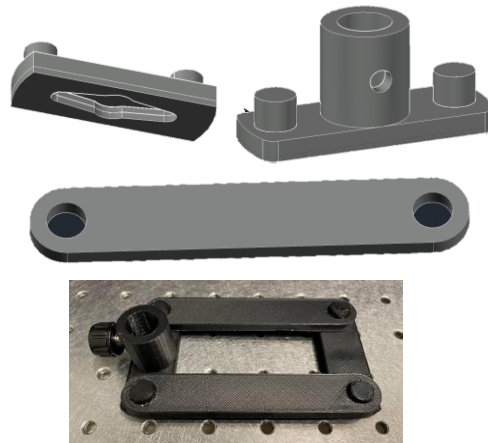


Figure 3, Coupler Servo-Motor Interface

The final parts our group had to develop and design were a mounting table for our optical elements and a housing for the positional servo motor. Early in the development of these parts, we decided to connect the two so we could reduce the number of optical posts used in setting up the system. By doing this, the total number of posts in set-up is 3, with only one of those posts being needed for our parts (1 post for the laser, 1 for the coupler, and 1 for the optics table). The design of these elements was relatively simple; the main concern was ensuring that our optics and the servo motor's center of rotation would be aligned along the same axis as the beam. Surprisingly, the servo motors center was skewed toward the side, requiring us to slightly redraft our design for the servo cage on multiple occasions. Another consideration in the design was making it so that the required spacing between this unit and the coupler was easily identifiable, thus we purposely spaced the elements so that the distance between the optical posts of the cage-mount unit and the optical post of the coupler unit are spaced 6 bore holes apart on a standard optical breadboard, roughly 6 inches.

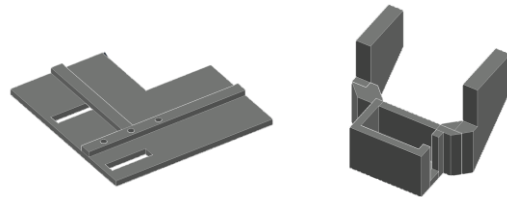


Figure 7, Optical Track and Stand Motor Housing

Project Budgeting and Finance

This section will contain tabulations for the various expected expenditures our group will incur over the development of this project (tables 34-40). Costs will be separated by their designation in either Electrical, Mechanical, or Optical categories. Due to the large number of optical elements in the system, the optical elements will be further sub-divided based off their involvement in either the beam profiler or power meter. If they are found in neither subsystem, they will be categorized as miscellaneous optical. Some cells within tables may be highlighted, explanations for these will be denoted. Furthermore, we have included price ranges for certain elements which we are undecided upon. These ranges are reflected in the sub-tallies and final price tally. Due to the volatility of component pricing (especially in a stunted semiconductor supply chain) and the hidden nature of shipping and convenience costs, it is probable that true costs will exceed the listings below. At the moment, we are borrowing many system elements from various CREOL professors and research labs. If they decided to withdraw the lent-out materials, the projects price could significantly increase.

Electrical Components:

Component	Price Range (\$)	Count	Total (\$)
LM2596 DC converter	10.99	6	11
Raspberry Pi 4 2GB	62.45	1	55
Raspberry Pi Pico	8	1	8
Raspberry Pi USB-C Charger	0	1	0
PCB	23.76	5	23.76
Total			127-136

Table 34: Electrical components

Mechanical Components:

Component	Price Range (\$)	Count	Total (\$)
Clamps	7	20	7
Gear/ Pinion Set	0	0	0
WEISE DS3218 positional motor	15	1	15
FEETECH FT90R continuous motor	14.95	2	16
Total			38

Table 35: Mechanical components

Optical Components:

Power Meter

Component	Price Range (\$)	Count	Total (\$)
-----------	------------------	-------	------------

Photodiode	10 - 16	1	10-16
Attenuator	21 - 30	1	21-30
Laser Cavity	Borrowed	1	0
Laser Pump	Borrowed	1	0
Output Couplers	Borrowed	2	0
Coupler Mounts	Borrowed	2	0
Total			31-46

Table 36: Optical Components (Power Meter)

Beam Profiler

Component	Price Range(\$)	Count	Total (\$)
Focusing Lens	50-100	1	50-100
CCD Camera	150-200	1	150-200
ND Filter	30-100	1	30-100
Total			210-400

Table 37: Optical Components (Beam Profiler)

Miscellaneous Optical

Component	Price Range (\$)	Count	Total (\$)
Beam Splitter	10-50	1	10-50
Optical Fiber	3	<1 Foot	3
Bare Fiber Adapter	Borrowed	1	0
Mounted Fiber Adapter	Borrowed	1	0
Bare Fiber Coupler	Borrowed	1	0
Total			13-53

Table 38: Miscellaneous
(Highlight Denotes Materials used for Proof-of-Concept Test)

Combined Optical

Classification	Cost (\$)
Power Meter	31-46
Beam Profiler	210-400
Miscellaneous	13-53
Total	257-499

Table 39: Combined Optical Costs

Replacement Cost

Component	Cost (\$)
Raspberry Pi Camera	90
Raspberry Pi Pico	8
FS90R rotational servo	15
Total	105

Combined Component Cost

Component Classification	Cost (\$)
Electrical	127
Mechanical	38
Optical	205
Replacements	105
Total	476

Table 40: Combined component costs

House of Quality Trade-off Table

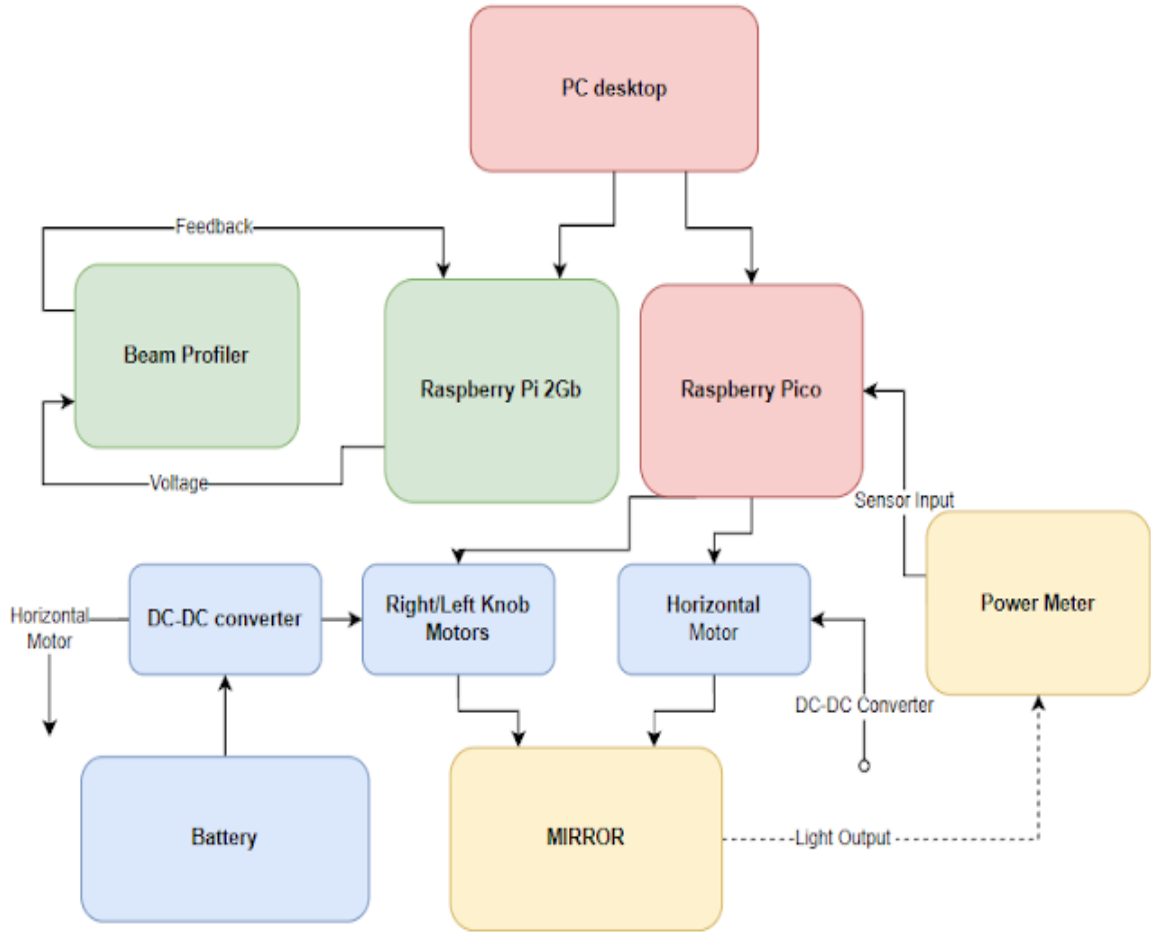
Correlations	
Positive	+
Negative	-
No Correlation	

Direction of Improvement	
Maximize	▲
Target	◇
Minimize	▼

		Column #					
		1	2	3	4	5	6
Direction of Improvement		▼	▼	▼	▲	▲	▼
Row #	Customer Requirements						
	Functional Requirements	Time to Lase	System Weight and Size	Cost	Workable Laser Wavelength Range	Data Refresh Rate	Power Consumption
1	Time to Lase	▼		+	-	+	+
2	System Weight and Size	▼		+	-	-	+
3	Cost	▼	-	+		-	+
4	Noise Disturbance	▼	+	+	-		+
5	Vibrational Impact	▼	+	+	-		+
6	Power Consumption	▼	+	+	+	-	-
7	Requirements		< 5 minutes	< 6.0 kg < 1 ft^3	< \$500	300nm - 1500nm	60 Hz < 20W

Figure 46: House of Quality Trade-off Table

Hardware Block Diagram



AJ assist: Bryce
Bryce assist: AJ
Nick assist: Matt
Matt assist: Nick

Figure 47: Hardware block diagram

Optical Subsystems Diagram

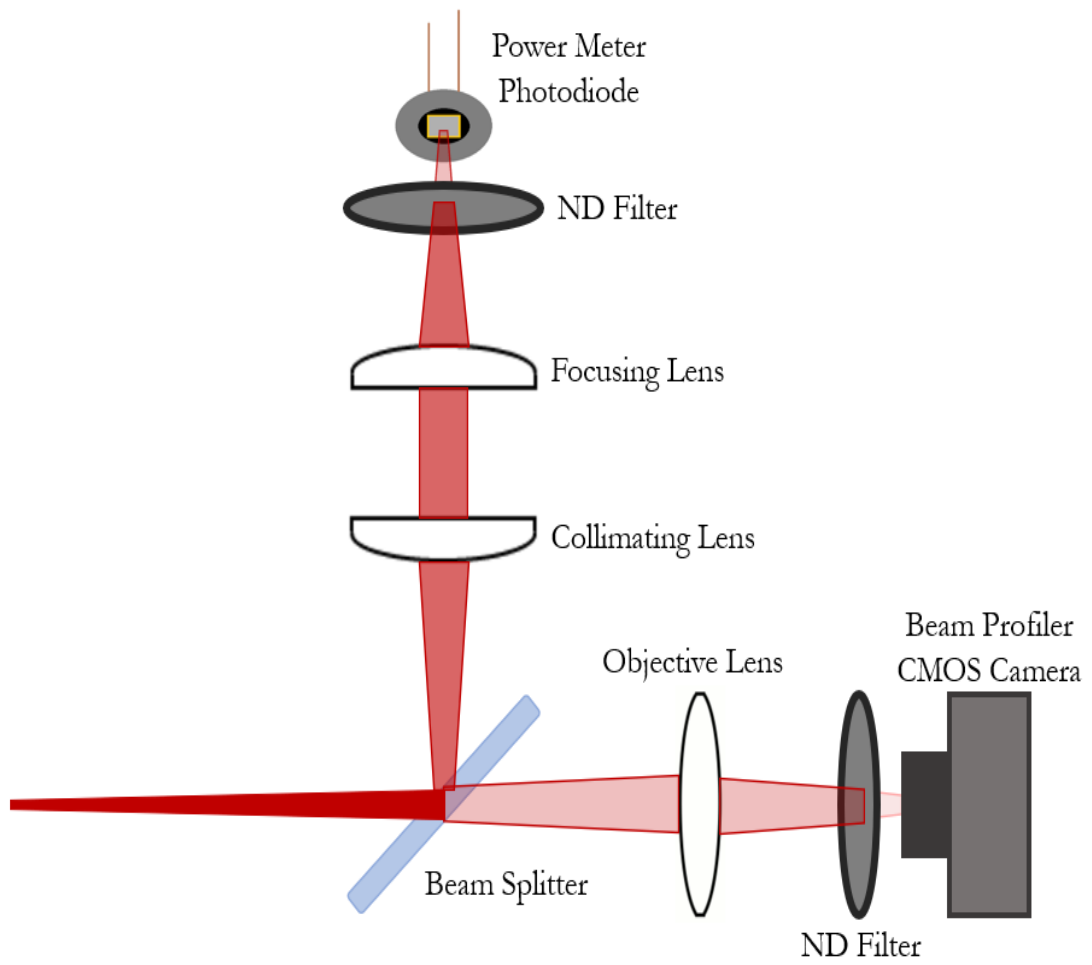


Figure 48: Optical subsystems diagram

Software Block Diagram

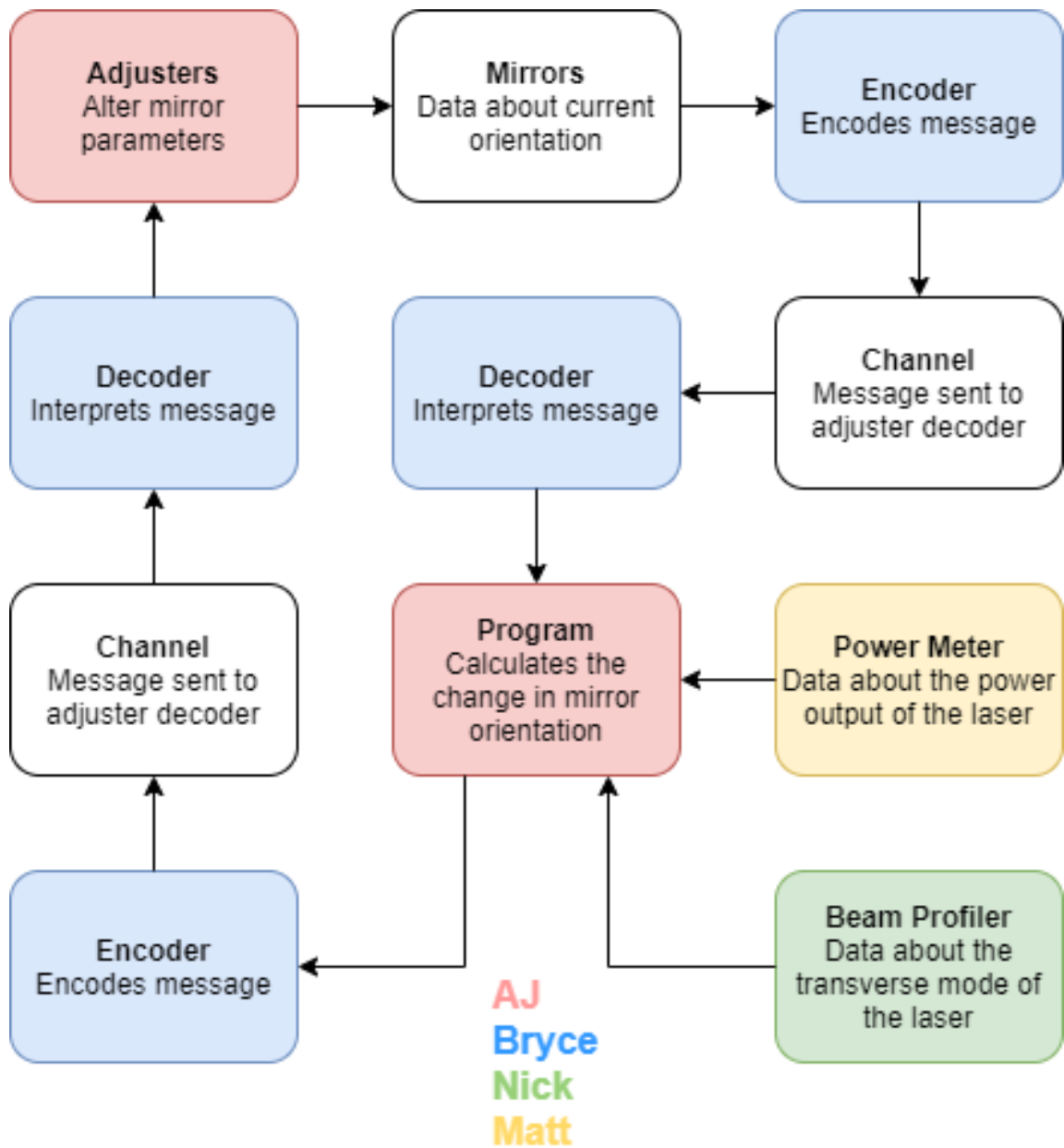


Figure 49: Software block diagram

Software Design

Just as important as the interconnected physical elements of our system, the software we design is vital to our projects function. This software will act both as the communication between the hardware elements of the system, and act as the intermediary between our system and the user. In this section, we discuss the design rationale behind our systems graphical user interface, as well as outlining all the internal software logic present within the system.

Combined Beam-Profiler/Power Meter Graphical User Interface (GUI):

The project software will have a developed program that will streamline the process of displaying the beam profiler and power meter readings, allowing the user to input their desired beam parameters and watch the values change in real time as the mirror mounts adjust. The GUI consists of five major modules: unprocessed camera feed, color coded camera feed, live parameters, desired parameters, and a function tab. The camera modules roughly mirror each other, as do the parameter modules. A rough visualization of the spacing and placement of the modules within a window is provided here in Fig. 50.

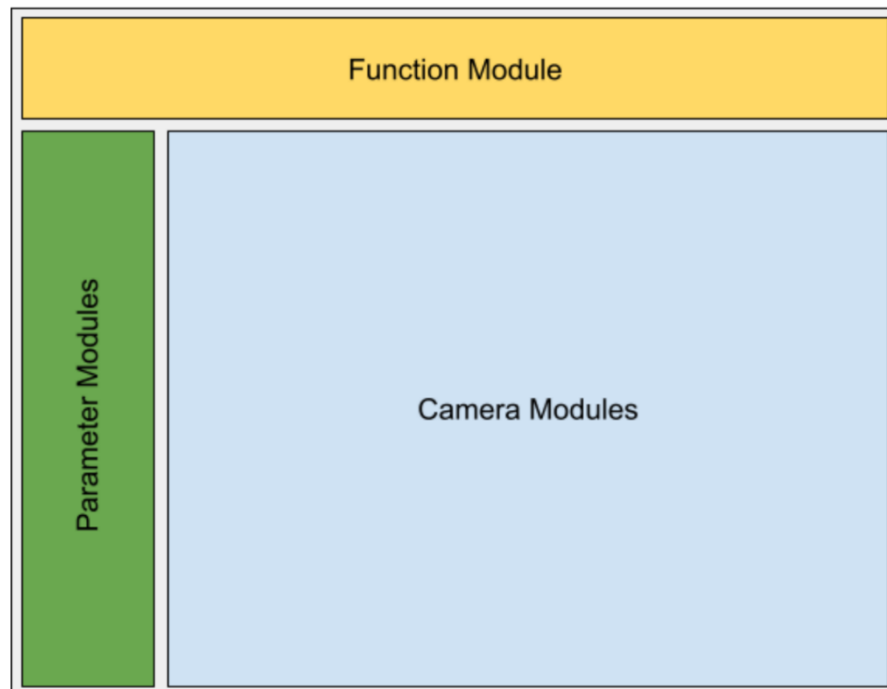


Figure 50: Pictorial Representation of the software layout

Designing the interface to be user friendly and easily understandable was the largest consideration when selecting the layout and what features to prominently display. Using the two camera and two parameter modules, the most major elements of the connected power-meter beam-profiler system are immediately present and identifiable. The areas to input data are front and center, directly next to the live measurements, so the user won't have to worry about finding the correct menu or clicking on the correct tab. However, we also want there to be a level of depth and customization in the software, which is why the functions tab exists. Besides allowing for the user to tinker with units, time divisions, etc., it will house the software's start, stop, and pause buttons. The function module will also house access to beam parameters that the system is able to identify but were deemed not worthy of inclusion in the parameter modules. Each individual module is touched upon in more depth here.

Unprocessed Camera Feed:

Displays a totally raw image from the camera, acting essentially as a live unedited feed of the laser at the camera sensor plane. Included because it potentially can be easier to observe the true shape of the beam and any aberrations than with the color coding.

Color Coded Camera Feed:

Shows the processed camera feed, color coded to showcase the beam intensity in different regions. A color bar located somewhere in the module will indicate which colors are correlated to lower or higher intensities, relatively. This is depicted in Fig. 51.

Both these modules will take up the same amount of space, will likely be placed next to each other, and will each feature a central "reticle" overlay to roughly indicate whether the beam is roughly centered on the sensor plane. In addition, tic marks at the bottom of each camera feed window will indicate physical dimensions. The unit for these ticks are some division of millimeters. Either within the functions tab or directly within the camera modules are the option to minimize either camera feed and use the leftover space to display just one of the camera feeds.

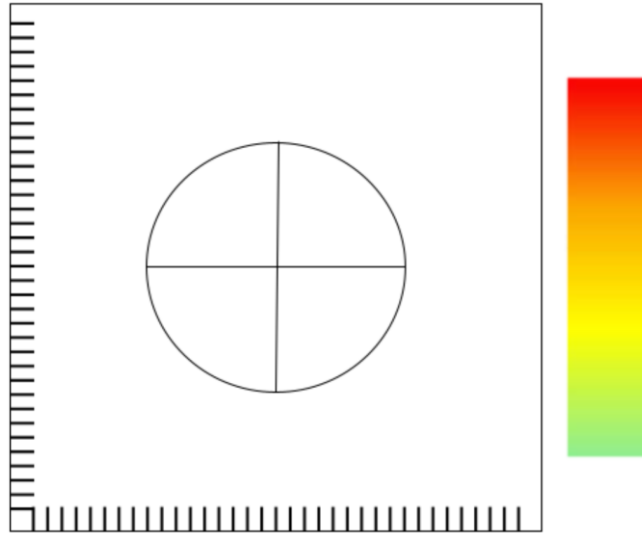


Figure 51: Potential design for color corrected camera module

Live Parameters:

Houses boxes for values for all the pertinent beam profiler and power meter measurements. The corresponding unit is displayed next to the value, with measurements being either instantaneous or time averaged. The function tab could include a feature to choose whether the displayed values are instantaneous or average, and if they are averaged, the time interval to average them over.

Desired Parameters:

A duplicate of the live parameter module, but all the value boxes will initially be empty. The user is able to input the value they hope the system will induce upon the laser into these empty cells. Initially, doing so will have no effect. However, once the “Start” Button in the function tab is clicked, the system will start adjusting the mirrors to try to achieve the user specified parameters. As it is unlikely that the parameters will all move towards the desired values in unison with the mirror movement, a ‘tier’ system will likely be needed. These tiers would essentially dictate to the mirror adjusters which input parameter should be prioritized over the others.

The desired parameters and the live parameters will use the same unit and take up the same area in the GUI. In an ideal situation, the system is able to achieve the desired parameters, and the two modules will mirror each other, albeit with fluctuations from the actual readings.

Function Tab:

Similar in application to a settings bar, the function tabs main components is a start, pause, and stop button. As previously mentioned, the start button will initiate the systems adjustors to bring about the user input laser parameters. If no parameters are inputted, it will instead simply try to maximize output power. Clicking the pause button will momentarily halt system operation, which will resume upon pressing the start button again. Hitting the stop button will depower the motors and clear the input parameters. In addition to these functions, the tab will also feature a save button that can save a copy of the camera images and beam parameters in a folder somewhere on the connected computer. The saved file will likely be a folder containing both image file type of the camera feeds (at the moment of saving) and the parameters in a text or excel file. Time and knowledge permitting, the ability to save a video file of the camera feeds as the mirrors adjust would be beneficial. Some sort of time variant representation of the parameters could accompany the video, providing an educational tool in observing how the different parameters change in reference to each other and the overall spatial characteristics of the beam. There will also be a setting button that can be used to adjust the time scale for the measurements. In addition, a zoom option can be accessed which will allow the user to select a region in the camera feed to focus on and increase the size of.

Final Design:

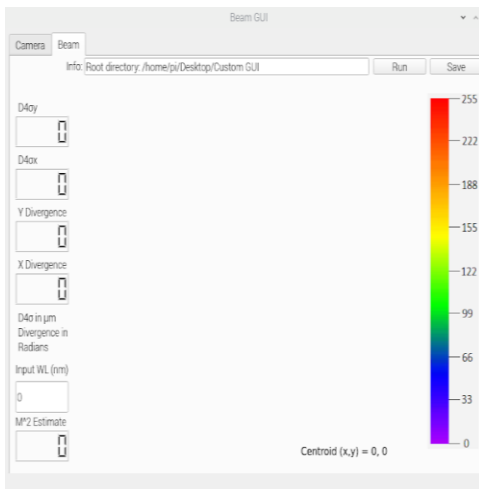


Figure 52: Final GUI Design

The final design of the GUI incorporated most of the elements listed above, while also having some useful unmentioned features. Centroid tracking was instituted as a basis for centering the beam, rather than maximum pixel value, due to the tendency for the laser to oversaturate the camera, even with a ND filter. Furthermore, a save feature was added,

with which a user can save pngs of the color coded and natural camera profile, intensity profiles, and a text file with the beam parameters at the moment of saving.

Software Logic

Beam Profiler:

The entirety of the beam profiler is predicated solely on the measurements given by the CMOS camera unit. There are two major components at play here: the images captured by the camera itself and the information on the individual pixels.

Converting the camera feed into a viewable window within the GUI shouldn't be very difficult, especially for the live unedited feed. There may be some data conversion involved, but it shouldn't be too complex. The camera intakes individual intensity readings across each pixel in its sensor array. These pixels can be index matched to an image array, which is then displayed within the camera module of the software. The intensity values contained in each pixel will then inform what the image array cells will output. The color-coded feed is slightly more intensive and will require matching the individual pixel intensity to a color gradient. After this matching is done, it should be an identical process as to the unedited feed regarding displaying it within the GUI.

The displayed parameters, while involving a lesser degree of raw data, will nevertheless involve more computation. The first important measurement the profiler will display is the beam width. While primarily done via the software, this element will require some user input in adjusting the ND filter attached to the camera module.

As mentioned in the Mode Quality Measurement section contained in the Optical Engineering Technology Investigation module, the waist definition we have been using is the Full-Width at Half-Maximum metric. To use this definition, the beam profiler camera must be able to identify a singular maximum intensity incident on its pixel array. Ensuring this condition will require the user to manually adjust the attached ND filter so that none, or very few, camera pixels are fully saturated (meaning that the camera cannot register any intensity higher than that which it is receiving). If too many pixels are saturated, it is very likely that the true maximum intensity will still reside in one pixel, but there are many pixels with the same pseudo-maximum intensity. This pseudo-maximum is the saturation intensity. As FWHM is predicated off finding a true maximum, the step of adjusting the ND filter to minimize saturation is a must. Once the user has made this adjustment, the system can begin its width calculations.

First, the pixel or pixels of maximum intensity are identified and both its location within the pixel array and the registered intensity incident will be stored. Then, the software will perform a simple computation, dividing this maximum by two, arriving at the intensity value correlating to the beam width defined by FWHM measurements. The software will then scan that pixel array, both horizontally and vertically, from the maximum pixel location until the $\frac{1}{2}$ maximum intensity pixel is found (or whatever pixel is closest to this value). Once located, the number of pixels separating the $\frac{1}{2}$ maximum and the true

maximum pixels will be measured in both directions. This count can then be easily converted into a physical distance by multiplying the count by the pixel size. Upon doing so, the system will yield a FWHM beam width in both the vertical and horizontal directions. As lasers are rarely-if ever-truly circularly symmetric, the inclusion of both a horizontal width and a vertical width is both logical and simple.

From the above procedure, we arrive at the following formulae:

$$\begin{aligned} \text{Beam Width (X)} &= |X_{Max} - X_{1/2}| \times (\text{Pixel Width}) \\ \text{Beam Width (Y)} &= |Y_{Max} - Y_{1/2}| \times (\text{Pixel Height}) \end{aligned}$$

Where X_{Max} and Y_{Max} are the (X, Y) indices of the maximum intensity pixel, $X_{1/2}$ is the X index of the horizontal 1/2 maximum intensity pixel, and $Y_{1/2}$ is the Y index of the vertical 1/2 maximum intensity pixel.

Using these width definitions, the calculations the profiler must perform to arrive at the beam divergence are simple. For our envisioned system, we have been using a specified objective lens within the optical axis of the beam profiler. Using the known focal length of the lens (f), the full divergence angle of the beam can be defined in the vertical and horizontal planes with the below formulae:

$$\begin{aligned} \theta(X) &= \text{Beam Width (X)} \div f \\ \theta(Y) &= \text{Beam Width (Y)} \div f \end{aligned}$$

Although we have been using a set objective with our system, it is possible that users could want, for whatever reason, to substitute their own lens in the beam axis. Because of this, it may be beneficial to provide the user with a prompt to insert the focal length of the profiler lens, rather than setting the value to a fixed variable within the system.

Now that both the full angular divergence and beam width in both orientations are defined, all other relevant parameters can be easily calculated. The beam waist, in both orientations, are defined as:

$$\begin{aligned} \text{Beam Waist (X)} &= \lambda \div [\tan(\theta_X/2) \times \pi] \\ \text{Beam Waist (Y)} &= \lambda \div [\tan(\theta_Y/2) \times \pi] \end{aligned}$$

It should be noted that in these formulae, there is the presence of wavelength. As our project is designed to work with any number of laser systems, wavelength is clearly something that can vary, dependent on the laser. As such, our software must include functionality which lets the user input the operating wavelength for whatever laser cavity they are attaching our automatic adjusters onto. If this were to be excluded, the applicability of our project would be infinitely reduced, and it would only produce valid measurements for lasers with a wavelength equivalent to the preloaded system wavelength.

Now that the system has obtained all the more basic metrics of the laser beam, the M² value is within reach. Similar to the above measurements, the beam quality can be

defined in both vertical and horizontal orientations. The below formulae define M^2 in each orthogonal direction.

$$M^2(X) = [Waist(X) \times (\theta_X/2) \times \pi] \div \lambda$$

$$M^2(Y) = [Waist(Y) \times (\theta_Y/2) \times \pi] \div \lambda$$

*Waist(N) and θ_N refer to the beam waist and angular divergence in the N orientation

Once all the major metrics are calculated by the profiler, its initial job is complete. Following the processes outline above, it just needs to update these measurements if the user seeks to optimize any metric using the Desired Parameters module of the GUI. This process is primarily handled by the automatic adjustors, with the profiler simply refreshing its measurements and feeding this information back into the adjustors looping algorithm. However, there are still some measurements that, while deemed not especially relevant to the projects overall function, may be beneficial for some users. As such, they are not initially display within the parameter modules, but can be made visible via the functions tab. They are quickly mentioned below, and the relevant software calculations are displayed underneath.

Beam Parameter Product (BPP):

$$BPP(X) = Waist(X) \times (\theta_X/2)$$

$$BPP(Y) = Waist(Y) \times (\theta_Y/2)$$

1/e² Width:

$$1/e^2(X) = 1.699 \times Beam\ Width(X)$$

$$1/e^2(Y) = 1.699 \times Beam\ Width(Y)$$

Rayleigh Length:

$$Z_R = \lambda \div [\tan^2(\{\theta_X + \theta_Y\}/4) \times \pi]$$

It should be noted for the Rayleigh Length calculation, the $\{\theta_X + \theta_Y\}/4$ is the result of averaging the two divergences. Although many of the other parameters have been displayed in terms of both the vertical and horizontal orientations, our group has yet to come across any documentation showing the Rayleigh Length presented in such a manner. We have only seen it given as a singular value, thus we thought that averaging the two orthogonal angular divergences and putting that into the formula was most appropriate.

Confocal Beam Parameter:

$$B = 2 \times Z_R$$

Beyond calculating and optimizing the above parameters, the profiler also attempts to correct for spot asymmetry. This was monitored in reference to the beam centroid, corresponding to the maximum intensity pixel. From this point, symmetry is measured along the horizontal and vertical axes, comparing pixels on either side of the centroid. For

example, a pixel four pixels to the left of the centroid is symmetrically related to a pixel four pixels to the right. When the system is set to optimize symmetry, it seek to establish uniformity between symmetrically related pixels in both the horizontal and vertical axes of the centroid. It performs this by simply sweeping the adjusters and attempting to minimize the beam Asymmetry parameter (BSP) which we define below, where j is a distance, in pixels, from the centroid, r is the distance, in pixels, between the centroid and the beam radius, $I(j)$ is the intensity at the j th pixel, and $\Delta sym(j)$ is the intensity difference between symmetrically related pixels at the j th index.

$$\Delta sym(j) = |I(+j) - I(-j)|$$

$$BAP = \sum_{j=1}^{j=r} \frac{\Delta sym(j)}{r - 1}$$

Essentially, the Beam Asymmetry Parameter returns the normalized, averaged asymmetry in the pixels between the beam centroid and the defined beam radius. It can be calculated in any orientation, but for computational simplicity, it was done in the X and Y axes. Minimizing this value in turn minimizes beam asymmetry.

Reinforcement Learning Program Design

This section discusses a high level view of the reinforcement learning programs of the project. The software is divided into two main programs, a training program and an alignment program. The motivation behind this decision to split up the training and alignment has a few factors. The training only needs to be done once assuming the setup of the laser remains constant. The training may also need to be performed on a more powerful computer, and then the output file be transferred to the raspberry pi to be used as an input for the aligning program. These two programs were written in python. I decided that python was be the best fit for these applications because python has many useful libraries for performing mathematical operations and machine learning alike. Python is also able to run on the raspberry pi OS. A compilation of the training program functions and alignment program functions are given in Tables 41 and 42.

Training Program Functions

Function Name	Parameters	Return Type
getScrewOrientation	boolean	integer
setScrewOrientation	boolean, integer	void
scanAcross	void	void
writeFile	string	void

decideAction	integer, integer, double	void
calculateReward	integer, double	double
updateState	reward	void

Table 41: Training program functions

Training Program Function Descriptions

getScrewOrientation

This function gets the current orientation of a screw from the PCB. The input parameter for this function is a boolean which represents which screw value to return. A 0 represents the first screw, and a 1 represents the second screw. The return type of this function is an integer. This integer is the number of degrees that the screw has rotated from the default orientation.

setScrewOrientation

This function sends a signal to the PCB to change the screw's orientation. The input parameters for this function are a boolean which represents which screw is to be changed, and an integer representing how many degrees to rotate the screw. There is no return value for this function.

scanAcross

This function sends a signal to the PCB to make the mirror scan across horizontally. There are no input parameters for this function. There is no return value for this function.

writeFile

This function writes to an output file the result of the training so that it can be saved and used to run the alignment program. This function takes a string of the file name as an input parameter. There is no return value for this function since the output is a text file.

decideAction

This function decides how to adjust the screws. It bases this decision on the current state of the environment. The input parameters for this function are two integers which are the orientation of the screws, and a double which is the output of the power meter. There is no return value for this function.

calculateReward

This function calculates the reward for the agent based on the outcome of the actions which it performs. The input parameters for this function are an integer which is the seconds which it took to achieve a certain power output from the optical power meter, and a double which is the value of that output which was achieved. The return value for this function is a double representing the score assigned to that time and output value pair.

updateState

This function updates the current state of the agent based on the reward it received. The input parameter for this function is a double representing the reward the agent received. There is no return value for this function.

Alignment Program Functions

Function Name	Parameters	Return Type
getScrewOrientation	Void	integer
setScrewOrientation	Integer	void
scanAcross	void	void
readFile	string	void
decideAction	integer, integer, double	void

Table 42: Alignment program functions

Alignment Program Function Descriptions

getScrewOrientation

This function gets the current orientation of a screw from the PCB. The input parameter for this function is a boolean which represents which screw value to return. A 0 represents the first screw, and a 1 represents the second screw. The return type of this function is an integer. This integer is the number of degrees that the screw has rotated from the default orientation.

setScrewOrientation

This function sends a signal to the PCB to change the screw's orientation. The input parameters for this function are a boolean which represents which screw is to be changed, and an integer representing how many degrees to rotate the screw. There is no return value for this function.

scanAcross

This function sends a signal to the PCB to make the mirror scan across horizontally. There are no input parameters for this function. There is no return value for this function.

readFile

This function reads an input file which contains the result of the training so that the alignment program can run based off of a trained agent. This function takes a string of the file name as an input parameter. There is no return value for this function.

decideAction

This function decides how to adjust the screws. It bases this decision on the current state of the environment. The input parameters for this function are two integers which are the orientation of the screws, and a double which is the output of the power meter. There is no return value for this function.

Conclusion

Specification	Goal	Satisfaction
Minimum Achievable Output Power	75% Max	✓✓✓
Workable Laser Wavelength Range	400nm – 700nm	✓✓✓
Workable Laser Output Power Range	0.1mW – 1W	✓✓✓
Maximum Laser Beam Half-Angle Divergence	17.5 mrad	✓✓✓
Workable Laser Beam Diameter	1nm – 10nm	✓✓✓ ✓✓
Time to lase	<5 minutes	✓✓✓

Expectations Barely Met - ✓ Expectations Met - ✓✓ Exceeded Expectations - ✓✓✓

Table 43: Project Goals Satisfaction

The product fulfilled each of the primary goals outlined for the project – taking the laser from not lasing to lasing, finding the maximum laser power, provide beam diagnostics feed to the user via a beam profiler, and complete the tasks in a reasonable amount of time. As seen in table 43, all goals by the end of the project either met expectations or even exceeded them. During the development cycle of this project, each member of our team had to apply themselves to an engineering challenge beyond the scope of their academic training. Whether that be an optics student 3-D modeling mechanical elements or a computer science major analyzing focusing lenses, we each broadened our engineering skillset. Furthermore, we gained priceless experience in working in a multidisciplinary team towards a shared goal and developed our abilities at interpersonal communication. Overall, the team was able to overcome any constraints to complete the given goals and tasks in the afforded time. As a result of being able to stay on track, there to be enough time to test the design and make final adjustments to help improve the performance. Because of this, we were able to come in second place for “Best Demo” in the Senior Design Creole Competition of 2022.

Bibliography

Below are listed our citations used for researching and developing both this paper and our project as a whole. Much like earlier sections, we have roughly categorized our citations according to their relevance to optics, computer programming, and electrical engineering.

Computing:

Fumo, David. “Types of Machine Learning Algorithms You Should Know.” Medium, Towards Data Science, 17 Aug. 2017, <https://towardsdatascience.com/types-of-machine-learning-algorithms-you-should-know-953a08248861>.

Silver, David. “Lecture Notes.” David Silver, 11 Jan. 2021, <https://www.davidsilver.uk/teaching/>.

Stanley, Kenneth O., and Risto Miikkulainen. “Evolving Neural Networks through Augmenting Topologies.” *Evolutionary Computation*, vol. 10, no. 2, 2002, pp. 99–127., <https://doi.org/10.1162/106365602320169811>.

Sutton, Richard S., et al. *Reinforcement Learning: An Introduction*. MIT Press Ltd, 2018.

Electrical and Mechanical:

“Control Stepper Motor with L298n Motor Driver & Arduino.” Last Minute Engineers, Last Minute Engineers, 18 Dec. 2020, <https://lastminuteengineers.com/stepper-motor-l298n-arduino-tutorial/>.

Kammet, Joel. Exploring Robotics Supplemental Notes . https://www.sci.brooklyn.cuny.edu/~kammet/gear_notes.pdf.

Nedlevoski, Dejan. “How Servo Motor Works & How to Control Servos Using Arduino.” *HowToMechatronics*, 8 Oct. 2021, <https://howtomechatronics.com/how-it-works/how-servo-motors-work-how-to-control-servos-using-arduino/>.

Post, Helen. “Choosing the Right Motor For Your Project - DC vs Stepper vs Servo Motors.” Latest Open Tech From Seeed, 29 June 2021, <https://www.seeedstudio.com/blog/2019/04/01/choosing-the-right-motor-for-your-project-dc-vs-stepper-vs-servo-motors/>.

“Raspberry Pi Projects.” [Projects.raspberrypi.org](https://projects.raspberrypi.org), <https://projects.raspberrypi.org/en/projects/raspberry-pi-setting-up/0>.

Optical:

A., Saleh Bahaa E, and Malvin Carl Teich. Fundamentals of Photonics. John Wiley & Sons, Incorporated, 2019.

Dereniak, Eustace L., and Teresa D. Dereniak. Geometrical and Trigonometric Optics. Cambridge University Press, 2008.

“Difference between CMOS & CCD and Why CMOS Sensors Are Preferred for Machine Vision Cameras.” Phase1 Vision, <https://www.phase1vision.com/blog/difference-between-cmos-and-ccd>.

“IMX477/IMX477R: Datasheet PDF, Specs.” Arducam, 13 Jan. 2021, <https://www.arducam.com/sony/imx477/#imx477-specs>.

Paschotta, Dr. Rüdiger. “RP Photonics Encyclopedia.” RP Photonics , 26 Sept. 2021, <https://www.rp-photonics.com/index.html>.

Sears-Collins, Addison. “Why Use CMOS Instead of CCD Sensors in Mobile Phones.” Automatic Addison, 7 Oct. 2019, <https://automaticaddison.com/why-use-cmos-instead-of-ccd-sensors-in-mobile-phones/>.